

TALLINN UNIVERSITY OF TECHNOLOGY  
DOCTORAL THESIS  
58/2019

**Structural and Catalytic Aspects of the  
Catalase-Related Fatty Acid  
Hydroperoxide Lyase**

TARVI TEDER



TALLINN UNIVERSITY OF TECHNOLOGY

School of Science

Department of Chemistry and Biotechnology

This dissertation was accepted for the defense of the degree of Doctor of Philosophy in Chemistry: 18.11.2019

**Supervisor:** Prof. Nigulas Samel  
Department of Chemistry and Biotechnology  
Tallinn University of Technology  
Tallinn, Estonia

**Co-supervisor:** Dr. Helike Lõhelaid  
Department of Chemistry and Biotechnology  
Tallinn University of Technology  
Tallinn, Estonia

**Opponents:** Prof. Ernst H. Oliw  
Department of Pharmaceutical Biosciences  
Faculty of Pharmacy  
Uppsala University  
Uppsala, Sweden

Prof. Ago Rinke  
Institute of Chemistry  
Faculty of Science and Technology  
University of Tartu  
Tartu, Estonia

**Defense of the thesis:** 13.12.2019, Tallinn

**Declaration:**

I hereby declare that this doctoral thesis, submitted for the doctoral degree at Tallinn University of Technology, is my original investigation and achievement and has not been previously submitted for a doctoral or an equivalent academic degree.

**Tarvi Teder**

---



European Union  
European Regional  
Development Fund



Investing  
in your future

Copyright: Tarvi Teder, 2019

ISSN 2585-6898 (publication)

ISBN 978-9949-83-509-6 (publication)

ISSN 2585-6901 (PDF)

ISBN 978-9949-83-510-2 (PDF)

TALLINNA TEHNIKAÜLIKOOL  
DOKTORITÖÖ  
58/2019

# **Katalaasilaadse hüdroperoksiidlüaasi struktuursed ja katalüütilised omadused**

TARVI TEDER

**TAL  
TECH**  
KIRJASTUS



# CONTENTS

LIST OF PUBLICATIONS.....	6
INTRODUCTION.....	7
ABBREVIATIONS.....	8
1 LITERATURE OVERVIEW.....	9
1.1 Oxylipins.....	9
1.1.1 Oxylipins in animals.....	9
1.1.2 Oxylipins in plants.....	10
1.1.3 Oxylipins in other organisms.....	11
1.2 Lipoxygenase-dependent pathways.....	12
1.2.1 Lipoxygenase.....	12
1.2.2 The Cyp74 family.....	16
1.3 Coral lipoxygenase-allene oxide synthase pathway.....	19
2 AIMS OF THE STUDY.....	24
3 MATERIALS AND METHODS.....	25
4 RESULTS.....	26
4.1 The protein characterization of <i>C. imbricata</i> cAOS-b and 8R-LOX (I).....	26
4.2 The reaction mechanism of <i>C. imbricata</i> cAOS-b (II).....	26
4.3 Sequence and structural analysis of <i>C. imbricata</i> cHPL (II).....	27
4.4 Docking simulations of <i>P. homomalla</i> cAOS (II, III).....	28
4.5 Docking simulations of <i>C. imbricata</i> cHPL (II, III).....	29
4.6 Residues involved in the reaction specificity of <i>C. imbricata</i> cHPL (II).....	30
4.7 Determinants in the substrate binding of cHPL and cAOS (III).....	31
4.8 Substrate preferences of coral cHPL and cAOS (III).....	34
5 DISCUSSION.....	36
CONCLUSIONS.....	42
REFERENCES.....	43
ACKNOWLEDGMENTS.....	53
ABSTRACT.....	54
KOKKUVÖTE.....	56
PUBLICATION I.....	59
PUBLICATION II.....	71
PUBLICATION III.....	91
CURRICULUM VITAE.....	103
ELULOOKIRJELDUS.....	106

## LIST OF PUBLICATIONS

The publications used in the thesis are listed as follows:

- I **T. Teder**, H. Lõhelaid, W. E. Boeglin, A. R. Brash, N. Samel. (2015). A catalase-related hemoprotein in coral is specialized for synthesis of short-chain aldehydes: discovery of P450-type hydroperoxide lyase activity in a catalase – *Journal of Biological Chemistry*, 290(32), 19823–32.
- II **T. Teder**, H. Lõhelaid, N. Samel. (2017). Structural and functional insights into the reaction specificity of catalase-related hydroperoxide lyase: A shift from lyase activity to allene oxide synthase by site-directed mutagenesis – *PLoS One*, 12(9), e0185291.
- III **T. Teder**, N. Samel, H. Lõhelaid. (2019). Distinct characteristics of the substrate binding between highly homologous catalase-related allene oxide synthase and hydroperoxide lyase – *Archives of Biochemistry and Biophysics*, 676, 108216.

## AUTHOR'S CONTRIBUTION

**Publications I-III:** *The author contributed to designing the experiments, performed the experimental work, analyzed and interpreted the data, and wrote the manuscript.*

## OTHER PUBLICATIONS BY THE AUTHOR (NOT DISCUSSED IN THIS THESIS)

1. **T. Teder**, W. E. Boeglin, A. R. Brash. (2017). Oxidation of C18 hydroxy-polyunsaturated fatty acids to epoxide or ketone by catalase-related hemoproteins activated with iodosylbenzene – *Lipids*, 52(7), 587–597.
2. **T. Teder**, W. E. Boeglin, C. Schneider, A. R. Brash. (2017). A fungal catalase reacts selectively with the 13S fatty acid hydroperoxide products of the adjacent lipoxygenase gene and exhibits 13S-hydroperoxide-dependent peroxidase activity – *Biochim Biophys Acta Mol Cell Biol Lipids*, 1862(7), 706–715.
3. H. Lõhelaid, **T. Teder**, N. Samel. (2015). Lipoxygenase-allene oxide synthase pathway in octocoral thermal stress response – *Coral Reefs*, 34, 143–154.
4. **T. Teder**, W. E. Boeglin, A. R. Brash. (2014). Lipoxygenase-catalyzed transformation of epoxy fatty acids to hydroxyendoperoxides: A potential P450 and lipoxygenase interaction – *Journal of Lipid Research*, 55, 2587–2596.
5. H. Lõhelaid, **T. Teder**, K. Töldsepp, M. Ekins, N. Samel. (2014). Up-regulated expression of AOS-LOXa and increased eicosanoid synthesis in response to coral wounding – *PLoS One* 9(2), e89215.

## INTRODUCTION

Oxygenated polyunsaturated fatty acids, collectively called oxylipins, are essential lipid mediators present in plants and animals. Oxylipins regulate a wide array of cellular activities, including gene regulation, energy production and signaling pathways. In mammals, the bioactive lipid mediators involved in many physiological processes are produced mainly by cyclooxygenases (COX) and lipoxygenases (LOX). These enzymes are also conserved in lower animals, including corals. So far, COX, LOX and the unique catalase-related allene oxide synthase-lipoxygenase (cAOS-LOX) fusion protein have been identified from several soft corals (*Animalia, Cnidaria*).

In the soft coral *Capnella imbricata*, two cAOS-LOX fusion proteins (cAOS-LOX-a and -b) with the amino acid identity of 88% have been identified. Although the LOX domain of both fusion proteins dioxygenates arachidonic acid (AA) to 8*R*-hydroperoxyeicosatetraenoic acid (8*R*-HpETE), the reaction specificities of the N-terminal domains differ. Specifically, the cAOS-a domain catalyzes the formation of allene oxide from 8*R*-HpETE, while the cAOS-b gives rise to unidentified short-chain aldehydes. A precedent can be found in plants where LOX-derived fatty acid hydroperoxides are metabolized by highly identical cytochrome P450-type AOS and HPL which however have different genetic origins and are structurally incomparable to coral enzymes. In regard to the biological role of coral fusion proteins, it has been shown that the gene expression and catalytic activity of cAOS-LOX-a are elevated in the mechanical and thermal stress response of corals. However, the biological role of cAOS-LOX-b needs further investigation. It should be noted that oxylipins derived by plant AOS and HPL are necessary for their defense and stress signaling.

The X-ray structures of the cAOS domain (PDB ID: 1u5u), the fusion protein (PDB ID: 3dy5) and the AA-bound LOX domain (PDB ID: 4qwt) of the soft coral *Plexaura homomalla* cAOS-LOX revealed the high structural similarity between coral cAOS and human erythrocyte catalase (HEC), while the 8*R*-LOX domain was the most similar to coral 11*R*-LOX and the pharmacologically important human 5*S*-LOX. Moreover, the heme coordinating residues, the distal heme residues, and the proximal heme ligand of cAOS are identical to the corresponding residues of catalase. Despite the homology between catalase-related enzymes and true catalases, cAOS prefers fatty acid hydroperoxides, while catalases exclusively metabolize hydrogen peroxide (H<sub>2</sub>O<sub>2</sub>).

Two highly homologous enzymes, cAOS-a and cAOS-b, with distinct reaction specificities evoked the interest about their structural and catalytic characteristics. One of the main objective of this thesis was to determine the unidentified polar compounds and propose the reaction mechanism of cAOS-b. In that regard, cAOS-b was identified as the first animal catalase-related hydroperoxide lyase (cHPL) catalyzing the scission of 8*R*-HpETE to aldehydic fragments. In addition, it was important to understand the determinants in the reaction mechanism and the substrate binding of cHPL in a relation to cAOS. For this, *in silico* and *in vitro* approaches were applied. The residues responsible for the cHPL-specific reaction were determined via site-directed mutagenesis. The differences in the substrate anchoring and the substrate preferences between cAOS and cHPL indicate their distinct usage of fatty acid hydroperoxides *in vivo*. As with Cyp74 enzymes, cAOS and cHPL contribute to the formation of versatile oxylipins, which may regulate multifaceted physiological processes of corals.

## ABBREVIATIONS

$\alpha$ -ketol	8-hydroxy-9-keto-(5Z, 11Z, 14Z)-eicosatrienoic acid
AA	arachidonic acid; (5Z, 8Z, 11Z, 14Z)-eicosatetraenoic acid
ALA	$\alpha$ -linolenic acid; (9Z, 12Z, 15Z)-octadecatrienoic acid
AO	allene oxide; 8,9-epoxy-(5Z, 9E, 11Z, 14Z)-eicosatetraenoic acid
AOC	allene oxide cyclase
AOS	allene oxide synthase
AOS-LOX	allene oxide synthase-lipoxygenase fusion protein
COX	cyclooxygenase
CAOS	catalase-related allene oxide synthase
CHPL	catalase-related hydroperoxide lyase
cyclopentenone	9-oxo-prosta-(5Z, 10, 14Z)-trienoic acid
CYP450	proteins of cytochrome P450 superfamily
DES	divinyl ether synthase
DHA	(4Z, 7Z, 10Z, 13Z, 16Z, 19Z)-docosahexaenoic acid
EPA	(5Z, 8Z, 11Z, 14Z, 17Z)-eicosapentaenoic acid
GLA	$\gamma$ -linolenic acid; 6Z, 9Z, 12Z-octadecatrienoic acid
HPL	hydroperoxide lyase
H(p)DHE	hydro(pero)xydocosahexaenoic acid
H(p)EPE	hydro(pero)xyeicosapentaenoic acid
H(p)ETE	hydro(pero)xyeicosatetraenoic acid
H(p)ODE	hydro(pero)xyoctadecadienoic acid
H(p)OTE	hydro(pero)xyoctadecatrienoic acid
JA	jasmonic acid; (+)-7- iso-jasmonic acid
LA	linoleic acid; (9Z, 12Z)-octadecadienoic acid
LOX	lipoxygenase
PCR	polymerase chain reaction
PUFA	polyunsaturated fatty acid
RP- or SP-HPLC	reverse phase or straight phase-high performance liquid chromatography



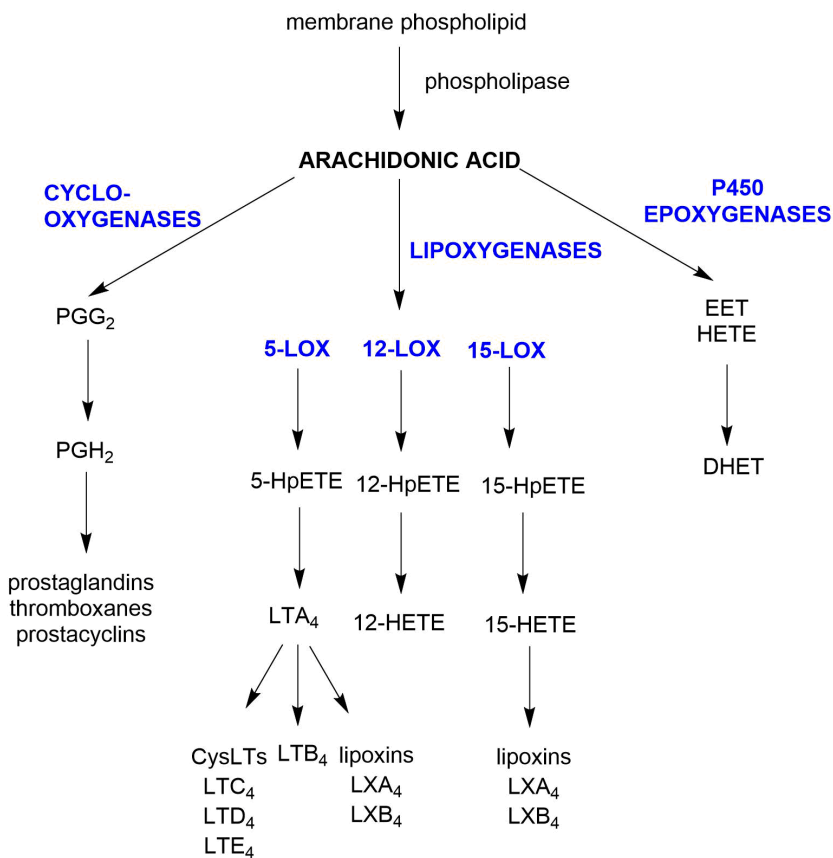
# 1 LITERATURE OVERVIEW

## 1.1 Oxylipins

Oxylipins are a major group of oxygenated long-chain polyunsaturated fatty acids (PUFAs) produced by aerobic organisms [1]. The double bonds of PUFAs are targets for regio- and stereospecific oxygenation by mono- or dioxygenases, or oxidized non-enzymatically by reactive oxygen species [2, 3]. Oxylipins are formed in primary and secondary oxygenation pathways. Primary pathways give rise to oxidized PUFA derivatives, e.g. PUFA hydroperoxides, whereas the secondary or downstream pathways catalyze the intra- or intermolecular rearrangements of functional groups within primary oxylipins. For instance, primary oxylipins in plants are mainly synthesized by lipoxygenases (LOX) [3]. Formed PUFA hydroperoxides are substrates for downstream enzymes, such as Cyp74 enzymes [4]. In animals, three major pathways responsible for the formation of primary oxygenated lipid mediators are cyclooxygenase (COX), LOX and cytochrome P450 (CYP450)[5]. All of the oxygenated products are catalyzed to secondary metabolites by corresponding enzymes (Scheme 1).

### 1.1.1 Oxylipins in animals

In animals, eicosanoids as 20-carbon oxylipins are derived by LOX, COX or CYP450 (Scheme 1) [5]. In animals, eicosanoids as 20-carbon oxylipins are catalyzed by three major pathways, LOX, COX or CYP450 (Scheme 1) [5]. COX and LOX catalyze the dioxygenation of AA to prostaglandins (PGs) and PUFA hydroperoxides (HpETEs), respectively, while NADPH-dependent P450 epoxygenases give rise to PUFA epoxides (EETs) and hydroxides (HETEs). Besides AA, eicosapentaenoic acid (EPA, C20:5n-3), dihomo- $\gamma$ -linolenic acid (DGLA) and docosahexaenoic acid (DHA, C22:6n-3) are the major precursors for the downstream lipid mediators [5–7]. COX-derived prostaglandin H<sub>2</sub> is catalyzed to thromboxane A<sub>2</sub> (TXA<sub>2</sub>) by TXA<sub>2</sub> synthase and prostacyclins (PGI<sub>2</sub>) by PGI<sub>2</sub> synthase (Scheme 2) [5]. Different HpETEs are metabolized to lipoxins (LXs), leukotrienes (LTs) and cysteinyl-leukotrienes (Cys-LTs) by corresponding enzymes [5]. EETs by CYP450 epoxygenase are targets for epoxy hydrolases resulting in the formation of dihydroxy PUFAs (DHET) [8]. Most of the COX- and LOX-derived mediators react with their respective receptors to regulate different physiological processes [5].

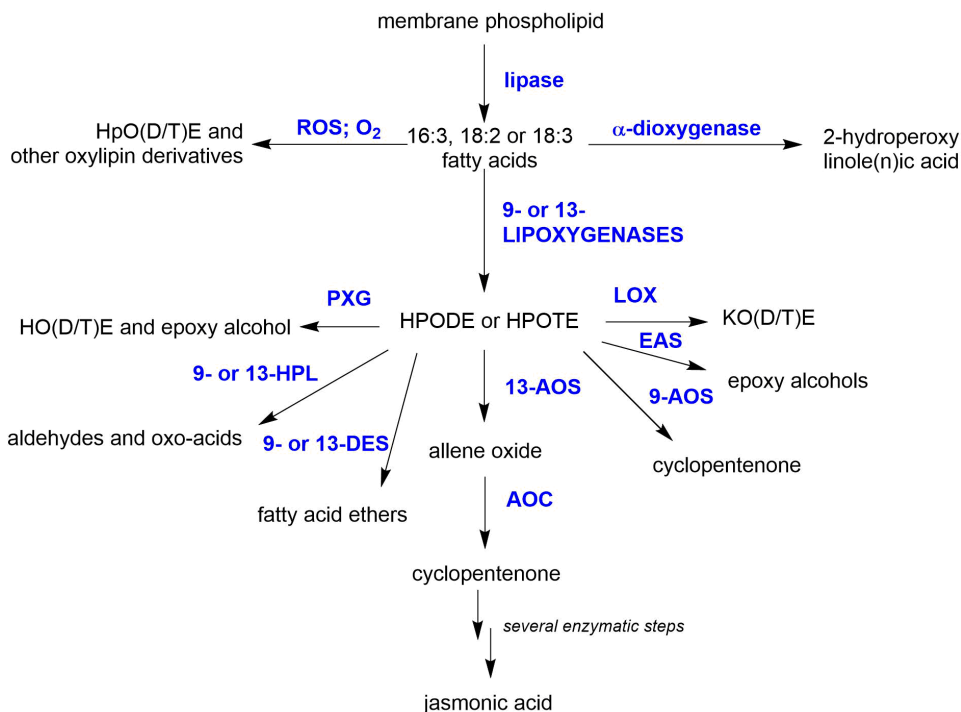


**Scheme 1. The eicosanoid synthesis in animals [5].** DHET – dihydroxyeicosatetraenoic acid; EET – epoxyeicosatetraenoic acid; H(p)ETE – hydro(pero)xyeicosatetraenoic acid; LTB<sub>4</sub>, LTC<sub>4</sub>, LTD<sub>4</sub> and LTE<sub>4</sub> – leukotriene B<sub>4</sub>, C<sub>4</sub>, D<sub>4</sub> and E<sub>4</sub>; LXA<sub>4</sub> and LXB<sub>4</sub> – lipoxin A<sub>4</sub> and B<sub>4</sub>; PGG<sub>2</sub> and PGH<sub>2</sub> – prostaglandin G<sub>2</sub> and H<sub>2</sub>.

### 1.1.2 Oxylipins in plants

In plants, oxylipins are 16- and 18-carbon PUFAs oxidized by LOX [9] or  $\alpha$ -dioxygenases ( $\alpha$ -DOX) [10]. Although the PUFA precursors need to be released from membranes by lipases prior to the oxygenation, it has been reported that some of LOXs are able to metabolize membrane-bound PUFAs as well [11, 12]. The heme-containing  $\alpha$ -DOX catalyzes the dioxygenation of the  $\alpha$ -carbon of PUFAs, resulting in the formation of 2-hydroperoxy derivatives [10]. In contrast to LOXs, its catalysis is independent from the *cis,cis*-1,4-pentadiene moiety. In addition,  $\alpha$ -DOX shows homology to the mammalian COX enzymes [10]. LOX-derived PUFA hydroperoxides are substrates for downstream enzymes such as peroxygenases (PXG) and Cyp74 enzymes, e.g. allene oxide synthase (AOS), hydroperoxide lyase (HPL), divinyl ether synthase (DES) and epoxy alcohol synthase (EAS) [1] (Scheme 2).

In contrast to most plants, moss as a non-flowering plant contains C18 and C20 PUFAs [2]. Interestingly, some of the LOXs from mosses have 12-LOX activity with AA in addition to 13-LOX activity with C18 PUFAs [2]. However, it seems that mosses lack 9-LOX activity. LOXs in mosses share an amino acid identity of 40% with plant LOXs, indicating the divergence of respective LOXs during evolution. As with plant Cyp74 enzymes, moss *Physcomitrella patens* contains HPL [13] and AOS [14].



**Scheme 2. The oxylipin pathway in plants [1].** AOC – allene oxide cyclase; AOS – allene oxide synthase; DES – divinyl ether synthase; EAS – epoxy alcohol synthase; HO(D/T)E – hydroxy octadecadi(tri)enoic acid; HPL – hydroperoxide lyase; HpO(D/T)E – hydroperoxy octadecadi(tri)enoic acid; KO(D/T)E – keto octadecadi(tri)enoic acid; PXG – peroxygenase; ROS – reactive oxygen species.

### 1.1.3 Oxylipins in other organisms

A variety of dioxygenases have been isolated from fungi, eukaryotic algae and prokaryotes [2]. In fungi, both activities, LOX and COX, are present. However, no fungal COXs have been isolated due to the sequence dissimilarities to known COXs. As some of the pathogenic fungi contain only a small amount of C20 PUFAs, prostaglandins are produced from AA derived from its host. Contrary to COXs, many fungal LOXs have been isolated and characterized. Fungal LOXs prefer either C18 or C20 substrates and some of them are also bifunctional [2]. The best characterized LOX from fungi is the manganese-containing LOX [15]. Upon the activation of manganese LOX,  $Mn^{2+}$  is oxidized to  $Mn^{3+}$ , which correspond to  $Fe^{2+}$  and  $Fe^{3+}$  in iron-containing LOXs. In addition to LOX and COX, fungi contains linoleate diol synthase (LDS), which catalyzes the dioxygenation and subsequent dihydroxylation of linoleate [16]. Although AOS activity has been detected in different fungal species [17–19], HPL activity is absent, probably due to the antifungal properties of aldehydes [20].

Eukaryotic algae contain different LOXs and COXs which contribute to the production of a vast array of bioactive oxylipins [2]. It was believed that the oxylipin metabolism was present only in eukaryotes. However, several dioxygenases have been isolated and characterized from prokaryotes in the last decade [2], mostly from cyanobacteria [21, 22].

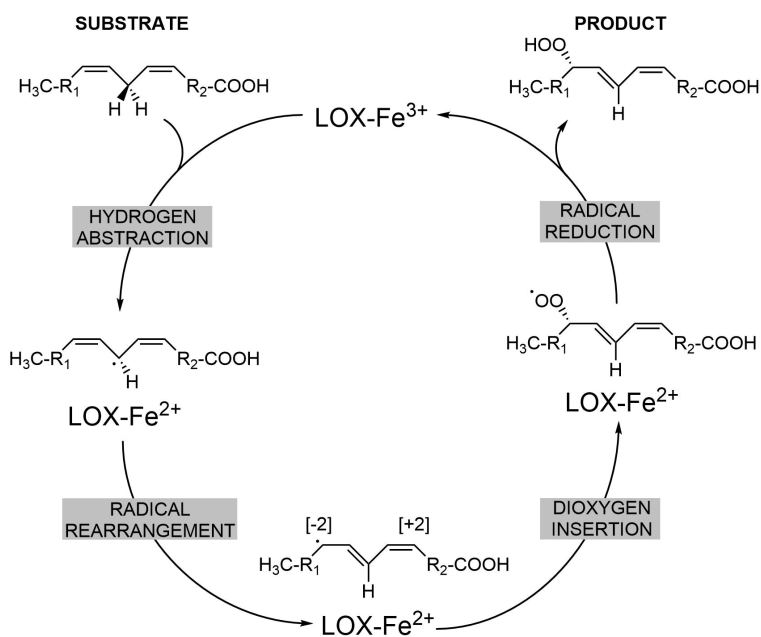
## 1.2 Lipoxygenase-dependent pathways

### 1.2.1 Lipoxygenase

Lipoxygenases (LOX) (EC 1.13.11.-) are ubiquitous non-heme iron-containing dioxygenases that catalyze the regio- and stereospecific formation of fatty acid hydroperoxides by introducing molecular oxygen to the *cis,cis*-1,4-pentadiene moiety of PUFAs.

#### *Mechanism of catalysis*

Catalysis by LOX is divided into four steps, as follows (Scheme 3): a) position-specific hydrogen abstraction from a bis-allylic methylene ( $R_1\text{-CH}_2\text{-R}_2$ ), which results in the formation of a pentadienyl radical, b) the rearrangement of the radical either in the direction of the methyl terminus (+2 rearrangement) or in the direction of the carboxyl terminus (-2 rearrangement) of PUFAs, 3) the introduction of molecular oxygen to the antarafacial plane (the opposite side of a substrate), producing a peroxy radical with a specific chiral center (*R* or *S*), and 4) the reduction of a peroxy radical to form the fatty acid hydroperoxide.



**Scheme 3. LOX-catalyzed hydrogen abstraction from AA and the subsequent formation of PUFA hydroperoxide.** The abstracted hydrogen and formed hydroperoxy group are antarafacially positioned [23]. Figure is reproduced from Ivanov et al. 2010 [24].

#### *Nomenclature*

LOXs are classified based on their stereo- and regiospecificity (Fig. 1). For example, coral 8*R*-LOX catalyzes the formation of 8*R*-hydroperoxy-eicosatetraenoic acid (8*R*-HpETE) from AA [25]. In addition, two human 12-LOX isozymes with different stereospecificities

have been named, 12S-LOX and 12R-LOX. Moreover, the location or the cell type of LOXs with the same stereospecificity has been specified, e.g. the platelet, epidermal or leukocyte type of 12-LOX [26].

All of the plant LOXs and some of the animal LOXs catalyze the formation of products with *S* stereoconfiguration. However, the *R*-lipoxygenases seem to be more prevalent in animals and have also been identified in marine invertebrates [25, 27]. The possible regio- and stereoisomers of PUFA hydroperoxides produced by LOXs are presented in Figure 1. The Ala-to-Gly mutation as the “Coffa/Brash determinant” [28, 29] of LOXs has been postulated to be the switch from *S*- to *R*-regiospecificity, however, this rule is not applicable to all of the LOXs [30].

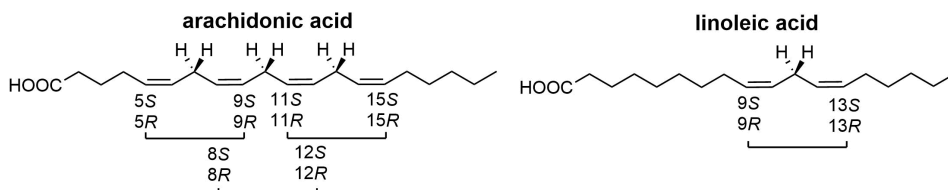


**Figure 1. Potential regio- and stereoisomers of LOX-derived PUFA hydroperoxides [23].**

To date, 5S-LOX, 8S-LOX, 12S-LOX, 12R-LOX and 15S-LOX have been identified from mammals [31] (Table 1). In addition, 9R-, 9S- and 13S-LOX [32] can be found in plants while 8R-LOX [33], 5R-LOX [34] and 11R-LOX [27, 35] seem to be only specific to marine invertebrates. It should be noted that plant LOXs react only with C18 PUFAs, e.g. LA, a-LA, whereas animal LOXs prefer C20 or longer PUFAs [32].

**Table 1. Human lipoxygenases [36].**

Gene name	Common names	Main substrate	Main product	Biological function
ALOX5	5-LOX	AA	5S-HpETE, LTA <sub>4</sub>	LT production, inflammatory mediators
ALOX12	Epidermal 12-LOX	AA	12S-HpETE	modulation of platelet aggregation
ALOX12b	12R-LOX	linoleoyl- $\omega$ -hydroxyceramide	9R-Hp-linoleoyl- $\omega$ -hydroxyceramide	maintenance of epidermal permeability barrier
ALOXE3	eLOX3	9R-hydroperoxy-linoleoyl- $\omega$ -hydroxyceramide	9R,10R-epoxy-13R-hydroxylinoleoyl- $\omega$ -hydroxyceramide	maintenance of epidermal permeability barrier
ALOX15	15-LOX-1, 12/15-LOX, leukocyte 12-LOX	free and esterified PUFAs	15S- and 12S-HpETE	inflammatory mediators, membrane oxidation
ALOX15b	15-LOX-2	AA	15S-HpETE	negative cell cycle regulation, tumor suppression

## Enzyme structure

The first crystal structure of *Glycine max* LOX was described in 1993 [37]. So far, four plant, seven animal and three bacterial LOX structures are available at the Protein Data Bank (PDB) [38]. Although the  $\alpha$ -helical catalytic and the N-terminal  $\beta$ -barrel domains are conserved between animal and plant LOXs, the molecular weight of plant LOXs is around 100 kDa, while animal LOXs are about 20 kDa smaller [39] (Fig. 2). In addition, the iron of LOXs is coordinated primarily by conserved histidines and an N-terminal isoleucine. The inactive enzyme contains the iron in the ferric form ( $\text{Fe}^{3+}$ ), which in catalysis is oxidized to the ferrous form ( $\text{Fe}^{2+}$ ) (Scheme 3). The N-terminal  $\beta$ -barrel domain of LOXs shares homology with the C-terminal C2 domain of lipases [40] and has been labeled as the PLAT (Polycystin-1, Lipoxigenase, Alpha-Toxin) domain in animal LOXs (Fig. [40] and has been labeled the PLAT (Polycystin-1, Lipoxigenase, Alpha-Toxin) domain in animal LOXs (Fig. 2B). Although most of the LOXs are cytosolic, the  $\beta$ -barrel of animal LOXs is necessary to obtain the substrate from the hydrophobic environment via calcium activation. However, the role of the  $\beta$ -barrel domain of plant LOX in membrane binding has not been shown.

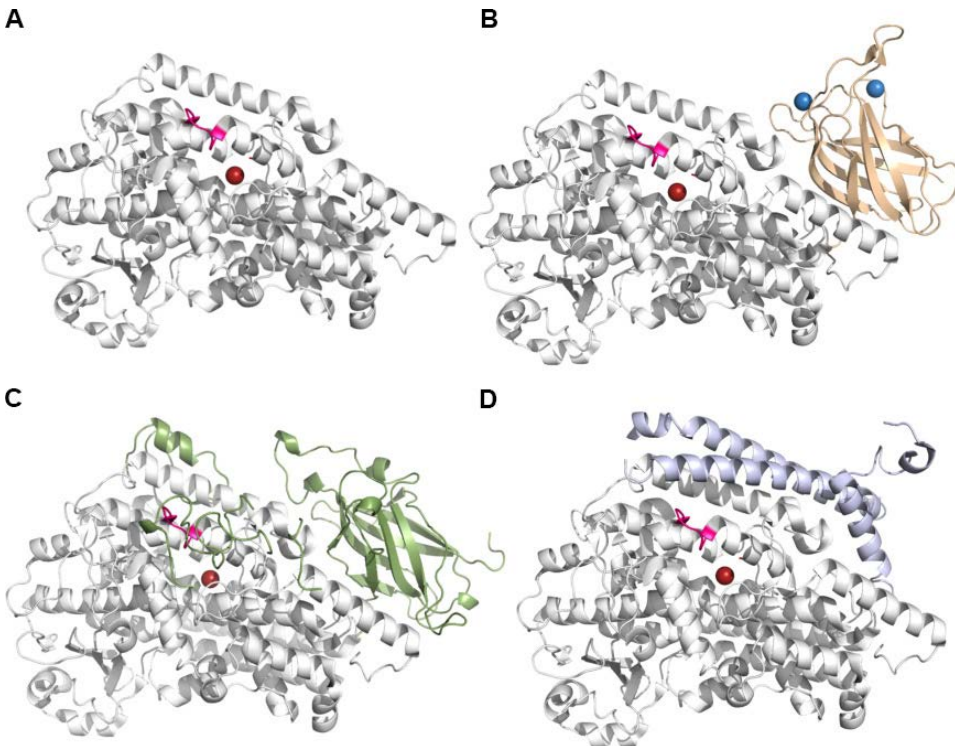


**Figure 2. The conserved core structure of plant, animal and bacterial LOXs.** (A) The overall structure of LOXs with the catalytic iron (red). The helical part in the active site is indicated in pink. The animal (B) and plant (C) LOXs with distinct N-terminal domains possibly involved in the membrane binding. The calcium ions are presented in blue. (D) The bacterial LOX with additional helices instead of the N-terminal PLAT domain. Figure is reproduced from Newcomer et al. 2015 [38].

Soybean LOX L-1 [41], *Gersemia fruticosa* 11R-LOX [42] and *Fusarium graminearum* 13S-LOX [43] contain tubular channelings for molecular oxygen. Directing the oxygen by specific residues might be involved in the regio- and stereospecificity of the dioxygenation [38]. However, the structural data of different LOXs regarding oxygen channeling is not clear.

### Substrate positioning

The substrate positioning in the active site is a key factor in controlling oxygenation by LOXs. LOXs can bind PUFAs in a tail-to-head (“tail first”) or a head-to-tail (“head first”) orientation. It has been reported that only 13S-LOX can oxidize either membrane-bound or free PUFAs. This indicates that 13S-LOX binds substrates in a tail-to-head orientation while substrates of 9S-LOX can enter the substrate channel only in a “head-first” orientation [44]. In addition, 15S-LOX-2 binds substrates as “tail-first”, whereas in 5-LOX, substrates enter the substrate channel as a carboxy group first (Fig. 3). The same principle applies to 12-LOX and 8-LOX.

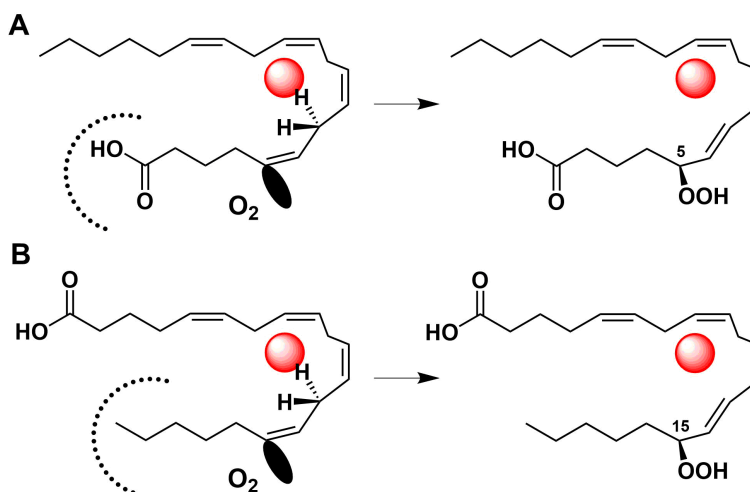


**Figure 3.** The inverse positioning of AA in the active sites of 5-LOX and 15-LOX-2. AA bound in a head-to-tail orientation by 5-LOX (A) and in a tail-to-head orientation by 15-LOX-2 (B). The non-heme iron is presented in red. The cavity depths of corresponding LOXs are in correlation with the schematic presentation. Figure is reproduced from Newcomer et al. 2015 [38].

### Substrate specificity and availability

Most of the LOXs prefer free PUFAs as substrates which have been released from a membrane by specific phospholipases [45]. Even though LOXs are positioned near membranes via the PLAT domain, the phospholipid membrane *per se* is not necessary for the activity of most LOXs. However, mammalian 15-LOX [46] and coral 11R-LOX [47] become catalytically active in the presence of lipid membranes through a structural reorganization of the PLAT domain. Only few LOXs are able to metabolize either free or esterified substrates, e.g. plant 13-LOX [44].

## Biological function

Overall, mammalian LOXs are involved in 1) the modification of lipid-protein complexes, 2) the regulation of the intracellular redox state and 3) the synthesis of bioactive lipid mediators (Fig. 4, upper part). Specifically, the modification of membrane-bound substrates by LOX increases the membrane permeability via hydrophilic pores and may result in the dysfunction of a cell. The cellular redox state is influenced by the pro- and anti-oxidative processes initiated by LOXs. The redox state affects gene expression and the transcription of redox-sensitive genes, which may control the phenotype of a cell [48].

Mammalian LOXs give rise to a variety of bioactive lipid mediators which include leukotrienes [49], lipoxins [50], hepxilins [51], eoxins [52], resolvins [6], protectins [53], maresins [7] and other oxylipins. These LOX-derived lipid mediators are involved in different pathophysiological processes including inflammatory, metabolic, infectious, neurodegenerative and other disorders. Therefore, as LOXs are involved in many pathogenesises of human diseases, they are potential targets in drug research.

In plants, 9-LOX is involved in cell death via hydroxy acids, whereas 13-LOX participates in processes which involve lipid peroxidation, the wounding response, daytime sensing, fertility and development (Fig. 4, lower part) [54].

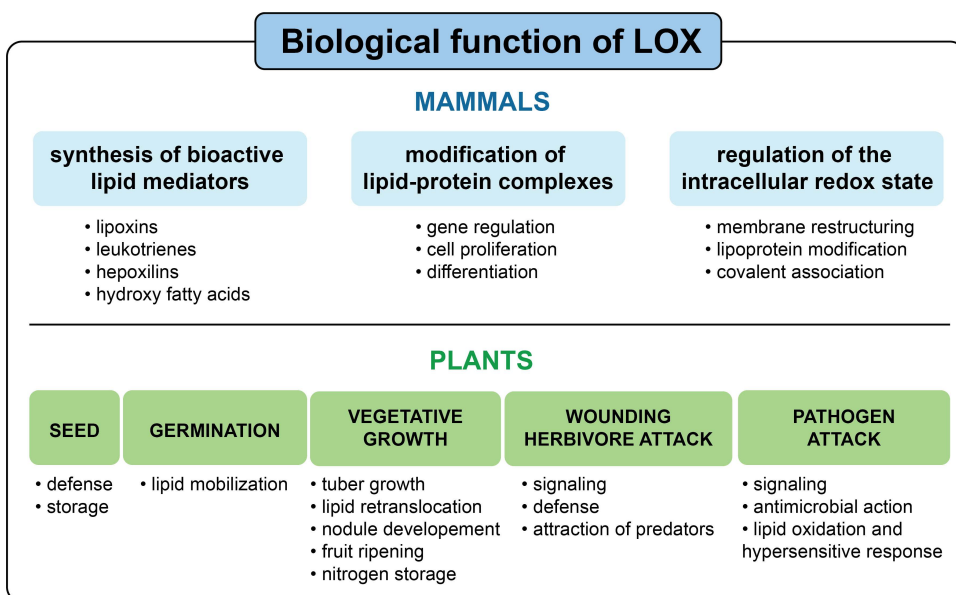
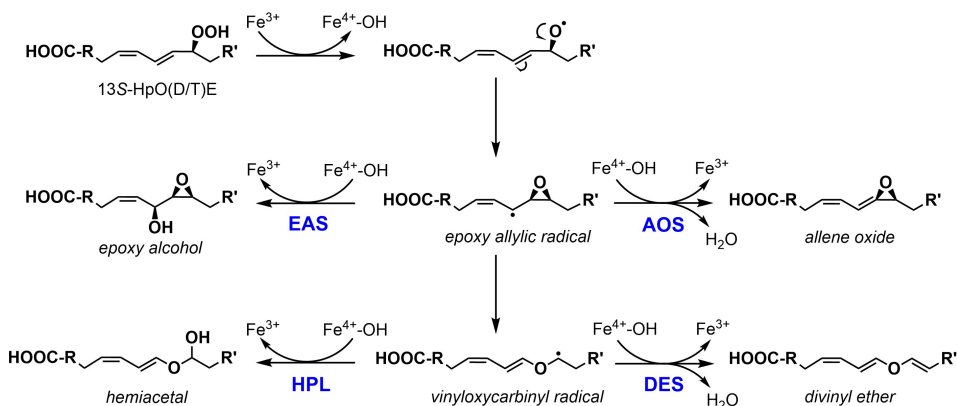


**Figure 4. Biological functions of LOXs.** In mammals (upper part), LOXs contribute to the synthesis of lipid mediators, the rearrangement of lipid-protein complexes and the control of the intracellular redox state via gene expression [48]. In plants (lower part), LOXs are involved in different steps of the life cycle of plants [55].

### 1.2.2 The Cyp74 family

In plants, the Cyp74 family of CYP450 consist of AOS, HPL, DES and EAS [56]. These enzymes are atypical CYP450 due to the fact they do not need NADPH or molecular oxygen as co-factors. The Cyp74 enzymes catalyze the formation of a common intermediate, epoxy allylic radical, which is converted to either allene oxide (AO), epoxy alcohol, hemiacetal or divinyl ether via intramolecular rearrangements (Scheme 4).





**Scheme 4. The catalytic mechanisms of plant AOS, HPL, DES and EAS.** EAS catalyzes the insertion of a hydroxy radical to the epoxy allylic radical as a common intermediate of Cyp74 enzymes to produce epoxy alcohol. AOS conducts the dehydration of epoxy allylic radical to allene oxide via oxidation and subsequent proton loss. The common intermediate for the formation of hemiacetal or divinyl ether by HPL or DES, respectively, is a vinyloxy carbonyl radical. Although the AOS reaction can be explained using the carbocation intermediate, the existence of a purely radical or carbocation-containing pathway remains unclear. However, as the HPL reaction involves the formation of radicals, the reactions catalyzed by the members of the Cyp74 family are presented as radical. Scheme is reproduced from [57].

#### Allene oxide synthase

AOs are chemically derived from an allene group by oxidation [58]. In plants, AOs are synthesized from either 9S- or 13S-hydroperoxides of ALA or LA by AOS of the Cyp74A family [59]. It should be noted that only 13S-hydroperoxide-derived AOs are converted to jasmonic acid (JA), an essential plant mediator, whereas 9S-hydroperoxides are utilized by alternative pathways [44]. Although plant AOSs prefer either 9S- or 13S-hydroperoxides, dual positional specificities of AOS have been identified from rice [60] and barley [61]. Due to the differences in the sequences between plant 9-AOS and 13-AOS, 9-AOS and 9/13-AOS belong to the Cyp74C group instead of Cyp74A [59].

The crystal structures of plant *Arabidopsis thaliana* AOS [62] and *Parthenium argentatum* AOS [63] with substrate and intermediate analogs revealed the structural attributes necessary for substrate binding and catalysis. Based on the structural information of AOS and the sequence alignments of Cyp74 enzymes, several single amino acids have been proposed to be determinants in the reaction specificity of Cyp74 enzymes. One of the most appealing regions of AOS and HPL, the substrate recognition site, contains conserved Phe and Leu, respectively [62, 64]. Single amino acid exchanges of the substrate cavity have led to the conversion from AOS to HPL [14, 65], DES to AOS [66] or EAS to AOS [57], illustrating the high homology between the members of the Cyp74 family (Table 2). Attempts to alter the activity from plant HPL to AOS have not been very successful. However, a cucumber EAS having HPL activity only with 13S-hydroperoxides was converted to AOS via site-directed mutagenesis recently [57].

**Table 2. The conversion of reaction specificity between the Cyp74 enzymes via site-directed mutagenesis. The choice of mutations is explained in corresponding publications. The measurements were conducted with 9S-HpODE or 13S-HpODE from LA (n-6), and 9S-HpOTE or 13S-HpOTE from ALA (n-3).**

Enzyme	Mutation	Substrate	Activity	Ref.
<i>Lycopersicon esculentum</i> AOS3	F108L	9S-HpODE, 9S-HpOTE (n-3) 13S-HpODE, 13S-HpOTE (n-3)	AOS → AOS, EAS AOS → EAS	
<i>Physcomitrella patens</i> * AOS2 (PpAOS2)	F93L	9S-HpODE, 9S-HpOTE (n-3) 13S-HpODE, 13S-HpOTE (n-3)	AOS → EAS AOS → AOS, EAS, HPL	[64]
<i>Zea mays</i> AOS1 (ZmAOS1)	F95L	9S-HpODE, 9S-HOTE (n-3) 13S-HpODE, 13S-HpOTE (n-3)	AOS → AOS, EAS, HPL	
<i>Linum usitatissimum</i> AOS (LuAOS)	F150L	9S-HpODE, 9S-HOTE (n-3) 13S-HpODE, 13S-HpOTE (n-3)	AOS → no change	
<i>Medicago truncatula</i> CYP74C13_MT	L97F	9S-HpODE, 9S-HOTE (n-3) 13S-HpODE, 13S-HpOTE (n-3)	EAS → AOS HPL → AOS	
<i>Cucumis sativus</i> CYP74C1_CS <i>C. sativus</i> CYP74C31	L93F/G283A L98F/A287G			[57]
LuDES <i>Nicotiana tabacum</i> DES	E292G V379F	13S-HpOTE (n-3), 9S-HpODE	DES → AOS	[66]
<i>P. patens</i> * AOS1	F93L	9S-HpODE, 13S-HpODE, 9S- HPOTE (n-3) 13S-HpOTE (n-3)	AOS → HPL AOS → AOS, HPL	[14]
<i>L. esculentum</i> AOS3	K302S T336Y	9S-HpODE	AOS → HPL	[67]
<i>L. esculentum</i> AOS3	F295I S297A	9S-HpODE	AOS → HPL	[65]
<i>A. thaliana</i> AOS	F137L	13S-HpODE 13S-HpOTE (n-3)	AOS → HPL AOS → AOS, HPL	[62]

\* - *P. patens* is a moss used as a model organism in plant research.

### Hydroperoxide lyase

Plant HPL designated as Cyp74B catalyzes the scission of fatty acid hydroperoxides to short-chain aldehydes [59]. Specifically, the 13S- or 9S-hydroperoxy fatty acid of LA is converted to 12-oxo-(9Z)-dodecenoic acid as traumatin and (3Z)-hexenal or 9-oxo-nonanoic acid and (3Z,6Z)-nonadienal by 13-HPL or 9-HPL, respectively [68]. HPL with dual activity, 9/13-HPL as Cyp74C, reacts with 13S-hydroperoxides and 9S-hydroperoxides similarly [69]. Although it is known that HPL is involved in plant defense and gene expression, the activity and the location of 9- and 13-HPL vary between different plant species and even within the plant [68]. For instance, 13-HPL has been identified from soybean seedlings and tea leaves, while 9-HPL has been identified from cucumber fruits [68], pear fruits [70] and lipid bodies of almonds [71]. Cucumber seedlings contain both activities, 9- and 13-HPL [68]. This correlates with the notion that the C6-aldehydes are associated with the smell of fresh grass, while the (3Z,6Z)-nonadienal or (3Z)-nonenal are similar to the odor of a cucumber [68].

Formed (3Z)-aldehydes isomerize enzymatically [72] or non-enzymatically [69] to (3E)-aldehydes. It has been shown that both isomers, (3Z)-hexenal and (2E)-hexenal, are biologically active in plants [72]. For instance, (3Z)-hexenal and (2E)-hexenal regulate the expression of stress-related genes [73] and due to the electrophilic characteristics of the  $\alpha,\beta$ -unsaturated carbonyl moiety of (2E)-hexenal [3, 74], it has antibacterial [72] and

antifungal properties [75]. (*E*)-aldehydes are reduced to alcohol derivatives by alcohol dehydrogenase or reductases [72] to avoid the high reactivity and harmful effects on photosynthetic systems in plants.

#### *Biological function*

The HPL and AOS pathways compete for the same substrate, although, their cellular location and the regulatory aspects indicate that there are specific lipases and LOXs for specific branches [76]. For example, two distinct LOX pathways in tomato and potato are designated either for the HPL or AOS branch [44]. The AOS pathway is involved in the plant defense via the synthesis of JA, while green leaf volatiles formed by HPL act as signaling compounds for natural enemies and are necessary in communicating with undamaged plants. Moreover, several silencing experiments have demonstrated cross-talk between the AOS and HPL branch [77, 78].

### **1.3 Coral lipoxygenase-allene oxide synthase pathway**

In corals, an 8*R*-lipoxygenase (8*R*-LOX) and a catalase-related allene oxide synthase (cAOS) are expressed together as a cAOS-LOX fusion protein [25]. The name cAOS-LOX is based on the sequence order in the gene, having the cAOS sequence located at the 5' end and the LOX sequence at the 3' end [25]. However, the enzymatic reaction is initiated by the C-terminal 8*R*-LOX domain, followed by the N-terminal cAOS domain. Specifically, the 8*R*-LOX domain catalyzes the conversion of AA to 8*R*-HpETE, which subsequently is converted to AO by the N-terminal cAOS domain. Due to the unstable properties of AO, it is detected as its stable end-products: 8-hydroxy-9-keto-(5*Z*, 11*Z*, 14*Z*)-eicosatrienoic acid as  $\alpha$ -ketol and 9-oxo-prosta-5*Z*,10,14*Z*-trienoic acid as cyclopentenone or precavulone A [25].

#### *Occurrence*

The cAOS-LOX fusion proteins have been identified from the soft corals *Plexarua homomalla* [25], *G. fruticosa* [79] and *Capnella imbricata* [80], and the full sequence from *Clavularia viridis* is available at the NCBI database (NCBI ID: AB188528). The amino acid identity between cAOS-LOXs from different coral species is around 80-90%. The sequence data of stony corals also suggests the existence of cAOS-LOX in hexacorals [81]. In the soft coral *G. fruticosa*, the cAOS-LOX [79] pathway co-exists with the independent 11*R*-LOX [27], however, no other LOX activity besides 8*R*-LOX has been reported from other corals.

#### *Biological function*

The gene expression of cAOS-LOX is elevated in response to white band disease [82], UV radiation [83] and temperature [84]. The increased enzymatic activity of cAOS-LOX, together with elevated eicosanoid levels during mechanical and thermal stress, have been shown [80]. This demonstrates that cAOS-LOX plays a central role in the stress response of corals. The cAOS-LOX pathway has been suggested to be a biomarker of endangered coral species in connection with climate warming and pollution [80, 85].

## Structure

The crystal structures of the *P. homomalla* cAOS-LOX fusion protein (PDB ID: 3dy5) [86] and the stand-alone domains, cAOS (PDB ID: 1u5u) [87] and 8R-LOX (PDB ID: 4qwt) [88] (Fig. 5) have been reported. The structure of 8R-LOX with AA demonstrated its similarity to mammalian LOXs rather than plant LOXs [88]. 8R-LOX as a typical animal LOX contains the core domain with the non-heme iron in the catalytic center and the PLAT domain with calcium binding sites. 8R-LOX has a U-shaped substrate channel which binds AA in a tail-to-head orientation (Fig. 5A). Arg182 in the substrate entry site of 8R-LOX is necessary for the productive binding of AA [88]. In contrast to coral 11R-LOX, the activity of 8R-LOX is not membrane-dependent, however, the presence of calcium ions [89] and/or the membrane [90] enhance the catalytic rate of 8R-LOX. It has been suggested that the PLAT domain of 8R-LOX plays a role only in membrane targeting and does not affect the catalytic activity *in vivo* [90]. Although cAOS and 8R-LOX can be expressed individually as active proteins, the covalent linkage between cAOS and 8R-LOX appears to be necessary for membrane targeting [86].

Despite the low amino acid identity, ~11%, between cAOS and human erythrocyte catalase (HEC), the core structures and their catalytic centers are conserved (Fig. 5B and 5C). Specifically, the heme coordinating residues, Arg64, Arg102 and Arg360, the distal heme residues, His67 and Asn137, and the proximal heme ligand, Tyr353 of cAOS, are identical to the corresponding residues of catalase [91]. However, coral cAOS with the larger substrate channel prefers fatty acid hydroperoxides as substrates instead of hydrogen peroxide (H<sub>2</sub>O<sub>2</sub>) [25].

The most notable difference in catalytic centers between true catalases and cAOS is the Val66 in catalases instead of the Thr66 of cAOS (Fig. 5C) [25]. The T66V (Thr66Val) mutation of cAOS did not alter the reaction specificity, but the formation of AO decreased drastically in parallel with the increased consumption of hydrogen peroxide (H<sub>2</sub>O<sub>2</sub>) [92]. The inverse mutation of HEC, V66T, reduced the decomposition of H<sub>2</sub>O<sub>2</sub> which confirmed the specific role of Val66 in the interaction with H<sub>2</sub>O<sub>2</sub> [93].

In addition, the replacements of Asn137 (Fig. 5C) lowered the turnover rate of cAOS but did not alter the reaction specificity of cAOS [94]. Most likely, Asn137 is not involved in the catalysis but it is necessary for the productive binding of a substrate.

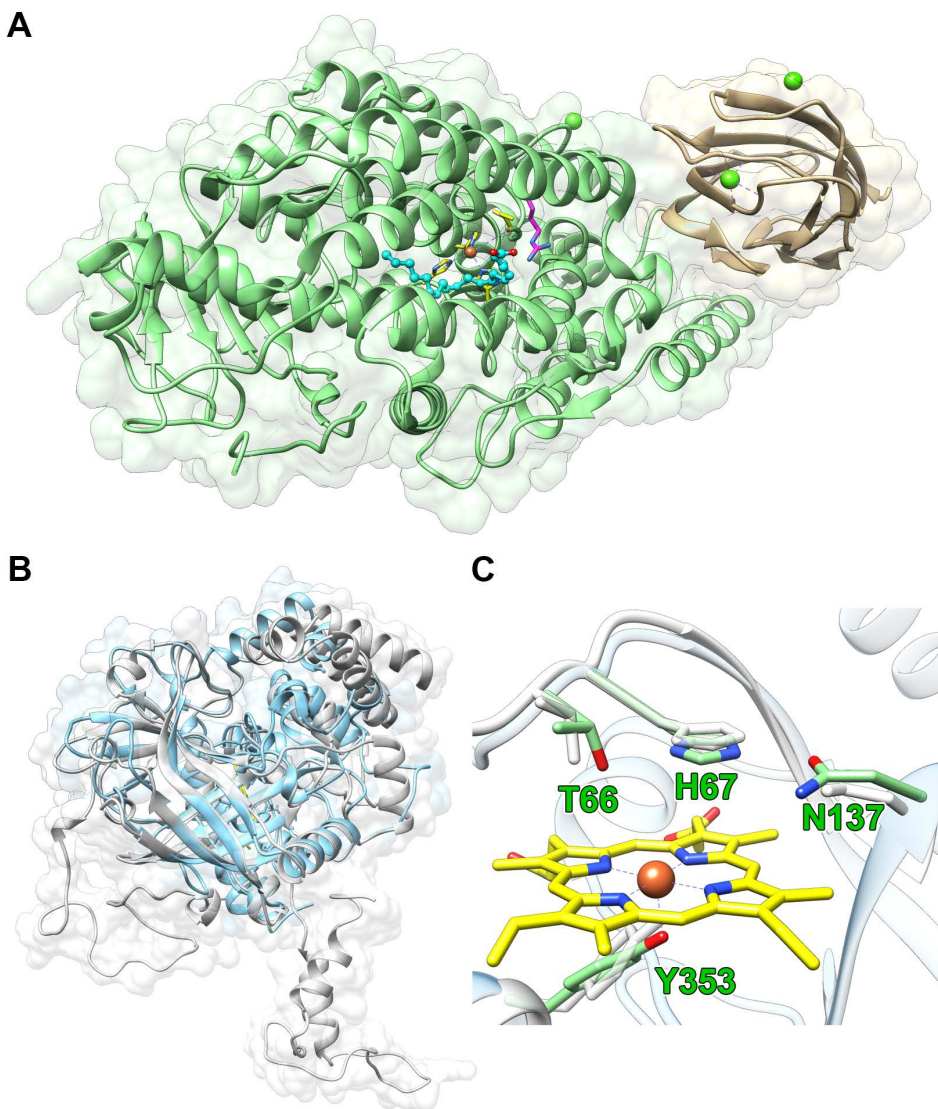
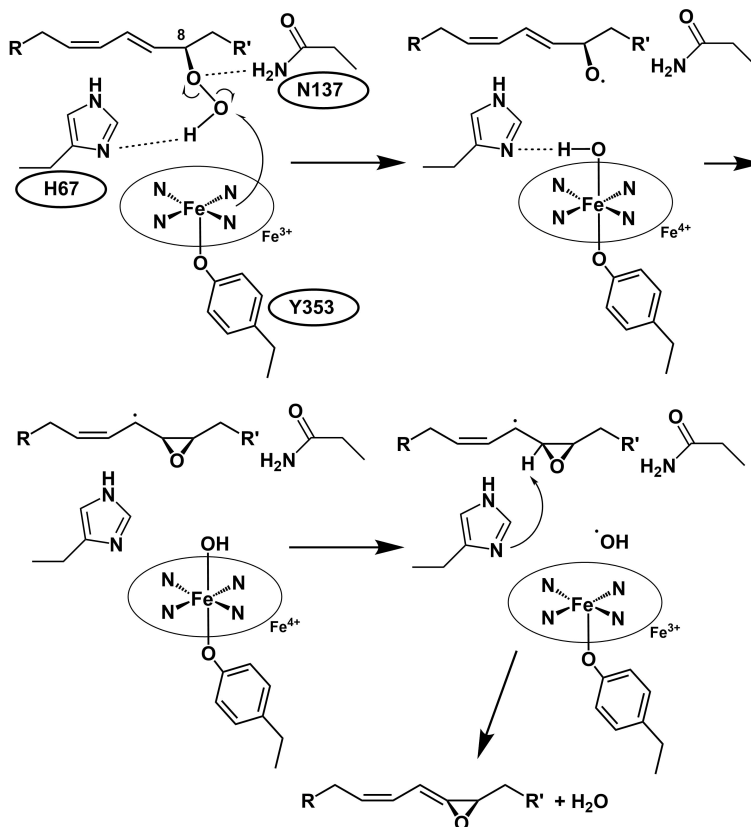


**Figure 5. The crystal structures of *P. homomalla* 8R-LOX and cAOS. (A)** The crystal structure of 8R-LOX with AA (cyan) (PDB ID: 4qwt). The conserved residues, His384, His389, His570 and Ile693, coordinating the non-heme iron are shown in yellow. The positively charged Arg182 interacting with the carboxy group of AA is presented in pink. The PLAT domain and calcium ions are presented as brown and light green, respectively. **(B)** The superimposed structures of *P. homomalla* cAOS (PDB ID: 1u5u) and HEC (PDB ID: 1dgf) are presented in blue and gray. The heme is presented in yellow. **(C)** The conserved active center between cAOS and HEC. The residues in the active site, Thr66, His67 and Asn137, and the proximal heme ligand, Tyr353, are presented in green.

## The mechanism of catalysis of cAOS

The structural data of cAOS suggests that His67 interacts with the hydroperoxy group via hydrogen bonding, which is necessary for homolytic cleavage by the heme iron. The cleavage of the hydroperoxy group results in the formation of an alkoxyl radical and the Fe<sup>4+</sup>-OH of cAOS as Compound II (Scheme 5). Similarly to plant AOS, allene oxide is formed from the epoxy allylic radical intermediate as a result of deprotonation.



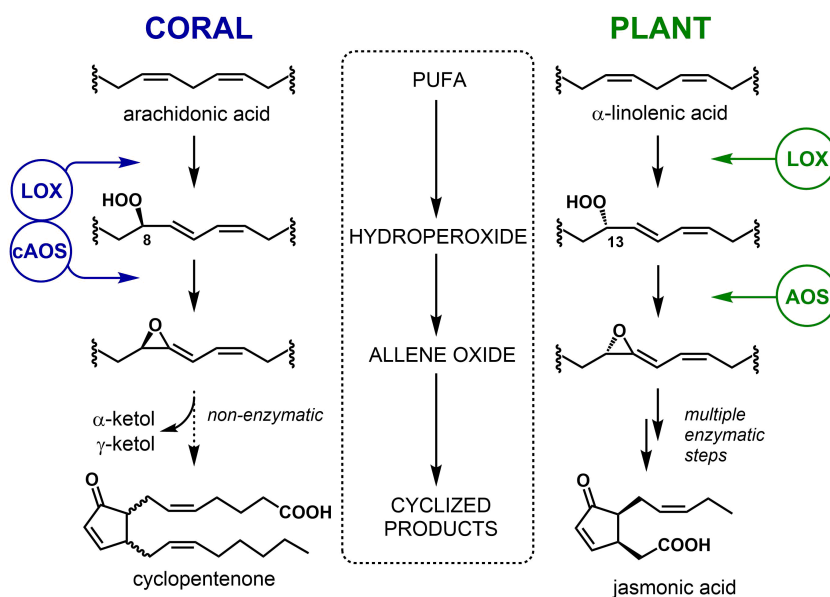
**Scheme 5.** The putative reaction mechanism of coral cAOS. The hydrogen bond between the His67 of cAOS and the hydroperoxy group of 8R-HpETE is necessary for homolytic cleavage by the heme group. The formation of an alkoxyl radical is followed by the epoxy allylic radical and corresponding carbocation. The latter is deprotonated to an AO. Scheme is adapted from [87].

## Comparison of coral and plant AOSs

Coral cAOS do not need any additional co-factors similarly to the CYP450-type plant AOS (Cyp74), TxA<sub>2</sub> synthase (Cyp5) and PGI<sub>2</sub> synthase (Cyp82) [56]. However, a heme group with catalytically relevant residues in the active site plays an important role in their mechanisms. Despite the LOX-dependency and the identical reactions catalyzed by coral cAOS and plant AOS, there are several differences between corresponding oxylipin pathways (Scheme 6):

- i) coral cAOS and LOX are fused together [25], whereas plant enzymes are expressed individually [54];

- ii) although coral cAOS and plant AOS are heme-containing and PUFA hydroperoxides metabolizing proteins, they are not structurally related. The former enzyme is catalase-related and the latter belongs to the CYP450 superfamily [58];
- iii) plant LOX catalyzes the formation C18 PUFA hydroperoxide in *S* stereoconfiguration, while the cAOS-LOX pathway produces *R*-hydroperoxides of AA;
- iv) no allene oxide cyclase has been detected from corals, but the JA pathway in plants contains several enzymes involved in the production of cyclic oxylipins from AO [95];
- v) plant AOSs are membrane-associated [96], while coral cAOS-LOX and its domains are fully active without the presence of lipid bilayers [89].



**Scheme 6. The formation of allene oxides in coral (left) and plant (right) LOX-dependent pathways.** In corals, allene oxide is synthesized by the cAOS-LOX fusion protein, while in plants two individual enzymes catalyze the distinct steps of the pathway. Plant AO is converted to cyclized derivatives by allene oxide cyclase, whereas coral cyclopentenone together with ketols are formed non-enzymatically.

Regardless of the distinct genetic origin of coral and plant AOS, the biological role of both pathways seems to be involved in the synthesis of oxylipins in response to abiotic and biotic stressors [44, 80, 85]. From an evolutionary standpoint, the properties of oxygenated PUFAs appear to be necessary for specific signaling via intracellular proteins or via membrane-bound receptors in different organisms [31].

## 2 AIMS OF THE STUDY

The general aims of the current study were to determine the reaction mechanism of *C. imbricata* cAOS-b and compare the structural-functional properties of highly identical *C. imbricata* cAOS-b and *P. homomalla* cAOS.

The specific goals of the study were:

- identification of products and elucidation of reaction mechanism for cAOS-b;
- determination of residues responsible for distinct reaction specificities of highly conserved cAOS and cAOS-b;
- comparison of structural and functional aspects between cAOS and cAOS-b in terms of substrate binding;
- ascertainment of substrate preferences of cAOS and cAOS-b.



### 3 MATERIALS AND METHODS

The brief description of materials and methods used in the thesis are listed below. The detailed protocols are presented in the corresponding publications.

#### *In silico* analysis

- Structural analysis of *P. homomalla* cAOS was performed to evaluate the structural differences between *P. homomalla* cAOS and *C. imbricata* cAOS-b (**Publications II and III**).
- Docking simulations were carried out to establish the interactions between the enzyme as template and the substrate as ligand (**II, III**).
- The homology modeling of *C. imbricata* cAOS-b was conducted to understand the structural characteristics necessary for lyase activity and the substrate binding (**II, III**).

#### Protein expression and characterization

- The expression constructs of *C. imbricata* cAOS-a, cAOS-b, 8R-LOX and *P. homomalla* cAOS were prepared using PCR cloning (**I-III**).
- The site-directed mutagenesis of *C. imbricata* cAOS-a, cAOS-b and *P. homomalla* cAOS was performed by using the whole plasmid PCR method to establish the role of a single amino acid on the substrate binding and product synthesis (**II, III**).
- Recombinant *C. imbricata* cAOS-a, cAOS-b and *P. homomalla* cAOS domains and the corresponding mutants with a C-terminal, and *C. imbricata* LOX domain with an N-terminal His-tag were expressed in *Escherichia coli* BL21(DE3) cells (**I-III**).
- Expressed enzyme variants were purified using nickel-affinity chromatography (**I-III**).
- Oligomerization states of wild-type enzymes and mutants were analyzed with size-exclusion chromatography (**II**).
- Kinetic parameters of enzyme variants were assayed spectrophotometrically (**I-III**).

#### Product identification

- The products of *C. imbricata* cAOS-b and 8R-LOX were analyzed and collected with RP- and SP-HPLC, and identified by using LC-MS and NMR (**I**).
- The products of *C. imbricata* cAOS-b and *P. homomalla* cAOS mutants were analyzed by using RP-HPLC coupled with ESI-Q-TOF-MSMS and radiodetector (**II, III**).
- The metabolites synthesized from alternative fatty acid hydroperoxy substrates by *C. imbricata* cAOS-b and *P. homomalla* cAOS were analyzed in the same way described previously (**III**).

## 4 RESULTS

### 4.1 The protein characterization of *C. imbricata* cAOS-b and 8R-LOX (I)

The recombinant *C. imbricata* cAOS-LOX-b (122 kDa) fusion protein, cAOS-b (43 kDa) and 8R-LOX (79 kDa) domains were expressed and purified as active proteins. The cAOS-LOX-b fusion protein and 8R-LOX eluted on the size exclusion column as monomers, while cAOS-b tended to oligomerize. Although this indicated that 8R-LOX is necessary for the stability of cAOS-b, the reaction rate and specificity of the cAOS-b domain alone or as a part of the fusion protein were identical. However, the factors of the oligomerization of cAOS-b remained unclear. The regio- and stereospecificity of *C. imbricata* 8R-LOX was confirmed by co-eluting the reduced product with 8R-HETE by *G. furticosa* 8R-LOX [97] and the racemic standard of 8-HETE as references on a chiral column. *C. imbricata* cAOS-b as a hemeprotein contains the  $\lambda$  maximum at 407 nm, while the corresponding value of cAOS is at 406 nm [25].

### 4.2 The reaction mechanism of *C. imbricata* cAOS-b (II)

*C. imbricata* cAOS-b catalyzed the cleavage of 8R-HpETE to short-chain aldehydes, (5Z)-8-oxo-octenoic acid as C8-oxo acid and (3Z,6Z)-dodecadienal as C12 aldehyde (Fig. 6). This type of enzymatic scission of PUFA hydroperoxides is typical for HPL [98]. Therefore, cAOS-b [80] was designated as the first animal HPL, and the abbreviation of cHPL will be used from now on. In an aqueous solution, C8-oxo acid and C12 aldehyde isomerized to the (5E)- and (3E)-derivatives, respectively, containing the  $\alpha,\beta$ -unsaturated carbonyl moiety (Fig. 6A). The non-enzymatic isomerization was detected with the shift in the UV chromophore from 205 nm to 220 nm by SP- and RP-HPLC. The initial products were determined as reduced derivatives of aldehydes, C8-hydroxy acid and C12 alcohol. The hydroxy derivatives contained the non-isomerized *cis* double bonds with the *cis* configuration (Fig. 6A).

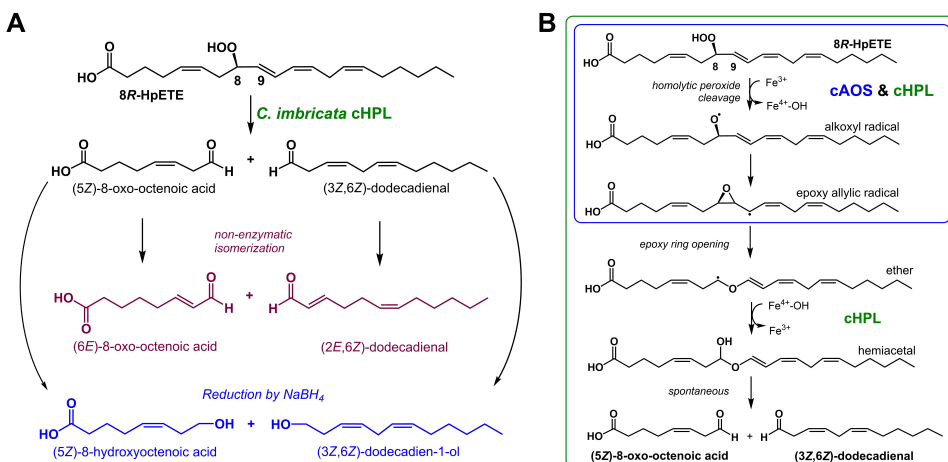


**Figure 6. The proposed reaction mechanism of cHPL. (A)** The enzymatic cleavage of 8R-HpETE into (5Z)-8-oxo-octenoic acid as C8-oxo acid and (3Z,6Z)-dodecadienal as C12 aldehyde which in an aqueous solution isomerize non-enzymatically to (6E)- and (2E)-derivatives (green), respectively. The primary products of cHPL can be analyzed as reduced derivatives of C8-oxo acid and C12 aldehyde (blue). **(B)** The steps in the formation of the hemiacetal intermediate by cHPL and its breakage into aldehydic fragments. Both catalase-related enzymes, cAOS and cHPL, give rise to a common intermediate, an epoxy allylic radical, which is transformed to a divinyl ether radical only by cHPL. The common and distinct steps in the reaction mechanisms between cAOS and cHPL are indicated by the blue and the green boxes, respectively (Publication I).

The isotopic analysis of the products by cHPL demonstrated that the oxygens in the oxo groups of C8-oxo acid and C12-aldehyde are retained from the hydroperoxy group of the 8R-HpETE substrate which excludes the involvement of water in the reaction (Fig. 6B). Based on the results and the reaction mechanism of plant HPL [99], the steps of the catalysis by cHPL are postulated in Figure 6B.

### 4.3 Sequence and structural analysis of *C. imbricata* cHPL (II)

*C. imbricata* cHPL and coral cAOSs as highly homologous enzymes have the amino acid identity of around 81-83%. In addition, all of the defined catalytically important residues, Thr66, His67 and Asn137, and the distal heme ligand, Tyr353, are conserved [25, 80, 85]. The differences in the sequences between the substrate channels of cHPL and cAOSs are presented in Figure 7A. To determine the structural characteristics of cHPL, the 3D homology model of cHPL was generated based on the crystal structure of *P. homomalla* cAOS (PDB ID: 1u5u) by using a SwissModel tool [100]. The good quality of the model with the Global Model Quality Estimation (GMQE) and Qualitative Model Energy Analysis (QMEAN) values of nearly 1 [101] was achieved with the high amino acid identity between cHPL and cAOS sequences and the good resolution of the template structure of *P. homomalla* cAOS. The superimposed structures of cHPL and cAOS with the differences in the residues are shown in Figure 7B and 7C.

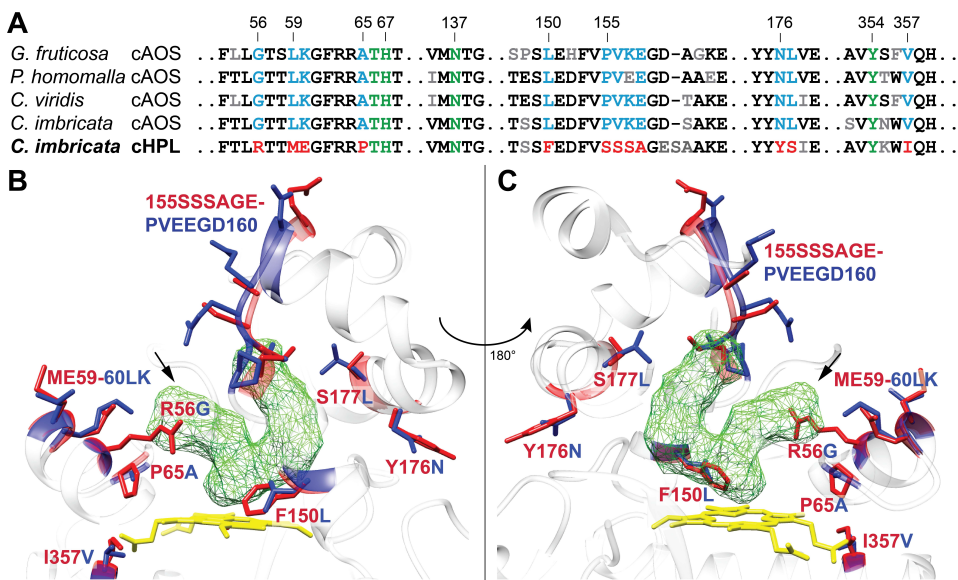


**Figure 7. The sequence and structure comparison between coral cAOS and cHPL. (A)** The amino acid alignment of the substrate channels of *P. homomalla* cAOS and *C. imbricata* cHPL. The invariant and variable residues of the sequences are shown in black and gray, respectively. The sequence differences between the substrate channels of cAOS and cHPL are indicated as light blue and red, respectively. The catalytically important residues and the distal heme ligand is presented as green. **(B)** The superimposition of the crystal structure of *P. homomalla* cAOS (blue) and the model of *C. imbricata* cHPL (red). The substrate entry site is located near R56G and is indicated with an arrow. The heme and the active site are presented in yellow and green, respectively. **(C)** The rotated view (180 degrees) of the superimposed structures (Publication II).

#### 4.4 Docking simulations of *P. homomalla* cAOS (II, III)

The 8*R*-HpETE substrate and the alternative fatty acid substrates, 8*R*-HpEPE, 10*R*-HpDHE, 9*R*-Hp-GLA, 8*R*-Hp-AEA, 8*R*-Hp-1-AG and 8*R*-Hp-1-AG were docked successfully into the substrate channel of *P. homomalla* cAOS. All of the ligands were placed in the substrate pocket in a catalytically productive conformation, with the carboxy group located near Lys107 or Lys60 and with the hydroperoxy group of a ligand interacting with the catalytically essential residues, Thr66 and His67, and the heme iron (Fig. 8). The docking simulations with 9*R*-Hp-ALA were unsuccessful probably due to the rigidity of the ligand and the incompatibility with the substrate channel of cAOS.

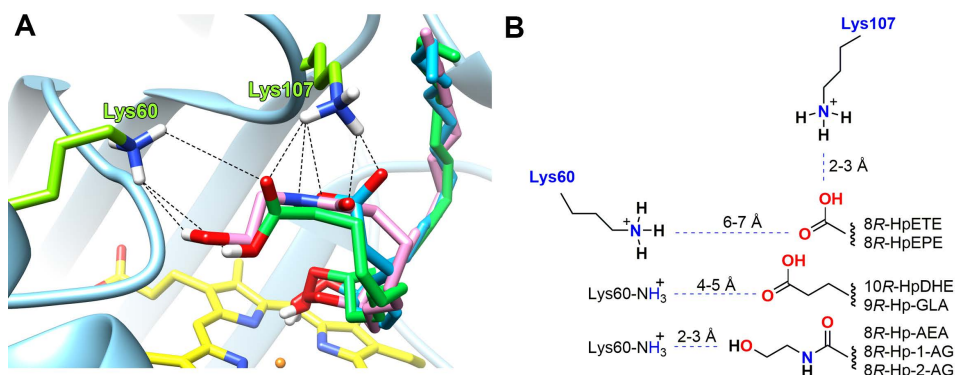


**Figure 8.** The docking simulations of the crystal structure of *P. homomalla* cAOS with PUFA hydroperoxides. (A) 8R-HpETE (cyan), 10R-HpDHE (green) and 9R-Hp-AEA (pink) placed in the substrate channel of *P. homomalla* cAOS. The interactions between the residues (green) and the head group of a ligand are indicated with dotted lines. The heme is shown in yellow. (B) The distances between the head group of ligands and the positively charged residues, Lys60 and Lys107. The proximity of Lys60 to the head group varied due to the distinct length of the ligands (Publications II and III).

#### 4.5 Docking simulations of *C. imbricata* cHPL (II, III)

The docking simulations of the model of *C. imbricata* cHPL resulted in unsuccessful docking attempts probably due to the structural constraints in the substrate channel (Fig. 9A). The major difference between the substrate entry sites of cHPL and cAOS was the SSSAGE loop of cHPL instead of the PVEEGD motif in cAOS. Most likely the SSSAGE loop has distinct backbone conformation compared to the PVEEGD motif of cAOS. Therefore, the SSSAGE loop of cHPL was remodeled using a MODELLER tool [102], which led to a wider substrate entry site (Fig. 9A). The refined loop of the remodeled cHPL (cHPL-SSSAGE) with the best score was used in the docking simulations with 8R-HpETE. The 8R-HpETE substrate was located in the substrate channel of the cHPL-SSSAGE model in a catalytically productive conformation (Fig. 9B). This indicated that the differences in the substrate entry sites between cHPL and cAOS, especially the SSSAGE loop, might influence the reaction specificity and the substrate preference.

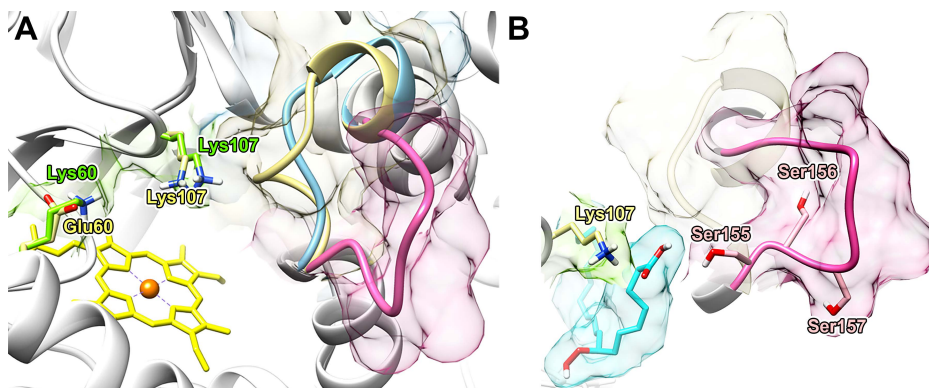


**Figure 9.** The refined model of cHPL. (A) The remodeled SSSAGE loop of cHPL (pink). The loops of cAOS and the initial model of cHPL are shown in blue and beige, respectively. The residues located in the substrate entry site of cAOS and cHPL are presented in beige and green, respectively. The heme is indicated in yellow. (B) The docking simulation of the cHPL-SSSAGE model with 8R-HpETE (cyan) (Publication III).

## 4.6 Residues involved in the reaction specificity of *C. imbricata* cHPL (II)

Based on the sequence and the structural analysis, the distinct residues of the substrate channel of wild-type (wt) cHPL were replaced with the corresponding residues in the wt cAOS sequence (Fig. 7A). Specifically, the R56G, P65A, LL108-109YP, F150L, YS176-177NL, Y176N, S177L, I357V and SSSAGE155-160PVVEEKG mutations of cHPL were prepared and analyzed. The kinetic parameters of the prepared mutants are presented in Table 3. The F150L, P65A and I357V mutations in the heme region and the ME59-60LK and SSSAGE155-160PVKEEG mutations in the substrate entry site lowered the  $k_{\text{cat}}$  value of cHPL. In contrast, YS176-177NL located at the bottom of the substrate channel and the R56G mutant in the substrate entry site increased the  $k_{\text{cat}}$  of cHPL.

**Table 3. The kinetic parameters of wt cHPL, wt cAOS, cHPL mutants and a cAOS mutant with 8R-HpETE.** The measurements were performed at an enzyme concentration of 5 nM. The kinetic parameters are presented with the corresponding standard error ( $n = 3$ ).

	Enzyme	$k_{\text{cat}}$ ( $\text{s}^{-1}$ )	$K_{\text{m}}$ ( $\mu\text{M}$ )	$k_{\text{cat}}/K_{\text{m}}$ ( $\text{s}^{-1}, \mu\text{M}^{-1}$ )
<i>C. imbricata</i> cHPL				
	<b>wild-type</b>	133.5 $\pm$ 5.0	4.0 $\pm$ 0.5	35.0 $\pm$ 5.0
Heme region	<b>F150L</b>	49.5 $\pm$ 1.5	2.0 $\pm$ 0.5	27.5 $\pm$ 6.0
	<b>P65A</b>	40.5 $\pm$ 2.5	15.5 $\pm$ 2.5	2.5 $\pm$ 0.5
	<b>I357V</b>	64.0 $\pm$ 3.0	5.0 $\pm$ 1.0	13.0 $\pm$ 2.5
	<b>R56G</b>	304.5 $\pm$ 23.0	19.0 $\pm$ 4.0	16.0 $\pm$ 3.5
Substrate channel	<b>YS176-177NL</b>	218.0 $\pm$ 14.0	4.0 $\pm$ 1.0	56.0 $\pm$ 13.5
	<b>ME59-60LK</b>	7.5 $\pm$ 0.5	7.5 $\pm$ 2.0	1.0 $\pm$ 0.5
	<b>SSSAGE155-160</b>	52.0 $\pm$ 3.5	2.0 $\pm$ 0.8	26.0 $\pm$ 10.5
	<b>PVKEEG fragment</b>			
<i>C. imbricata</i> cAOS				
	<b>wild-type</b>	1835.0 $\pm$ 196.5	46.5 $\pm$ 9.0	39.5 $\pm$ 8.5
Heme region	<b>L150F</b>	203.5 $\pm$ 8.0	6.5 $\pm$ 1.0	30.5 $\pm$ 4.5
<i>P. homomalla</i> cAOS*				
	<b>wild-type</b>	1409.0 $\pm$ 85.0	45.5 $\pm$ 7.5	31.0 $\pm$ 5.5

\* - values obtained from the article by Boutaud *et al.* [89].

Despite the fact that all of the mutants influenced the catalytic parameters of cHPL, only the F150L and YS176-177NL mutations resulted in a change of reaction specificity from cHPL to cAOS. The incubations with individual mutants, Y176N and S177L, revealed that only S177L was responsible for the altered catalysis (unpublished data). This is in correlation with the docking simulations of *P. homomalla* cAOS, which showed that only Phe150 and Ser177 interacted with the C6=C7 double bond and C16 of 8R-HpETE, respectively (Fig. 10A and 10B). The cHPL F150L mutant produced a mixture of cHPL and cAOS products (Fig. 10C, second panel), while the S177L substitution also gave rise to some additional products, epoxy alcohol and trihydroxy derivatives (Fig. 10C, third panel).

The inverse mutation of cAOS, L150F, was prepared to test the role of the Phe150 of cHPL in the cAOS sequence. Although the  $k_{\text{cat}}$  of cAOS L150F was about 10 times lower than wt cAOS, the reaction specificity remained unaltered.

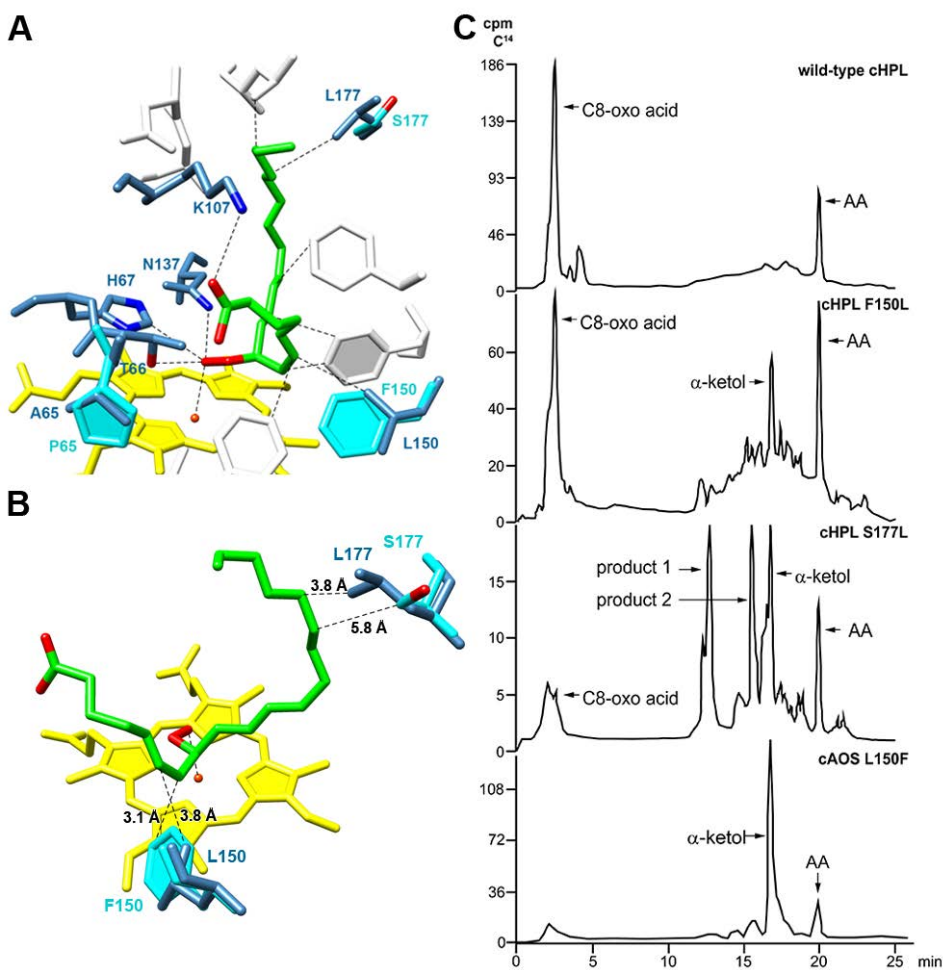


**Figure 10. The determinants of the reaction specificity of cHPL.** (A) The interaction between 8R-HpETE and the catalytically important amino acids and the residues in the substrate channel. The residues of cAOS and cHPL are presented in blue and cyan, respectively. The heme is shown in yellow. (B) The proximity between 8R-HpETE (green) and the residues influencing the reaction specificity of cHPL. The heme is presented in yellow. (C) The radiochromatograms of the products synthesized from [ $^{14}\text{C}$ ]-8R-HpETE by wt cHPL, its mutants and cAOS L150F. The cHPL F150L and S177L mutants gave rise to a mixture of cAOS and cHPL products (second and third panel). The product patterns of other cHPL mutants were identical to the products of wt cHPL (upper panel). The cAOS L150F mutation did not influence the reaction specificity of cAOS (lower panel) (Publication II).

#### 4.7 Determinants in the substrate binding of cHPL and cAOS (III)

The potential residues involved in the formation of a salt bridge (Fig. 8) with the negatively charged carboxy group of PUFA hydroperoxides were replaced with either a neutral amino acid, Met, or with a residue containing the opposite charge, Glu or Lys. Specifically, the K60M, K60E, K107M and K107E mutants of cAOS, and the E60M, E60K, K107M and K107E mutants of cHPL were prepared and analyzed. The kinetic parameters of each mutant determined with 8R-HpETE, 8R-HpEPE, 10R-HpDHE, 9R-Hp-ALA and 9R-Hp-GLA are presented in Table 4. In addition, the double mutation of cAOS,

K60M-K107M, was prepared to exclude the compensation of the loss of positive charge by either K60 or K107.

The K60M, K60E and K107M mutations did not influence the kinetic parameters of cAOS which indicates that Lys60 and Lys107 were not involved in the salt bridge formation and therefore, these residues are not necessary for the productive binding of 8*R*-HpETE. This result was in correlation with the K60M-K107M mutation, which had the same kinetic properties as determined for the individual mutants. The reduction of the kinetic parameters of cAOS by the K107E mutation can be explained by the altered structural conformation and/or the electrostatic interactions between the adjacent residues and the carboxy group of the 8*R*-HpETE substrate. However, the differences in the results between K107M and K107E indicate that the positive charge of Glu107 might influence the structural integrity and the electrostatic properties of the substrate entry site of cAOS. Yet, the K107M mutation illustrates that the loss of positive charge does not influence the substrate binding of the substrate.

The significantly lower  $k_{\text{cat}}$  and  $K_m$  values of cHPL due to the Glu60 mutations demonstrated that the Glu60 of cHPL is necessary for the productive binding of a substrate, even though the negative charge of Glu60 excludes the salt bridge formation with the carboxy group of 8*R*-HpETE. This notion is in correlation with the ME59-60LK mutation which similarly to the E60M mutation, attenuated the kinetic parameters of cHPL (Tables 3 and 4). In addition, the increased turnover rate of cHPL with replaced Lys107 demonstrated that the positively charged Lys107 is not necessary and even interrupts the electrostatic interactions with the PUFA hydroperoxides. However, as the Glu60 and Lys107 mutations influenced the kinetic parameters drastically, the interactions between the substrate entry site and 8*R*-HpETE are presumably more complex than expected.

The reaction specificity of cAOS or cHPL with the C18, C20 and a C22 PUFA hydroperoxides remained unaltered. Specifically, cAOS catalyzed the formation of corresponding  $\alpha$ -ketols from all of the different substrates, while cHPL gave rise to respective oxo-acids.

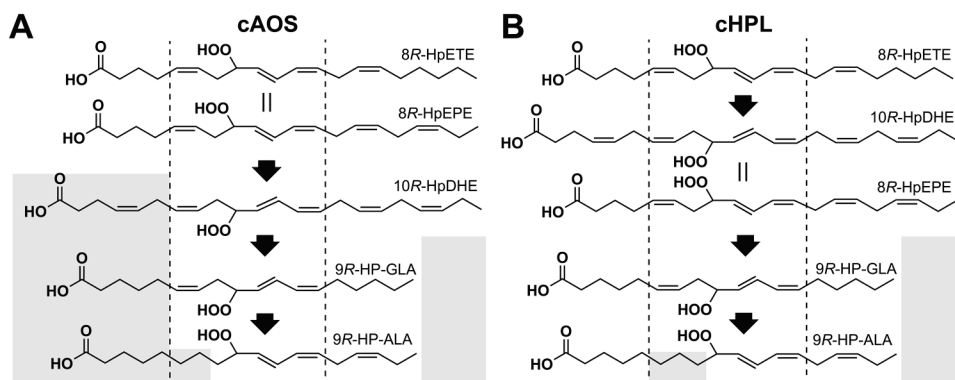


**Table 4. The kinetic parameters of wt cAOS, wt cHPL and mutants determined with PUFA hydroperoxides. The kinetic parameters are presented with the corresponding standard error ( $n = 3$ ). The catalytic efficiency ( $E_{cat}$ ) was obtained from the ratio of  $k_{cat}/K_m$  ( $s^{-1} \mu M^{-1}$ ). The measurements were performed at an enzyme concentration of 10 nM.**

Substrate		cAOS				
		wild-type	K60M	K60E	K107M	K107E
8R-HpETE	$k_{cat}$ ( $s^{-1}$ )	2360 ± 230	2580 ± 340	2670 ± 230	2400 ± 160	1080 ± 110
	$K_m$ ( $\mu M$ )	50 ± 10	50 ± 10	50 ± 10	50 ± 5	30 ± 5
	$k_{cat}/K_m$	50 ± 10	50 ± 15	50 ± 10	50 ± 5	35 ± 10
8R-HpEPE	$k_{cat}$ ( $s^{-1}$ )	2370 ± 230	2950 ± 730	2450 ± 390	2460 ± 180	1260 ± 100
	$K_m$ ( $\mu M$ )	40 ± 10	60 ± 20	70 ± 20	50 ± 5	25 ± 5
	$k_{cat}/K_m$	55 ± 10	50 ± 20	40 ± 10	55 ± 10	50 ± 10
10R-HpDHE	$k_{cat}$ ( $s^{-1}$ )	1400 ± 170	1100 ± 140	1040 ± 180	2800 ± 370	1030 ± 140
	$K_m$ ( $\mu M$ )	35 ± 10	20 ± 5	30 ± 10	50 ± 10	30 ± 10
	$k_{cat}/K_m$	40 ± 10	50 ± 15	40 ± 15	60 ± 15	40 ± 15
9R-Hp-ALA	$k_{cat}$ ( $s^{-1}$ )	1370 ± 130	2050 ± 510	1080 ± 120	1780 ± 280	700 ± 70
	$K_m$ ( $\mu M$ )	80 ± 10	90 ± 35	50 ± 10	80 ± 20	30 ± 5
	$k_{cat}/K_m$	15 ± 2	25 ± 10	20 ± 5	25 ± 5	25 ± 5
9R-Hp-GLA	$k_{cat}$ ( $s^{-1}$ )	1710 ± 200	1630 ± 340	1550 ± 160	2650 ± 290	1220 ± 100
	$K_m$ ( $\mu M$ )	75 ± 15	75 ± 30	90 ± 20	125 ± 20	60 ± 1
	$k_{cat}/K_m$	25 ± 6	20 ± 10	15 ± 5	20 ± 5	20 ± 5
Substrate		cHPL				
		wild-type	E60M	E60K	K107M	K107E
8R-HpETE	$k_{cat}$ ( $s^{-1}$ )	170 ± 10	90 ± 10	20 ± 1	580 ± 60	390 ± 30
	$K_m$ ( $\mu M$ )	12.0 ± 1.5	4.5 ± 1.5	1.5 ± 0.2	38.0 ± 6.5	12.5 ± 2.0
	$k_{cat}/K_m$	15 ± 2	20 ± 5	15 ± 2	15 ± 5	30 ± 5
8R-HpEPE	$k_{cat}$ ( $s^{-1}$ )	420 ± 30	200 ± 10	160 ± 20	720 ± 60	460 ± 30
	$K_m$ ( $\mu M$ )	50 ± 5	20 ± 2	40 ± 10	70 ± 10	20 ± 5
	$k_{cat}/K_m$	10 ± 1	10 ± 1	5 ± 1	10 ± 2	25 ± 5
10R-HpDHE	$k_{cat}$ ( $s^{-1}$ )	700 ± 70	300 ± 30	55 ± 2	1290 ± 220	620 ± 50
	$K_m$ ( $\mu M$ )	60 ± 10	30 ± 5	5 ± 1	90 ± 20	15 ± 5
	$k_{cat}/K_m$	10 ± 2	10 ± 2	10 ± 2	15 ± 5	40 ± 15
9R-Hp-ALA	$k_{cat}$ ( $s^{-1}$ )	340 ± 25	110 ± 10	80 ± 15	700 ± 180	490 ± 90
	$K_m$ ( $\mu M$ )	60 ± 10	25 ± 5	50 ± 15	140 ± 50	80 ± 20
	$k_{cat}/K_m$	5 ± 1	5 ± 1	2 ± 1	5 ± 2	5 ± 2
9R-Hp-GLA	$k_{cat}$ ( $s^{-1}$ )	550 ± 50	220 ± 15	70 ± 5	620 ± 90	460 ± 40
	$K_m$ ( $\mu M$ )	80 ± 15	60 ± 10	30 ± 5	80 ± 20	60 ± 10
	$k_{cat}/K_m$	6.5 ± 1.0	4.0 ± 0.5	2.0 ± 0.5	8.0 ± 2.5	8.5 ± 2.0

## 4.8 Substrate preferences of coral cHPL and cAOS (III)

The substrate preferences of *P. homomalla* cAOS and *C. imbricata* cHPL were determined based on the catalytic efficiencies obtained with 8*R*-HpETE, 8*R*-HpEPE, 10*R*-HpDHE, 9*R*-Hp-ALA and 9*R*-Hp-GLA (Table 4) [103]. The substrate preferences of *P. homomalla* cAOS from best to worst were determined as follows: 8*R*-HpETE > 8*R*-HpEPE > 10*R*-HpDHE > 9*R*-Hp-GLA > 9*R*-Hp-ALA (Scheme 7A). In parallel, the substrate preference of *C. imbricata* cHPL are presented as follows: 8*R*-HpETE = 8*R*-HpEPE > 10*R*-HpDHE > 9*R*-Hp-GLA > 9*R*-Hp-ALA (Scheme 7B). Even though the most preferred substrate of cAOS and cHPL was 8*R*-HpETE, the substrate selectivities with 8*R*-HpEPE and 10*R*-HpDHE were notably different. The 8*R*-HpEPE substrate was almost as good as 8*R*-HpETE, while 10*R*-HpDHE as a C22 fatty acid was metabolized with lower efficiency by cAOS. In contrast, as 8*R*-HpETE was the best substrate for cHPL, 8*R*-HpEPE and 10*R*-HpDHE were metabolized with similar efficiency. The much lower efficiency of cAOS and cHPL with 9*R*-Hp-ALA and 9*R*-Hp-GLA indicated that C18 fatty acid substrates was not preferred. However, the higher  $k_{cat}$  value with 9*R*-Hp-GLA was in correlation with the successful docking simulations only with 9*R*-Hp-GLA, suggesting that cHPL and cAOS prefer substrates with the C5=C6 double bond adjacent to the hydroperoxy group (Scheme 7).



**Scheme 7. The substrate preferences of cAOS (A) and cHPL (B) determined with PUFA hydroperoxides.** The substrate preferences starting with the best substrate are presented from top to bottom. The motifs possibly reducing the catalytic efficiency are indicated in gray. Similar catalytic efficiencies obtained with different PUFA hydroperoxides are indicated by the equal sign (Publication III).

The ability to metabolize neutral derivatives of PUFA hydroperoxides were tested with methylated 8*R*-HpETE (Met-8*R*-HpETE), Met-10*R*-HpDHE, 8*R*-Hp-AEA and 8*R*-Hp-1-AG (Fig. 11). In contrast to cAOS, only cHPL catalyzed the conversion of Met-8*R*-HpETE and Met-10*R*-HpDHE (Fig. 11B). In addition, the turnover rate of cHPL with 8*R*-Hp-1-AG and 8*R*-Hp-AEA was about four times higher than cAOS (Figs. 11C and 11D), while the turnover rate of cAOS with 8*R*-HpETE was 10 times higher compared to the value of cHPL (Fig. 11A). The capability of cHPL to metabolize endocannabinoid derivatives and 10*R*-HpDHE as C22 PUFA indicates the structural differences between the substrate entry sites of cAOS and cHPL.

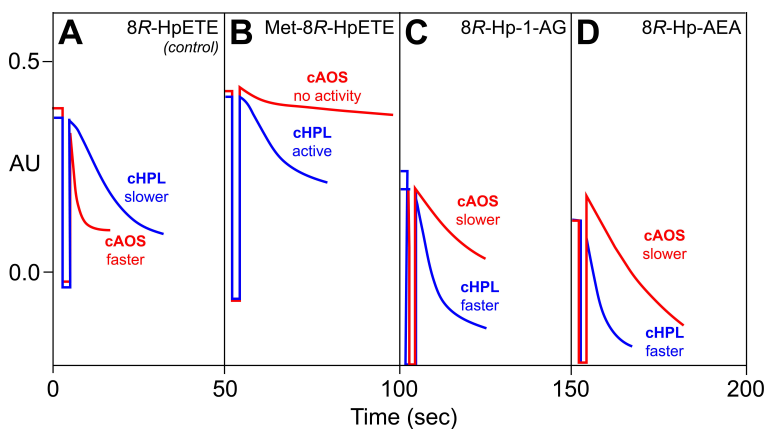


**Figure 11. The incubations of cAOS and cHPL with alternative substrates.** (A) The control reactions of cAOS and cHPL with free 8R-HpETE. (B) Activities with Met-8R-HpETE which were in correlation with the incubations with Met-10R-HpDHE (not shown). (C and D) The incubations with 8R-Hp-1-AG (C) and 8R-HpE-AEA (D), respectively. The loss of the conjugated diene of PUFA hydrpoperoxides at 235 nm was observed spectrophotometrically (Publication III).

The Met-8R-HpETE, 8R-Hp-1AG and 8R-Hp-AEA substrates were metabolized by cAOS and cHPL according to the reaction mechanism obtained with 8R-HpETE. This indicated that different head groups of the arachidonate derivatives do not influence the catalyzed reaction of cAOS or cHPL.

## 5 DISCUSSION

In the current study, the catalytic activity of the first animal HPL was determined. In addition, the structural and functional aspects between highly identical cHPL and cAOS were examined. The structural determinants of cHPL and cAOS necessary for the distinct reaction specificities and substrate binding will be discussed.

### *The independence of the individual domains of cHPL-LOX*

In order to study the isolated cHPL domain, the individual N-terminal domain of cHPL-LOX was expressed as an active protein. This correlates with the studies of functionally independent *P. homomalla* cAOS and 8R-LOX [89]. *In vivo*, the linkage between 8R-LOX and cHPL or cAOS is probably necessary to assure membrane targeting and the proximity of two domains [86, 90]. In plants, the regulatory aspects of LOX-dependent pathways are different due to the distinct localizations of 9S-LOX, 13S-LOX, AOS and HPL [59]. As the expression of plant LOX, AOS and AOC are all controlled by the transcription factor Col1, an artificial LOX-AOS-AOC complex was generated to study their possible co-occurrence and co-operativity in the inner envelope of chloroplasts [104]. In addition to coral cAOS-LOX and cHPL-LOX, several fungal fusion proteins with dioxygenase(DOX)-LDS, DOX-AOS or DOX-EAS activities have been identified [105].

### *Characterization of the reaction mechanism catalyzed by cHPL*

Although the active site, catalytically important residues and overall structure between coral cAOS and cHPL are conserved, cAOS and cHPL convert 8R-HpETE into different products.

The steps in the reaction catalyzed by cHPL correspond to the mechanism of plant HPL [99]. The reaction is initiated by the cleavage of the hydroperoxy group followed by sequential steps until the formation of short-chain aldehydes (Fig. 6B). Instead of the formation of the C9=C10 double bond as described in the cAOS reaction, cHPL catalyzes the breakage of the C8-C9 bond of the epoxy group (Fig. 12) and the subsequent formation of hemiacetal intermediate [106]. Currently, it is not known which factors are involved in the epoxy ring opening by cHPL. Two possible options can be proposed: a) the hydrogen at C8 is abstracted by the His67 of cHPL or by the Compound II ( $\text{Fe}^{4+}\text{-OH}$ ), or b) the epoxy ring opening occurs spontaneously due to the instability of the epoxy allylic radical. However, it should be emphasized that, compared to epoxy alcohol synthases, the radical at C10 of cAOS and cHPL is protected from the rebound of the hydroxy group of Compound II or the incorporation of molecular oxygen. Therefore, all of the intramolecular rearrangements by cAOS and cHPL occur only near C8 or C9 of the epoxy ring.

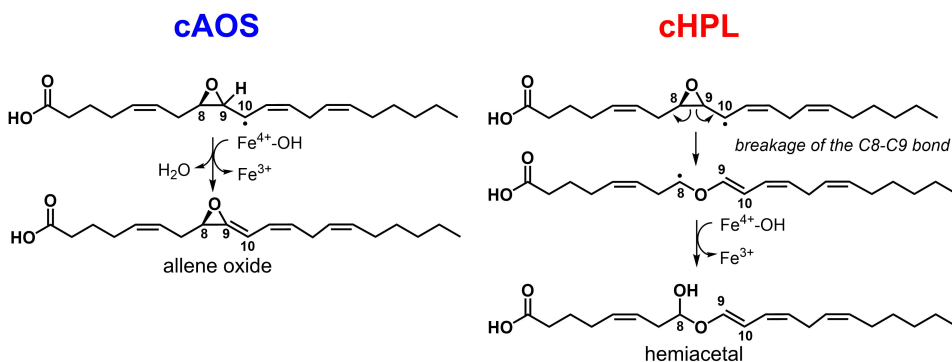


**Figure 12.** The distinct conversion of the epoxy allylic radical intermediate by cAOS (left) and cHPL (right). The hydrogen at C9 of an epoxy allylic radical is abstracted by cAOS, resulting in the formation of an allene oxide. In contrast, cHPL catalyzes the epoxy ring opening of the epoxy allylic radical instead of the hydrogen abstraction at C9 (Publication II).

The lyase-type activity can either induce “homolytic” cleavage, also known as  $\alpha$ -scission, or “heterolytic” as the  $\beta$ -scission of carbon-carbon bonds of fatty acid hydroperoxides [68]. Coral cHPL and plant HPL both catalyze the “heterolytic” cleavage of a fatty acid hydroperoxide. Specifically, cHPL catalyzes the cleavage of the C8-C9 bond between the hydroperoxy group and the C9=C10 double bond of 8*R*-HpETE, which results in the formation of C8-oxo acid and C12-aldehyde. The “homolytic” cleavage of 8*R*-HpETE takes place between the C7-C8 bond and this type of lyase-like activity has been reported in sea urchins [107], by LOXs in anaerobic conditions [108] and by non-enzymatic reactions with free heme [109].

The reaction mechanism of plant HPL has been presented either with [110] or without [99] the involvement of water. Although both mechanisms are valid on paper, the latter mechanism was confirmed with the isolation of hemiacetal intermediate containing both oxygens from the hydroperoxy group of a fatty acid substrate [99]. This result was supported by our study with the <sup>18</sup>O-labeled water showing that the oxygens of 8*R*-HpETE are retained in the oxo groups of C8-oxo acid and C12 aldehyde.

Coral cHPL catalyzes the reaction at a turnover rate about 10 times lower than cAOS and plant HPL [69, 111, 112]. The lower reaction efficiency of cHPL with 8*R*-HpETE compared to the value of cAOS is explained by the much lower  $K_m$  value in relation to the  $k_{cat}$  value of cHPL (Table 4). The lower  $K_m$  value of cHPL indicates that the interaction between the enzyme and the substrate is stronger. Even though cAOS and cHPL compete for the same substrate *in vivo*, the catalytic efficiency of LOX domains and the activity of lipases are the rate limiting steps prior to the reaction by cAOS or cHPL. Furthermore, the cellular locations and the regulatory aspects of cAOS-LOX and cHPL-LOX are not known.

#### *Determinants in the reaction mechanism of cHPL*

The residues involved in the reaction mechanism of cHPL, Phe150 and Ser177, were shown to be the interacting residues of the 8*R*-HpETE substrate by *in vitro* and *in silico* approaches. Most likely, the Phe150 of cHPL directs the substrate in a position necessary for the epoxy ring opening and the Leu177 of cHPL is involved in the coordinating of the aliphatic tail of the substrate. The mutations in these residues, F150L and S177L,

influenced the interactions with the substrate or intermediates resulting in the formation of cAOS products. Clearly, the properties of wt residues were necessary to catalyze only the cHPL-specific reaction and the F150L and S177L mutations restructured the substrate channel more similar to cAOS.

The inability of cAOS L150F to alter the reaction mechanism is in correlation with the results obtained with the Cyp74 enzymes. The opposite mutations in the residues of AOS which initially resulted in the conversion of AOS activity to HPL were not effective on the shift from HPL to AOS [65, 113]. This phenomenon can be explained by structural properties of the substrate channels of AOS and HPL. Most likely, the catalytic center of coral cHPL is more sensitive to single mutations than cAOS due to the distinct substrate positioning. The L150F mutation of cAOS did not influence substrate placement in the active site, probably due to the shape of the substrate entry site and/or the substrate channel. The most notable structural features that might be involved in directing the substrates are the PVEEGD and SSSAGE loops in the substrate entry sites of cAOS and cHPL, respectively. However, the SSSAGE-PVEEGD substitution did not result in the altered reaction specificity of cHPL. It can be speculated that cHPL arose from cAOS during the evolution of catalase-related enzymes due to gene duplication and modification. This is also explained by the inefficient conversion of cAOS to cHPL. However, as only the F150L mutation of cAOS was prepared during this study, the effects of single mutations on the cAOS-specific residues in the active site remain elusive.

#### *Structural characteristics of the substrate binding by cAOS and cHPL*

The substrate is bound to the U- or L-shaped channel of coral cAOS with its carboxy head located in the substrate entry site and the hydroperoxy group near the catalytically important residues (Figs. 7 and 8). Most of the fatty acid-binding enzymes interact with PUFA substrates in a similar fashion [42, 88, 115]. Two common criteria in the binding of PUFA substrates by fatty acid-binding proteins are as follows: (1) the electrostatic interactions between the carboxy group of a fatty acid and the polar residues of a protein, and (2) the hydrophobic interactions between the aliphatic tail of a fatty acid and the non-polar substrate pocket of a protein. Studies on the fatty acid binding enzymes, albumin [116] and lipid transfer proteins [117], have demonstrated that substrate binding is ensured mainly by hydrophobic interactions. In addition, COX-2 tolerates the lack of a carboxy group of substrates or substrate analogs [115, 118, 119]. In contrast, COX-1 [120] and coral 8R-LOX The substrate is bound to the U- or L-shaped channel of coral cAOS with its carboxy head located in the substrate entry site and the hydroperoxy group near the catalytically important residues (Figs. 8 and 9). Most of the fatty acid-binding enzymes interact with PUFA substrates in a similar fashion [42, 88, 114]. Two common criteria in the binding of PUFA substrates by fatty acid-binding proteins are as follows: (1) the electrostatic interactions between the carboxy group of a fatty acid and the polar residues of a protein, and (2) the hydrophobic interactions between the aliphatic tail of a fatty acid and the non-polar substrate pocket of a protein. Studies on the fatty acid binding enzymes, albumin [115] and lipid transfer proteins [116], have demonstrated that substrate binding is ensured mainly by hydrophobic interactions. In addition, COX-2 tolerates the lack of a carboxy group of substrates or substrate analogs [114, 117, 118]. In contrast, COX-1 [119] and coral 8R-LOX [88] cannot bind substrates without the involvement of positively charged Arg in their substrate entry sites.

Substrate preferences of PUFA-metabolizing enzymes are determined by the structural characteristics of the substrate channel. The length, the number of double bonds, the positioning and the stereoconfiguration of functional groups of PUFA substrates all together need to match with the properties of the substrate channel for productive binding and efficient catalysis. For example, the substrate selectivity of COX-1 and COX-2 differ mainly due to the wider channel opening of COX-2 [118]. Despite the differences in the substrate preference, COX-1 and COX-2 catalyze the same reaction and both prefer free AA as the substrate [120]. In contrast, highly homologous cAOS and cHPL catalyze different reactions and their substrate preferences are similar but not identical. Similar to COX isozymes [120], the reaction mechanism of cAOS and cHPL is preserved with substrates with different head groups. Therefore, even though cAOS and cHPL can bind alternative substrates, their catalytic center is well stabilized. To give an example of the opposite, *M. truncatula* HPL has EAS activity with 9S-HpODE and HPL activity with 13S-HpODE [57]. However, the reaction specificities remained unaltered with either ALA- or LA-derived hydroperoxides, suggesting that only the location of the hydroperoxy group was necessary for distinct reactions (Table 2). Coral cAOS and cHPL prefer only substrates with the hydroperoxy group located at the  $\omega$ 12 position from the methyl terminus, e.g. 8R-HpETE and 10R-HpDHE.

In the current thesis, the substrate preferences were determined based on the catalytic efficiency, which takes into account the  $k_{\text{cat}}$  and  $K_{\text{m}}$  values. This sort of specificity constant is used to determine the influence of different substrates or substrate analogs on the catalytic rate of an enzyme [103]. The catalytic efficiency has been misused in comparing the reactivity of different enzymes, e.g. mutants, on the same substrate [103, 121]. Therefore, the comparison between the reaction efficiencies of wt cAOS, wt cHPL and mutants determined with the same substrate might be misleading. Specifically, in the evaluation of the kinetic properties of cAOS mutants in relation to wt cAOS, the  $k_{\text{cat}}$  and  $K_{\text{m}}$  values need to be analyzed separately. For instance, even though the catalytic efficiencies between wt cAOS and mutants with 8R-HpEPE are similar (Table 4), the cAOS K107E mutant has about half the  $k_{\text{cat}}$  value. In addition, the catalytic efficiency of cHPL K107E with 10R-HpETE was the highest but the  $k_{\text{cat}}$  was comparable with the corresponding value of wt cHPL. This indicated that the catalytic efficiency of cHPL K107E was determined mainly by the  $K_{\text{m}}$  value.

Based on the analysis of protein-ligand interactions in the Protein Databank, the salt bridge interactions between a positively charged residue from a protein and a negatively charged oxygen from a ligand were two times higher than the opposite (approximately 5000 vs 2500) [123]. As mentioned earlier, PUFA dioxygenases such as LOX and COX contain mostly positively charged Arg in their substrate entry sites, whereas coral cAOS and cHPL have the positively charged Lys in the entrance of the substrate channel. When we compare the properties of Arg and Lys, the ionic interaction by the larger guanidinium group of Arg is stronger than by the smaller ammonium group of Lys. The potency of an ionic interaction by Arg or Lys is influenced by its neighboring residues and also by whether the salt bridge is buried or solvent-exposed [124]. Therefore, the existence of Lys in the substrate entry site might not necessarily denote that formed contacts are weaker. For example, Lys234 of bacterial enzyme  $\beta$ -lactamase is particularly obligatory for the catalysis of penicillin derivatives with the C3 carboxy group [125, 126]. The increase of the  $k_{\text{cat}}$  value of a CYP450, FA hydroxylase, with short chain FAs was achieved as a result of Leu187 replacement in the substrate channel with Lys and not with Arg [127]. Despite the fact that the Lys60 and Lys107 of coral cAOS are located in

the substrate entry site, the *in vitro* measurements demonstrated that these lysines are not essential for the productive binding of substrates. For instance, an NMR study of a liver fatty acid binding protein (FABP) revealed the electrostatic interactions between two oleates and corresponding binding sites [128]. However, mutational analysis demonstrated that the electrostatic interaction occurs only in one binding pocket. Therefore, even though the structural data confirmed the electrostatic interactions by wt protein, an alternative substrate accommodation was necessary to bind the second oleate. In regard to the coral cAOS, the interactions between the carboxy group of a fatty acid substrate and the Lys107 seem to be too weak or the substrate is bound in an alternative way. Based on the analysis of protein-ligand interactions in the Protein Databank, the salt bridge interactions between a positively charged residue from a protein and a negatively charged oxygen from a ligand were two times higher than the opposite (approximately 5000 vs 2500) [122]. As mentioned earlier, PUFA dioxygenases such as LOX and COX contain mostly positively charged Arg in their substrate entry sites, whereas coral cAOS and cHPL have the positively charged Lys in the entrance of the substrate channel. When we compare the properties of Arg and Lys, the ionic interaction by the larger guanidinium group of Arg is stronger than by the smaller ammonium group of Lys. The potency of an ionic interaction by Arg or Lys is influenced by its neighboring residues and also by whether the salt bridge is buried or solvent-exposed [123]. Therefore, the existence of Lys in the substrate entry site might not necessarily denote that formed contacts are weaker. For example, Lys234 of bacterial enzyme  $\beta$ -lactamase is particularly obligatory for the catalysis of penicillin derivatives with the C3 carboxy group [124, 125]. The increase of the  $k_{cat}$  value of a cytochrome P450 enzyme, FA hydroxylase, with short chain FAs was achieved as a result of Leu187 replacement in the substrate channel with Lys and not with Arg [126]. Despite the fact that the Lys60 and Lys107 of coral cAOS are located in the substrate entry site, the *in vitro* measurements demonstrated that these lysines are not essential for the productive binding of substrates. For instance, an NMR study of a liver fatty acid binding protein (FABP) revealed the electrostatic interactions between two oleates and corresponding binding sites [127]. However, mutational analysis demonstrated that the electrostatic interaction occurs only in one binding pocket. Therefore, even though the structural data confirmed the electrostatic interactions by wild-type protein, an alternative substrate accommodation was necessary to bind the second oleate. In regard to the coral cAOS, the interactions between the carboxy group of a fatty acid substrate and the Lys107 seem to be too weak or the substrate is bound in an alternative way.



### *Biological role of cHPL*

In corals, the biological role of cHPL-LOX is not clear, as mechanical and thermal stress do not induce the gene expression and activity of cHPL-LOX [80, 85]. In plants, short chain aldehydes are synthesized in response to abiotic and biotic stress [110]. Similarly, cHPL-LOX could be involved in the biotic defense via antimicrobial activity of aldehydes [74, 128, 129] or it could play a housekeeping role. In addition, the initial stress response, which happens in seconds or minutes, has not been analyzed in corals.

The most abundant PUFA in soft corals, including *P. homomalla* and *C. imbricata*, is AA. The amounts of EPA and DHA are significantly lower than AA, but their availability and the biological role in corals have not been investigated. Studies determining total lipid content of corals usually present their results without differentiating membrane-bound and free PUFAs, and therefore it is difficult to conclude about the availability of free PUFA substrates [130–132]. Moreover, the release of PUFAs from membranes is highly dependent on lipases. Although cAOS-LOX and cHPL-LOX are not membrane-dependent *in vitro*, the possibility of metabolizing membrane-bound substrates by these fusion proteins *in vivo* remains elusive. Although AA is most abundant in *C. imbricata*, cAOS and cHPL might catalyze the conversion of alternative PUFA hydroperoxides as well. The ability of cHPL to metabolize different PUFA hydroperoxides, including endocannabinoid derivatives, indicates that cHPL might contribute to the wider product pool. Currently, an endocannabinoid system of *Cnidaria* has been identified only in *Hydra* species [133].

## CONCLUSIONS

In the current thesis, the mechanistic aspects of the first animal HPL were described. In addition, the structural and functional characteristics between highly identical cHPL and cAOS were studied.

The main conclusions are presented as follows:

- *C. imbricata* cHPL catalyzes the formation of hemiacetal intermediate from 8*R*-HpETE. The hemiacetal breaks down into two fragments, C8-oxo acid and C12 aldehyde. The oxygens from the hydroperoxy group of 8*R*-HpETE are retained in the aldehydic fragments. Formed (*Z*)-aldehydes isomerize non-enzymatically to (*E*)-aldehydes. The latter contain highly reactive  $\alpha,\beta$ -unsaturated carbonyl moiety.
- Despite the high sequence identity and the conserved active sites between cHPL and cAOS, their reaction specificities differ. Two residues, Phe150 and Leu177, are responsible for the cHPL-specific activity, as replacements with the corresponding residues of cAOS result in a shift of activity from cHPL to cAOS.
- The main differences in the substrate entry sites between cHPL and cAOS are the SSSAGE loop of cHPL and the corresponding motif of cAOS, PVEEGD, respectively. These motifs do not influence the reaction specificity but most likely contribute to the distinct kinetic properties and the substrate preferences of cAOS and cHPL.
- The docking simulations demonstrated the electrostatic interactions between positively charged Lys60 and Lys107 of cAOS and the negatively charged carboxy group of fatty acid hydroperoxides. However, this was not confirmed by the mutational analysis. In contrast to cAOS, the substitutions in corresponding residues of cHPL, Glu60 and Lys107, resulted in altered kinetic parameters. As the Glu60 and Lys107 mutations had opposite effects on the turnover rates, the interactions between the substrate entry site of cHPL and a substrate are more complex than expected.
- The substrate preferences of cAOS from best to worst were determined as follows: 8*R*-HpETE = 8*R*-HpEPE > 10*R*-HpDHE > 9*R*-Hp-GLA > 9*R*-Hp-ALA. In parallel, the preferred substrates of cHPL were: 8*R*-HpETE > 10*R*-HpDHE = 8*R*-HpEPE, 9*R*-Hp-GLA > 9*R*-Hp-ALA.
- In contrast to cAOS, cHPL metabolized 8*R*-hydroperoxy endocannabinoid derivatives with larger head groups and also methylated substrates more efficiently, indicating differences in the opening of the substrate channels between cAOS and cHPL.

## REFERENCES

- [1] A. Mosblech, I. Feussner, I. Heilmann, Oxylipins: Structurally diverse metabolites from fatty acid oxidation, *Plant Physiol. Biochem.*, 47 (2009) 511–517.
- [2] A. Andreou, F. Brodhun, I. Feussner, Biosynthesis of oxylipins in non-mammals, *Prog. Lipid Res.*, 48 (2009) 148–170.
- [3] G. Griffiths, Biosynthesis and analysis of plant oxylipins, *Free Radic. Res.*, 49 (2015) 565–582.
- [4] A.R. Brash, Mechanistic aspects of CYP74 allene oxide synthases and related cytochrome P450 enzymes, *Phytochemistry*, 70 (2009) 1522–1531.
- [5] E.A. Dennis, P.C. Norris, Eicosanoid storm in infection and inflammation, *Nat. Rev. Immunol.*, 15 (2015) 511–523.
- [6] C.N. Serhan, B.D. Levy, Resolvins in inflammation: Emergence of the pro-resolving superfamily of mediators, *J. Clin. Invest.*, 128 (2018) 2657–2669.
- [7] C.N. Serhan, J. Dallil, R.A. Colas, J.W. Winkler, N. Chiang, Protectins and maresins: New pro-resolving families of mediators in acute inflammation and resolution bioactive metabolome, *Biochim. Biophys. Acta - Mol. Cell Biol. Lipids*, 1851 (2015) 397–413.
- [8] J.W. Newman, C. Morisseau, B.D. Hammock, Epoxide hydrolases: Their roles and interactions with lipid metabolism, *Prog. Lipid Res.*, 44 (2005) 1–51.
- [9] A. Liavonchanka, I. Feussner, Lipoxygenases: Occurrence, functions and catalysis, *J. Plant Physiol.*, 163 (2006) 348–357.
- [10] M. Hamberg, I.P. De Leon, M.J. Rodriguez, C. Castresana,  $\alpha$ -Dioxygenases, *Biochem. Biophys. Res. Commun.*, 338 (2005) 169–174.
- [11] A. Banaś, I. Johansson, S. Stymne, Plant microsomal phospholipases exhibit preference for phosphatidylcholine with oxygenated acyl groups, *Plant Sci.*, 84 (1992) 137–144.
- [12] M.X. Andersson, M. Hamberg, O. Kourtchenko, Å. Brunnström, K.L. McPhail, W.H. Gerwick, C. Göbel, I. Feussner, M. Ellerström, Oxylipin profiling of the hypersensitive response in *Arabidopsis thaliana*: Formation of a novel oxo-phytodienoic acid-containing galactolipid, arabidopside E, *J. Biol. Chem.*, 281 (2006) 31528–31537.
- [13] M. Stumpe, J. Bode, C. Göbel, T. Wichard, A. Schaaf, W. Frank, M. Frank, R. Reski, G. Pohnert, I. Feussner, Biosynthesis of C9-aldehydes in the moss *Physcomitrella patens*, *Biochim. Biophys. Acta - Mol. Cell Biol. Lipids*, 1761 (2006) 301–312.
- [14] J. Scholz, F. Brodhun, E. Hornung, C. Herrfurth, M. Stumpe, A.K. Beike, B. Faltin, W. Frank, R. Reski, I. Feussner, Biosynthesis of allene oxides in *Physcomitrella patens*, *BMC Plant Biol.*, 12 (2012).
- [15] A. Wennman, E.H. Oliw, S. Karkehabadi, Y. Chen, Crystal structure of manganese lipoxygenase of the rice blast fungus *Magnaporthe oryzae*, *J. Biol. Chem.*, 291 (2016) 8130–8139.

- [16] U. Garscha, E.H. Oliw, Critical amino acids for the 8(R)-dioxygenase activity of linoleate diol synthase A comparison with cyclooxygenases, *FEBS Lett.*, 582 (2008) 3547–3551.
- [17] E.H. Oliw, M. Hamberg, Biosynthesis of Jasmonates from Linoleic Acid by the Fungus *Fusarium oxysporum* Evidence for a Novel Allene Oxide Cyclase, *Lipids*, 54 (2019) 543–556.
- [18] I. Hoffmann, F. Jernerén, E.H. Oliw, Expression of fusion proteins of *Aspergillus terreus* reveals a novel allene oxide synthase, *J. Biol. Chem.*, 288 (2013) 11459–11469.
- [19] E.H. Oliw, Biosynthesis of Oxylipins by *Rhizoctonia solani* with Allene Oxide and Oleate 8S,9S-Diol Synthase Activities, *Lipids*, 53 (2018) 527–537.
- [20] I. Prost, S. Dhondt, G. Rothe, J. Vicente, M.J. Rodriguez, N. Kift, F. Carbonne, G. Griffiths, M.T. Esquerré-Tugayé, S. Rosahl, C. Castresana, M. Hamberg, J. Fournier, Evaluation of the antimicrobial activities of plant oxylipins supports their involvement in defense against pathogens, *Plant Physiol.*, 139 (2005) 1902–1913.
- [21] J. Newie, A. Andreou, P. Neumann, O. Einsle, I. Feussner, R. Ficner, Crystal structure of a lipoxygenase from *Cyanotheca* sp may reveal novel features for substrate acquisition, *J. Lipid Res.*, 57 (2016) 276–286.
- [22] A.R. Brash, N.P. Niraula, W.E. Boeglin, Z. Mashhadi, An ancient relative of cyclooxygenase in cyanobacteria is a linoleate 10S-dioxygenase that works in tandem with a catalase-related protein with specific 10S-hydroperoxide lyase activity, *J. Biol. Chem.*, 289 (2014) 13101–13111.
- [23] C. Schneider, D.A. Pratt, N.A. Porter, A.R. Brash, Control of Oxygenation in Lipoxygenase and Cyclooxygenase Catalysis, *Chem. Biol.*, 14 (2007) 473–488.
- [24] I. Ivanov, D. Heydeck, K. Hofheinz, J. Roffeis, V.B. O’Donnell, H. Kuhn, M. Walther, Molecular enzymology of lipoxygenases, *Arch. Biochem. Biophys.*, 503 (2010) 161–174.
- [25] R. Koljak, O. Boutaud, B.H. Shieh, N. Samel, A.R. Brash, Identification of a naturally occurring peroxidase-lipoxygenase fusion protein, *Science* (80- ), 277 (1997) 1994–1996.
- [26] H. Kuhn, M. Walther, R.J. Kuban, Mammalian arachidonate 15-lipoxygenases: Structure, function, and biological implications, *Prostaglandins Other Lipid Mediat.*, 68–69 (2002) 263–290.
- [27] M. Mortimer, R. Järving, A.R. Brash, N. Samel, I. Järving, Identification and characterization of an arachidonate 11R-lipoxygenase, *Arch. Biochem. Biophys.*, 445 (2006) 147–155.
- [28] G. Coffa, A.R. Brash, A single active site residue directs oxygenation stereospecificity in lipoxygenases: Stereocontrol is linked to the position of oxygenation, *Proc. Natl. Acad. Sci. U. S. A.*, 101 (2004) 15579–15584.
- [29] G. Coffa, A.N. Imber, B.C. Maguire, G. Laxmikanthan, C. Schneider, B.J. Gaffney, A.R. Brash, On the relationships of substrate orientation, hydrogen abstraction, and product stereochemistry in single and double dioxygenations by soybean lipoxygenase-1 and its Ala542Gly mutant, *J. Biol. Chem.*, 280 (2005) 38756–38766.

- [30] C. Jansen, K. Hofheinz, R. Vogel, J. Roffeis, M. Anton, P. Reddanna, H. Kuhn, M. Walther, Stereocontrol of arachidonic acid oxygenation by vertebrate lipoxygenases: Newly cloned zebrafish lipoxygenase 1 does not follow the ala-versus-gly concept, *J. Biol. Chem.*, 286 (2011) 37804–37812.
- [31] T. Horn, S. Adel, R. Schumann, S. Sur, K.R. Kakularam, A. Polamarasetty, P. Redanna, H. Kuhn, D. Heydeck, Evolutionary aspects of lipoxygenases and genetic diversity of human leukotriene signaling, *Prog. Lipid Res.*, 57 (2015) 13–39.
- [32] A. Andreou, I. Feussner, Lipoxygenases - Structure and reaction mechanism, *Phytochemistry*, 70 (2009) 1504–1510.
- [33] G.L. Bundy, E.G. Nidy, D.E. Epps, S.A. Mizsak, R.J. Wnuk, Discovery of an arachidonic acid C-8 lipoxygenase in the gorgonian coral *Pseudoplexaura porosa*, *J. Biol. Chem.*, 261 (1986) 747–751.
- [34] T. Hada, L.L. Swift, A.R. Brash, Discovery of 5R-lipoxygenase activity in oocytes of the surf clam: *Spisula solidissima*, *Biochim. Biophys. Acta - Lipids Lipid Metab.*, 1346 (1997) 109–119.
- [35] V. Di Marzo, C. Gianfrani, L. De Petrocellis, A. Milone, G. Cimino, Polyunsaturated-fatty-acid oxidation in Hydra: Regioselectivity, substratedependent enantioselectivity and possible biological role, *Biochem. J.*, 300 (1994) 501–507.
- [36] J.Z. Haeggström, C.D. Funk, Lipoxygenase and leukotriene pathways: Biochemistry, biology, and roles in disease, *Chem. Rev.*, 111 (2011) 5866–5896.
- [37] J.C. Boyington, B.J. Gaffney, L.M. Amzel, Crystallization and preliminary X-ray analysis of soybean lipoxygenase-1, a non-heme iron-containing dioxygenase, *J. Biol. Chem.*, 265 (1990) 12771–12773.
- [38] M.E. Newcomer, A.R. Brash, The structural basis for specificity in lipoxygenase catalysis, *Protein Sci.*, 24 (2015) 298–309.
- [39] A.R. Brash, Lipoxygenases: Occurrence, functions, catalysis, and acquisition of substrate, *J. Biol. Chem.*, 274 (1999) 23679–23682.
- [40] J.A. Corbin, J.H. Evans, K.E. Landgraf, J.J. Falke, Mechanism of specific membrane targeting by C2 domains: Localized pools of target lipids enhance Ca<sup>2+</sup> affinity, *Biochemistry*, 46 (2007) 4322–4336.
- [41] W. Minor, J. Steczko, B. Stec, Z. Otwinowski, J.T. Bolin, R. Walter, B. Axelrod, Crystal structure of soybean lipoxygenase L-1 at 14 Å resolution, *Biochemistry*, 35 (1996) 10687–10701.
- [42] P. Eek, R. Järving, I. Järving, N.C. Gilbert, M.E. Newcomer, N. Samel, Structure of a calcium-dependent 11R-lipoxygenase suggests a mechanism for Ca<sup>2+</sup> regulation, *J. Biol. Chem.*, 287 (2012) 22377–22386.
- [43] S. Pakhomova, W.E. Boeglin, D.B. Neau, S.G. Bartlett, A.R. Brash, M.E. Newcomer, An ensemble of lipoxygenase structures reveals novel conformations of the Fe coordination sphere, *Protein Sci.*, 28 (2019) 920–927.
- [44] C. Wasternack, I. Feussner, The Oxylipin Pathways: Biochemistry and Function, *Annu. Rev. Plant Biol.*, 69 (2018) 363–386.

- [45] A.M. Vasquez, V.D. Mouchlis, E.A. Dennis, Review of four major distinct types of human phospholipase A2, *Adv. Biol. Regul.*, 67 (2018) 212–218.
- [46] R. Brinckmann, K. Schnurr, D. Heydeck, T. Rosenbach, G. Kolde, H. Kühn, Membrane translocation of 15-lipoxygenase in hematopoietic cells is calcium-dependent and activates the oxygenase activity of the enzyme, *Blood*, 91 (1998) 64–74.
- [47] R. Järving, A. Löökene, R. Kurg, L. Siimon, I. Järving, N. Samel, Activation of 11R-lipoxygenase is fully Ca<sup>2+</sup>-dependent and controlled by the phospholipid composition of the target membrane, *Biochemistry*, 51 (2012) 3310–3320.
- [48] H. Kuhn, S. Banthiya, K. Van Leyen, Mammalian lipoxygenases and their biological relevance, *Biochim. Biophys. Acta - Mol. Cell Biol. Lipids*, 1851 (2015) 308–330.
- [49] J.Z. Haeggström, Leukotriene biosynthetic enzymes as therapeutic targets, *J. Clin. Invest.*, 128 (2018) 2680–2690.
- [50] M. Romano, E. Cianci, F. Simiele, A. Recchiuti, Lipoxins and aspirin-triggered lipoxins in resolution of inflammation, *Eur. J. Pharmacol.*, 760 (2015) 49–63.
- [51] C.R. Pace-Asciak, The hepoxilins and some analogues: A review of their biology, *Br. J. Pharmacol.*, 158 (2009) 972–981.
- [52] C. Sachs-Olsen, M. Sanak, A.M. Lang, A. Gielicz, P. Mowinckel, K.C. Lødrup Carlsen, K.H. Carlsen, A. Szczeklik, Eoxins: A new inflammatory pathway in childhood asthma, *J. Allergy Clin. Immunol.*, 126 (2010).
- [53] C.N. Serhan, N.A. Petasis, Resolvins and protectins in inflammation resolution, *Chem. Rev.*, 111 (2011) 5922–5943.
- [54] C. Wasternack, M. Strnad, Jasmonates: News on occurrence, biosynthesis, metabolism and action of an ancient group of signaling compounds, *Int. J. Mol. Sci.*, 19 (2018).
- [55] H. Porta, M. Rocha-Sosa, Plant lipoxygenases Physiological and molecular features, *Plant Physiol.*, 130 (2002) 15–21.
- [56] A.R. Brash, Mechanistic aspects of CYP74 allene oxide synthases and related cytochrome P450 enzymes, *Phytochemistry*, 70 (2009) 1522–1531.
- [57] Y.Y. Toporkova, S.S. Gorina, E.K. Bessolitsyna, E.O. Smirnova, V.S. Fatykhova, F. Brühlmann, T.M. Ilyina, L.S. Mukhtarova, A.N. Grechkin, Double function hydroperoxide lyases/epoxyalcohol synthases (CYP74C) of higher plants: identification and conversion into allene oxide synthases by site-directed mutagenesis, *Biochim. Biophys. Acta - Mol. Cell Biol. Lipids*, 1863 (2018) 369–378.
- [58] N. Tijet, A.R. Brash, Allene oxide synthases and allene oxides, *Prostaglandins Other Lipid Mediat.*, 68–69 (2002) 423–431.
- [59] E. Blée, Impact of phyto-oxylipins in plant defense, *Trends Plant Sci.*, 7 (2002) 315–322.
- [60] S. Yoeun, J. Il Kim, O. Han, Cellular localization and detergent dependent oligomerization of rice allene oxide synthase-1, *J. Plant Res.*, 128 (2014) 201–209.

- [61] H. Maucher, B. Hause, I. Feussner, J. Ziegler, C. Wasternack, Allene oxide synthases of barley (*Hordeum vulgare* cv Salome): Tissue specific regulation in seedling development, *Plant J.*, 21 (2000) 199–213.
- [62] D.S. Lee, P. Nioche, M. Hamberg, C.S. Raman, Structural insights into the evolutionary paths of oxylipin biosynthetic enzymes, *Nature*, 455 (2008) 363–368.
- [63] L. Li, Z. Chang, Z. Pan, Z.Q. Fu, X. Wang, Modes of heme binding and substrate access for cytochrome P450 CYP74A revealed by crystal structures of allene oxide synthase, *Proc. Natl. Acad. Sci. U. S. A.*, 105 (2008) 13883–13888.
- [64] Y.Y. Toporkova, E.O. Smirnova, L.S. Mukhtarova, S.S. Gorina, A.N. Grechkin, Catalysis by allene oxide synthases (CYP74A and CYP74C): Alterations by the Phe/Leu mutation at the SRS-1 region, *Phytochemistry*, 169 (2020).
- [65] Y.Y. Toporkova, Y. V. Gogolev, L.S. Mukhtarova, A.N. Grechkin, Determinants governing the CYP74 catalysis: Conversion of allene oxide synthase into hydroperoxide lyase by site-directed mutagenesis, *FEBS Lett.*, 582 (2008) 3423–3428.
- [66] Y.Y. Toporkova, V.S. Ermilova, S.S. Gorina, L.S. Mukhtarova, E.V. Osipova, Y.V. Gogolev, A.N. Grechkin, Structure-function relationship in the CYP74 family: Conversion of divinyl ether synthases into allene oxide synthases by site-directed mutagenesis, *FEBS Lett.*, 587 (2013) 2552–2558.
- [67] Y.Y. Toporkova, E. V. Osipova, L.S. Mukhtarova, Y. V. Gogolev, A.N. Grechkin, Alteration of Catalysis of CYP74C Subfamily Enzymes as a Result of Site-Directed Mutagenesis, *Dokl. Biochem. Biophys.*, 435 (2010) 287–290.
- [68] E. Blée, Phytooxylipins and plant defense reactions, *Prog. Lipid Res.*, 37 (1998) 33–72.
- [69] N. Tijet, C. Schneider, B.L. Muller, A.R. Brash, Biogenesis of volatile aldehydes from fatty acid hydroperoxides: Molecular cloning of a hydroperoxide lyase (CYP74C) with specificity for both the 9- and 13-hydroperoxides of linoleic and linolenic acids, *Arch. Biochem. Biophys.*, 386 (2001) 281–289.
- [70] I.S. Kim, W. Grosch, Partial Purification and Properties of a Hydroperoxide Lyase from Fruits of Pear, *J. Agric. Food Chem.*, 29 (1981) 1220–1225.
- [71] G. Mita, A. Quarta, P. Fasano, A. De Paolis, G. Pietro Di Sansebastiano, C. Perrotta, R. Iannacone, E. Belfield, R. Hughes, N. Tsesmetzis, R. Casey, A. Santino, Molecular cloning and characterization of an almond 9-hydroperoxide lyase, a new CYP74 targeted to lipid bodies, *J. Exp. Bot.*, 56 (2005) 2321–2333.
- [72] M. Kunishima, Y. Yamauchi, M. Mizutani, M. Kuse, H. Takikawa, Y. Sugimoto, Identification of (Z)-3:(E)-2-Hexenal isomerases essential to the production of the leaf aldehyde in plants, *J. Biol. Chem.*, 291 (2016) 14023–14033.
- [73] Y. Yamauchi, M. Kunishima, M. Mizutani, Y. Sugimoto, Reactive short-chain leaf volatiles act as powerful inducers of abiotic stress-related gene expression, *Sci. Rep.*, 5 (2015) 8030.
- [74] M.J. Mueller, S. Berger, Reactive electrophilic oxylipins: Pattern recognition and signalling, *Phytochemistry*, 70 (2009) 1511–1521.

- [75] Y.L. Krishnamurthy, J. Shashikala, B. Shankar Naik, Antifungal potential of some natural products against *Aspergillus flavus* in soybean seeds during storage, *J. Stored Prod. Res.*, 44 (2008) 305–309.
- [76] C. Wasternack, S. Song, Jasmonates: Biosynthesis, metabolism, and signaling by proteins activating and repressing transcription, *J. Exp. Bot.*, 68 (2017) 1303–1321.
- [77] T. Savchenko, I.S. Pearse, L. Ignatia, R. Karban, K. Dehesh, Insect herbivores selectively suppress the HPL branch of the oxylipin pathway in host plants, *Plant J.*, 73 (2013) 653–662.
- [78] X. Liu, F. Li, J. Tang, W. Wang, F. Zhang, G. Wang, J. Chu, C. Yan, T. Wang, C. Chu, C. Li, Activation of the Jasmonic Acid Pathway by Depletion of the Hydroperoxide Lyase OsHPL3 Reveals Crosstalk between the HPL and AOS Branches of the Oxylipin Pathway in Rice, *PLoS One*, 7 (2012).
- [79] H. Löhelaid, R. Järving, K. Valmsen, K. Varvas, M. Kreen, I. Järving, N. Samel, Identification of a functional allene oxide synthase-lipoxygenase fusion protein in the soft coral *Gersemia fruticosa* suggests the generality of this pathway in octocorals, *Biochim. Biophys. Acta - Gen. Subj.*, 1780 (2008) 315–321.
- [80] H. Löhelaid, T. Teder, K. Töldsepp, M. Ekins, N. Samel, Up-regulated expression of AOS-LOXa and increased eicosanoid synthesis in response to coral wounding, *PLoS One*, 9 (2014).
- [81] H. Löhelaid, N. Samel, Eicosanoid diversity of stony corals, *Mar. Drugs*, 16 (2018).
- [82] S. Libro, S.T. Kaluziak, S. V. Vollmer, RNA-seq profiles of immune related genes in the staghorn coral *Acropora cervicornis* Infected with white band disease, *PLoS One*, 8 (2013).
- [83] M. Aranda, A.T. Banaszak, T. Bayer, J.R. Luyten, M. Medina, C.R. Voolstra, Differential sensitivity of coral larvae to natural levels of ultraviolet radiation during the onset of larval competence, *Mol. Ecol.*, 20 (2011) 2955–2972.
- [84] N.R. Polato, N.S. Altman, I.B. Baums, Variation in the transcriptional response of threatened coral larvae to elevated temperatures, *Mol. Ecol.*, 22 (2013) 1366–1382.
- [85] H. Löhelaid, T. Teder, N. Samel, Lipoxygenase-allene oxide synthase pathway in octocoral thermal stress response, *Coral Reefs*, 34 (2015) 143–154.
- [86] N.C. Gilbert, M. Niebuhr, H. Tsuruta, T. Bordelon, O. Ridderbusch, A. Dassey, A.R. Brash, S.G. Bartlett, M.E. Newcomer, A covalent linker allows for membrane targeting of an oxylipin biosynthetic complex, *Biochemistry*, 47 (2008) 10665–10676.
- [87] M.L. Oldham, A.R. Brash, M.E. Newcomer, The structure of coral allene oxide synthase reveals a catalase adapted for metabolism of a fatty acid hydroperoxide, *Proc. Natl. Acad. Sci. U. S. A.*, 102 (2005) 297–302.
- [88] D.B. Neau, G. Bender, W.E. Boeglin, S.G. Bartlett, A.R. Brash, M.E. Newcomer, Crystal structure of a lipoxygenase in complex with substrate: The arachidonic acid-binding site of 8R-lipoxygenase, *J. Biol. Chem.*, 289 (2014) 31905–31913.
- [89] O. Boutaud, A.R. Brash, Purification and catalytic activities of the two domains of the allene oxide synthase-lipoxygenase fusion protein of the coral *Plexaura homomalla*, *J. Biol. Chem.*, 274 (1999) 33764–33770.



- [90] M.L. Oldham, A.R. Brash, M.E. Newcomer, Insights from the x-ray crystal structure of coral 8R-lipoxygenase: Calcium activation via a C2-like domain and a structural basis of product chirality, *J. Biol. Chem.*, 280 (2005) 39545–39552.
- [91] M.L. Oldham, A.R. Brash, M.E. Newcomer, The structure of coral allene oxide synthase reveals a catalase adapted for metabolism of a fatty acid hydroperoxide, *Proc. Natl. Acad. Sci. U. S. A.*, 102 (2005) 297–302.
- [92] T. Tosha, T. Uchida, A.R. Brash, T. Kitagawa, On the relationship of coral allene oxide synthase to catalase: A single active site mutation that induces catalase activity in coral allene oxide synthase, *J. Biol. Chem.*, 281 (2006) 12610–12617.
- [93] Z. Mashhadi, W.E. Boeglin, A.R. Brash, Inhibitory effects of a novel Val to Thr mutation on the distal heme of human catalase, *Biochimie*, 106 (2014) 180–183.
- [94] B. Gao, W.E. Boeglin, A.R. Brash, Role of the conserved distal heme asparagine of coral allene oxide synthase (Asn137) and human catalase (Asn148): Mutations affect the rate but not the essential chemistry of the enzymatic transformations, *Arch. Biochem. Biophys.*, 477 (2008) 285–290.
- [95] I. Stenzel, B. Hause, O. Miersch, T. Kurz, H. Maucher, H. Weichert, J. Ziegler, I. Feussner, C. Wasternack, Jasmonate biosynthesis and the allene oxide cyclase family of *Arabidopsis thaliana*, *Plant Mol. Biol.*, 51 (2003) 895–911.
- [96] R.K. Hughes, S. De Domenico, A. Santino, Plant cytochrome CYP74 family: Biochemical features, endocellular localisation, activation mechanism in plant defence and improvements for industrial applications, *ChemBioChem*, 10 (2009) 1122–1133.
- [97] H. Löhelaid, R. Järving, K. Valmsen, K. Varvas, M. Kreen, I. Järving, N. Samel, Identification of a functional allene oxide synthase-lipoxygenase fusion protein in the soft coral *Gersemia fruticosa* suggests the generality of this pathway in octocorals, *Biochim. Biophys. Acta - Gen. Subj.*, 1780 (2008) 315–321.
- [98] K. Matsui, H. Toyota, T. Kajiwara, T. Kakuno, A. Hatanaka, Fatty acid hydroperoxide cleaving enzyme, hydroperoxide lyase, from tea leaves, *Phytochemistry*, 30 (1991) 2109–2113.
- [99] A.N. Grechkin, M. Hamberg, The “heterolytic hydroperoxide lyase” is an isomerase producing a short-lived fatty acid hemiacetal, *Biochim. Biophys. Acta - Mol. Cell Biol. Lipids*, 1636 (2004) 47–58.
- [100] A. Waterhouse, M. Bertoni, S. Bienert, G. Studer, G. Tauriello, R. Gumienny, F.T. Heer, T.A.P. De Beer, C. Rempfer, L. Bordoli, R. Lepore, T. Schwede, SWISS-MODEL: Homology modelling of protein structures and complexes, *Nucleic Acids Res.*, 46 (2018) W296–W303.
- [101] P. Benkert, S.C.E. Tosatto, D. Schomburg, QMEAN: A comprehensive scoring function for model quality assessment, *Proteins Struct. Funct. Genet.*, 71 (2008) 261–277.
- [102] B. Webb, A. Sali, Comparative protein structure modeling using MODELLER, *Curr. Protoc. Bioinforma.*, 2016 (2016) 5.6.1–5.6.37.
- [103] R. Eisenthal, M.J. Danson, D.W. Hough, Catalytic efficiency and kcat/KM: a useful comparator?, *Trends Biotechnol.*, 25 (2007) 247–249.

- [104] S. Pollmann, A. Springer, S. Rustgi, D. Von Wettstein, C.H. Kang, C. Reinbothe, S. Reinbothe, Substrate channeling in oxylipin biosynthesis through a protein complex in the plastid envelope of *Arabidopsis thaliana*, *J. Exp. Bot.*, 70 (2019) 1497–1511.
- [105] E.H. Oliw, M. Aragón, Y. Chen, F. Jernerén, A new class of fatty acid allene oxide formed by the DOX-P450 fusion proteins of human and plant pathogenic fungi, *C. immitis* and *Z. tritici*, *J. Lipid Res.*, 57 (2016) 1518–1528.
- [106] L.S. Mukhtarova, F. Brühlmann, M. Hamberg, B.I. Khairutdinov, A.N. Grechkin, Plant hydroperoxide-cleaving enzymes (CYP74 family) function as hemiacetal synthases: Structural proof of hemiacetals by NMR spectroscopy, *Biochim. Biophys. Acta - Mol. Cell Biol. Lipids*, 1863 (2018) 1316–1322.
- [107] A.R. Brash, M.A. Hughes, D.J. Hawkins, W.E. Boeglin, W.C. Song, L. Meijer, Allene oxide and aldehyde biosynthesis in starfish oocytes, *J. Biol. Chem.*, 266 (1991) 22926–22931.
- [108] G.J. Garssen, J.F. Vliegthart, J. Boldingh, An anaerobic reaction between lipoxigenase, linoleic acid and its hydroperoxides, *Biochem. J.*, 122 (1971) 327–332.
- [109] J. Delcarte, P. Jacques, M.L. Fauconnier, P. Hoyaux, K. Matsui, M. Marlier, P. Thonart, The homolytic and heterolytic fatty acid hydroperoxide lyase-like activities of hematin, *Biochem. Biophys. Res. Commun.*, 286 (2001) 28–32.
- [110] M.A. Noordermeer, G.A. Veldink, J.F.G. Vliegthart, Fatty Acid Hydroperoxide Lyase: A Plant Cytochrome P450 Enzyme Involved in Wound Healing and Pest Resistance, *ChemBioChem*, 2 (2001) 494–504.
- [111] K. Matsui, C. Miyahara, J. Wilkinson, B. Hiatt, V. Knauf, T. Kajiwara, Fatty acid hydroperoxide lyase in tomato fruits: Cloning and properties of a recombinant enzyme expressed in *escherichia coli*, *Biosci. Biotechnol. Biochem.*, 64 (2000) 1189–1196.
- [112] M.A. Noordermeer, A.J.H. van Dijken, S.C.M. Smeekens, G.A. Veldink, J.F.G. Vliegthart, Characterization of three cloned and expressed 13-hydroperoxide lyase isoenzymes from alfalfa with unusual N-terminal sequences and different enzyme kinetics, *Eur. J. Biochem.*, 267 (2000) 2473–2482.
- [113] Y.Y. Toporkova, L.S. Mukhtarova, Y. V. Gogolev, A.N. Grechkin, Origins of the diversity of cytochrome P450 CYP74 family based on the results of site-directed mutagenesis, *Moscow Univ. Biol. Sci. Bull.*, 65 (2010) 155–157.
- [114] C.A. Rouzer, L.J. Marnett, Cyclooxygenases: Structural and functional insights, *J. Lipid Res.*, 50 (2009).
- [115] M. Fasano, S. Curry, E. Terreno, M. Galliano, G. Fanali, P. Narciso, S. Notari, P. Ascenzi, The extraordinary ligand binding properties of human serum albumin, *IUBMB Life*, 57 (2005) 787–796.
- [116] H.-C. Cheng, P.-T. Cheng, P. Peng, P.-C. Lyu, Y.-J. Sun, Lipid binding in rice nonspecific lipid transfer protein-1 complexes from *Oryza sativa*, *Protein Sci.*, 13 (2004) 2304–2315.
- [117] A.L. Blobaum, L.J. Marnett, Structural and functional basis of cyclooxygenase inhibition, *J. Med. Chem.*, 50 (2007) 1425–1441.

- [118] K.M. Knights, A.A. Mangoni, J.O. Miners, Defining the COX inhibitor selectivity of NSAIDs: Implications for understanding toxicity, *Expert Rev. Clin. Pharmacol.*, 3 (2010) 769–776.
- [119] E.D. Thuresson, K.M. Lakkides, C.J. Rieke, Y. Sun, B.A. Wingerd, R. Micielli, A.M. Mulichak, M.G. Malkowski, R.M. Garavito, W.L. Smith, Prostaglandin endoperoxide H synthase-1: The functions of cyclooxygenase active site residues in the binding, positioning, and oxygenation of arachidonic acid, *J. Biol. Chem.*, 276 (2001) 10347–10357.
- [120] O. Laneuville, D.K. Breuer, N. Xu, Z.H. Huang, D.A. Gage, J.T. Watson, M. Lagarde, D.L. DeWitt, W.L. Smith, Fatty acid substrate specificities of human prostaglandin-endoperoxide H synthase-1 and -2 Formation of 12-hydroxy-(9Z,13E/Z,15Z)-octadecatrienoic acids from  $\alpha$ -linolenic acid, *J. Biol. Chem.*, 270 (1995) 19330–19336.
- [121] N. Carrillo, E.A. Ceccarelli, O.A. Roveri, Usefulness of kinetic enzyme parameters in biotechnological practice, *Biotechnol. Genet. Eng. Rev.*, 27 (2010) 367–382.
- [122] R. Ferreira De Freitas, M. Schapira, A systematic analysis of atomic protein-ligand interactions in the PDB, *Medchemcomm*, 8 (2017) 1970–1981.
- [123] C.D. Waldburger, J.F. Schildbach, R.T. Sauer, Are buried salt bridges important for protein stability and conformational specificity?, *Nat. Struct. Biol.*, 2 (1995) 122–128.
- [124] L.M. Ellerby, W.A. Escobar, A.L. Fink, C. Mitchinson, J.A. Wells, The role of lysine-234 in  $\beta$ -lactamase catalysis probed by site-directed mutagenesis, *Biochemistry*, 29 (1990) 5797–5806.
- [125] D. Verma, D.J. Jacobs, D.R. Livesay, Variations within Class-A  $\beta$ -Lactamase Physicochemical Properties Reflect Evolutionary and Environmental Patterns, but not Antibiotic Specificity, *PLoS Comput. Biol.*, 9 (2013).
- [126] T.W.B. Ost, C.S. Miles, J. Murdoch, Y.F. Cheung, G.A. Reid, S.K. Chapman, A.W. Munro, Rational re-design of the substrate binding site of flavocytochrome P450 BM3, *FEBS Lett.*, 486 (2000) 173–177.
- [127] Y. He, R. Estephan, X. Yang, A. Vela, H. Wang, C. Bernard, R.E. Stark, A nuclear magnetic resonance-based structural rationale for contrasting stoichiometry and ligand binding site(s) in fatty acid-binding proteins, *Biochemistry*, 50 (2011) 1283–1295.
- [128] A. Higdon, A.R. Diers, J.Y. Oh, A. Landar, V.M. Darley-Usmar, Cell signalling by reactive lipid species: New concepts and molecular mechanisms, *Biochem. J.*, 442 (2012) 453–464.
- [129] E.E. Farmer, C. Davoine, Reactive electrophile species, *Curr. Opin. Plant Biol.*, 10 (2007) 380–386.
- [130] A.B. Imbs, D.A. Demidkova, T.N. Dautova, Lipids and fatty acids of cold-water soft corals and hydrocorals: a comparison with tropical species and implications for coral nutrition, *Mar. Biol.*, 163 (2016).
- [131] A.B. Imbs, O.A. Demina, D.A. Demidkova, Lipid class and fatty acid composition of the boreal soft coral *Gersemia rubiformis*, *Lipids*, 41 (2006) 721–725.

- [132] A.B. Imbs, N.A. Latyshev, T.N. Dautova, Y.Y. Latypov, Distribution of lipids and fatty acids in corals by their taxonomic position and presence of zooxanthellae, *Mar. Ecol. Prog. Ser.*, 409 (2010) 65–75.
- [133] L. De Petrocellis, D. Melck, T. Bisogno, A. Milone, V. Di Marzo, Finding of the endocannabinoid signalling system in Hydra, a very primitive organism: Possible role in the feeding response, *Neuroscience*, 92 (1999) 377–387.

## ACKNOWLEDGMENTS

*“From a little spark may burst a flame.”*

Dante Alighieri

I would like to thank:

- Prof. Nigulas Samel and Dr. Helike Lõhelaid, who introduced me to the world of lipids. They gave me the chance to be actively involved in the research and see nature from a different perspective. With them, I got the opportunity to develop, become more independent and do the science I really enjoy.
- all of my colleagues for their much appreciated support and enjoyable company.
- one of my main collaborators, Prof. Alan R. Brash, who complemented my skill set and contributed to my future as a scientist.
- my family and especially my grandmother, who supported my studies throughout these years.
- all the funding sources that supported my participation in international science meetings and courses. Specifically, this work has been partially supported by “TUT Institutional Development Program for 2016-2022” Graduate School in Biomedicine and Biotechnology receiving funding from the European Regional Development Fund under program ASTRA 2014-2020.4.01.16-0032 in Estonia. In addition, some of the travels to science meetings were funded by DORA Plus program (Archimedes).

## ABSTRACT

### Structural and catalytic aspects of the catalase-related fatty acid hydroperoxide lyase

A unique fusion protein, catalase-related allene oxide synthase-lipoxygenase (cAOS-LOX), plays a central role in the oxylipin synthesis of corals (*Animalia*, *Cnidaria*). The cAOS-LOX fusion protein catalyzes the conversion of arachidonic acid (AA) to 8*R*-hydroperoxy-eicosatetraenoic acid (8*R*-HpETE), which subsequently is metabolized to allene oxide, detected as stable end-products,  $\alpha$ -ketol and cyclopentenone. Two highly homologous fusion proteins, cAOS-LOX-a and -b, were identified in the soft coral *Capnella imbricata*. It was shown that the gene expression and activity of cAOS-LOX-a was elevated in response to abiotic stressors, while the levels and the activity of cAOS-LOX-b remained unaltered. This indicated the involvement of cAOS-LOX-a in the stress response of corals, although, the biological role of cAOS-LOX-b remains elusive.

The initial product analysis revealed that instead of the formation of  $\alpha$ -ketol and cyclopentenone, cAOS-LOX-b gives rise to unknown polar compounds. In the current thesis, these products were identified as (5*Z*)-8-oxo-octenoic acid and (3*Z*,6*Z*)-dodecadienal. This type of enzymatic activity is unprecedented among animals. Therefore, the N-terminal domains of cAOS-LOX-a and cAOS-LOX-b were designated as cAOS and cHPL, respectively. Specifically, cHPL catalyzed the conversion of 8*R*-HpETE to the hemiacetal intermediate, which breaks down into two short-chain fragments. The cHPL-catalyzed reaction corresponds to the reaction mechanism of plant HPL. In addition, both of the oxygens from the hydroperoxy group of 8*R*-HpETE are retained in the oxo groups of aldehydes, which excludes the involvement of water in the reaction mechanism. Although coral cAOS and cHPL catalyze the same reactions as corresponding plant enzymes, they originate from different gene families. As plant AOS and HPL belong to the subfamily of cytochrome P450, the core structure and the active site of cAOS are highly identical to catalases.

The differences in the substrate channels between cAOS and cHPL possibly involved in the reaction specificity and substrate binding were determined based on sequence alignment and structural analysis. The residues responsible for the reaction specificity of cHPL were identified as Phe150 and Ser177 by using the site-directed mutagenesis approach. Specifically, the replacements in these residues resulted in a shift in the activity from cHPL to cAOS.

Based on the X-ray structure of *Plexaura homomalla* cAOS (PDB IDs: 1u5u), positively charged Lys60 and Lys107 in the substrate entry site were postulated to be anchoring residues of the negatively charged carboxy group of 8*R*-HpETE. This was confirmed by docking simulations with different polyunsaturated fatty acid (PUFA) hydroperoxides. To understand their influence on the catalytic reaction, the Lys60 and Lys107 of cAOS were replaced with either Met, as a neutral residue, or Glu, as a negatively charged residue. In parallel, the corresponding residues of cHPL, Glu60 and Lys107, were substituted using the same strategy. Despite the data on the electrostatic interactions *in silico*, the mutations of Lys60 and Lys107 of cAOS did not influence the substrate binding *in vitro*. In contrast, substitutions of the Glu60 of cHPL reduced the reaction rate of cHPL significantly, indicating its essential role in the proper binding of substrates. As the replacements of the Lys107 of cHPL resulted in an increased turnover

rate, more complex interactions between the residues in the substrate entry site and the carboxy group of a PUFA hydroperoxide are anticipated.

The substrate preferences of cAOS and cHPL with free PUFA hydroperoxides were determined based on the corresponding catalytic efficiencies. Although 8*R*-HpETE was metabolized with the best efficiency by cAOS and cHPL, 10*R*-hydroperoxy-docosahexaenoic acid (10*R*-HpDHE) was a more suitable substrate for cHPL. The C18 PUFA hydroperoxy derivatives, 9*R*-Hp-ALA and 9*R*-Hp-GLA, were metabolized with the lowest efficiency by both enzymes.

Incubations with neutral PUFA hydroperoxides revealed that cHPL can catalyze the conversion of 8*R*-hydroperoxy derivatives of methylated AA, docosahexaenoic acid (DHA) and endocannabinoid derivatives, anandamide (AEA) and 1-arachidonoyl glycerol (1-AG). In contrast, even though cAOS was able to catalyze endocannabinoid derivatives with lower activity, no reaction was detected with methylated substrates. This refers to distinct characteristics of the substrate entry sites of cAOS and cHPL.

In conclusion, two parallel pathways, cAOS-LOX and cHPL-LOX, were identified in the soft coral *C. imbricata*. Despite the high sequence identity, cAOS and cHPL catalyze the conversion of 8*R*-HpETE to different products. As with the plant Cyp74 enzymes, the shift from HPL to AOS can be achieved by single mutations in the amino acid sequence. In addition, due to variations in the substrate entry sites, the substrate binding and the substrate preference between cAOS and cHPL are different. The ability to metabolize alternative PUFA hydroperoxides by cHPL suggests the versatile usage of the substrate pool *in vivo*. Although cAOS and cHPL contribute to the multifaceted production of oxylipins, the cross-talk between oxylipin-mediated signaling pathways in corals needs further investigation.

## KOKKUVÕTE

### Katalaasilaadse hüdroperoksiidlüaasi struktuursed ja katalüütilised omadused

Pehme korallide arahhidoonhappe (AA) metabolismis on kesksel kohal unikaalne liitvalk, katalaasilaadne alleenoksiidsüntaas-lipoksügenaas (cAOS-LOX). Liitvalgu C-terminaalne LOX domeen katalüüsib AA oksüdatsiooni 8R-hüdroperoksü-eikosatetraeenhappeks (8R-HpETEks), mis N-terminaalse cAOS domeeni poolt konverteeritakse alleenoksiidiks (AO). AO-d kui ebastabiilset produkti detekteeritakse tema stabiilsete lõpp-ühendite,  $\alpha$ -ketooli ja tsüklopentenooni, kaudu. Hiljuti identifitseeriti pehmet korallist *Capnella imbricata* kaks kõrge identisusega liitvalku, cAOS-LOX-a ja cAOS-LOX-b. Stressikatsed pehme koralliga *C. imbricata* näitasid kõrgeenenud cAOS-LOX-a geeniekspressiooni ja aktiivsust, kusjuures cAOS-LOX-b tase jäi muutumatuks. Antud katsega näidati, et cAOS-LOX-a on seotud koralli üldise stressivastusega, kuid cAOS-LOX-b funktsioon vajab edasist uurimist.

Esmase produktide analüüsi põhjal selgus, et cAOS-LOX-b katalüüsib  $\alpha$ -ketooli ja tsüklopentenooni asemel tundmatuid polaarseid ühendeid. Käesolevas teesis näidati, et cAOS-LOX-b liitvalgu LOX domeen katalüüsib AA-st 8R-HpETE, mis N-terminaalse domeeni poolt konverteeritakse (5Z)-8-okso-okateenhappeks ehk C8-oksohappeks ja (3Z,6Z)-dodekadienaaliks ehk C12-aldehüüdiks. Kusjuures mõlemate aldehüüdsete fragmentide oksorühmad sisaldavad hapnikke 8R-HpETE hüdroperoksürühmast. See tähendab, et hemiatsetaalse vaheühendi moodustamisel vesi ei osale. Seesugust taimedele omast lüaasist aktiivsust ei ole varem loomades täheldatud. Koralli cAOS-b ja taime hüdroperoksiidlüaas (HPL) katalüüsivad identset reaktsiooni, mistõttu antud töös nimetati cAOS-b katalaasilaadseks hüdroperoksiidlüaasiks (cHPL).

Hoolimata sellest, et koralli cAOS/cHPL ja taime AOS/HPL katalüüsivad samu reaktsioone, on taime ja koralli ensüümid erinevatest geeniperekondadest ja seetõttu ka struktuurilt erinevad. *Plexaura homomalla* cAOS kristallstruktuuri (PDB ID: 1u5u) ja järjestuse põhjal on koralli cAOS-i katalüütiline tsenter ning üldine struktuur identne katalaasidega. Hoolimata kõrge struktuursest sarnasusest, eelistab cAOS rasvhappe hüdroperoksiide ning katalaas katalüüsib ainult vesinikperoksiidi lagunemist.

Kõrgelt identsete cAOS-i ja cHPL-i järjestus- ning struktuurianalüüsi põhjal määrati nende substraadikanalite aminohappelised erinevused, mis võiksid olla seotud reaktsioonimehhanismi ja substraadisidumisega. Koht-spetsiifilise mutageneesi abil määrati, et aminohapped, Phe150 ja Leu177, on seotud cHPL-spetsiifilise reaktsiooniga. Täpsemalt, antud mutatsioonide tulemusena cHPL katalüüsib nii cHPL kui ka cAOS produktide teket.

*P. homomalla* cAOS-i kristallstruktuuri põhjal täheldati kahe positiivselt laetud aminohappe, Lys60 ja Lys107, potentsiaalset rolli elektrostaatilisest interaktsioonist rasvhappe karboksüülrühmaga, mida kinnitasid dokkimissimulatsioonid erinevate ligandidega. Koht-spetsiifilise mutageneesi abil asendati antud lüsiinid vastavalt neutraalse metioniini või positiivselt laetud glutamaadiga. Paralleelselt muteeriti vastavad jäägid, Glu60 ja Lys107, cHPL-i järjestuses neutraalse või vastasmärgilise jäägiga. Mutatsioonide tulemusel selgus, et erinevalt *in silico* tulemustest, cAOS-i substraadikanalis olevad lüsiinid ei mõjuta kineetilisi parameetreid, mistõttu ei ole nad vajalikud substraadi sidumisel. Vastupidiselt cAOS-le, Glu60 asendused alandasid cHPL-i reaktsioonikiirust märkimisväärselt, mis ilmestab Glu60 olulisust substraadi



produktiivses sidumises. Erinevalt cAOS-le, Lys107 asendused tõstsid cHPL-i reaktsioonikiirust, mis viitab komplekssetele interaktsioonidele cHPL-i substraadikani suudmes.

Katalüütiliste efektiivsute põhjal oli nii cAOS-le kui ja cHPL-le parimaks substraadiks 8R-HpETE. Suurim erinevus oli 10R-hüdroperoksü-dokosaheksaneehappe (10R-HpDHE), C22 hüdroperoksiidi, eelistuse osas. Kui cAOS-i efektiivsus langes 10R-HpDHE-ga märkimisväärselt, siis cHPL kasutas 10R-HpDHE-d pea samasuguse efektiivsusega kui 8R-hüdroperoksü-eikosapentaenahapet (8R-HpEPE-t). Mõlema ensüümi puhul täheldati, et 9R-Hp-ALA ja 9R-Hp-GLA kui C18 hüdroperoksü rasvhappeid metaboliseeritakse madalaima efektiivsusega.

Inkubatsioonidest alternatiivsete substraatidega selgus, et cHPL on võimeline konverteerima nii 8R-hüdroperoksü-endokannabinoidide kui ka metüleeritud 8R-HpETE-t ja 10R-HpDHE-d. Erinevalt cHPL-st oli cAOS-i reaktsioonikiirus endokannabinoididega umbes neli korda madalam ning metüleeritud substraate ei metaboliseeritud üldse. See asjaolu viitab märkimisväärssetele struktuursetele erinevustele cAOS-i ja cHPL-i substraadikani suudmes.

Kokkuvõtteks, korallis *C. imbricata* on kaks paralleelset oksüliipine sünteesivat rada, cAOS-LOX ja cHPL-LOX. Hoolimata cAOS-i ja cHPL-i kõrgest järjestuse identsusest, katalüüsivad nad 8R-HpETE-st erinevaidprodukte. Sarnaselt taime Cyp74 ensüümidega, on üksikute mutatsioonide abil võimalik suunata cHPL-i sünteesima cAOS-i produkte. Erinevused cAOS-i ja cHPL-i substraadisidumises ja -eelistuses on tingitud eelkõige substraadikani suudme struktuurist. Eeskätt cHPL-i võimekus metaboliseerida alternatiivseid rasvhappe hüdroperoksiide viitab cHPL-i ja cAOS-i substraadikasutuse eripäradele *in vivo*. Hoolimata sellest, et cAOS ja cHPL panustavad pehme koralli *C. imbricata* oksüliipiinide metabolismi, nende osalus ja koostoime korallide signaalradades vajab edasist uurimist.



## PUBLICATION I

T. Teder, H. Löhelaid, W. E. Boeglin, A. R. Brash, N. Samel

**A catalase-related hemoprotein in coral is specialized for synthesis of short-chain aldehydes: discovery of P450-type hydroperoxide lyase activity in a catalase**

*Journal of Biological Chemistry* 290 (2015) 19823–32



# A Catalase-related Hemoprotein in Coral Is Specialized for Synthesis of Short-chain Aldehydes

## DISCOVERY OF P450-TYPE HYDROPEROXIDE LYASE ACTIVITY IN A CATALASE\*

Received for publication, April 20, 2015, and in revised form, June 18, 2015. Published, JBC Papers in Press, June 22, 2015, DOI 10.1074/jbc.M115.660282

Tarvi Teder<sup>†‡§</sup>, Helike Löhela<sup>†</sup>, William E. Boeglin<sup>§</sup>, Wade M. Calcutt<sup>¶</sup>, Alan R. Brash<sup>§</sup>, and Nigulas Samel<sup>†‡1</sup>

From the <sup>†</sup>Department of Chemistry, Tallinn University of Technology, 12618 Tallinn, Estonia, <sup>§</sup>Department of Pharmacology and the Vanderbilt Institute of Chemical Biology, Vanderbilt University, Nashville, Tennessee 37232, and <sup>¶</sup>Department of Biochemistry, Vanderbilt University, Nashville, Tennessee

**Background:** Biosynthetic transformation of fatty acid peroxides commonly is catalyzed by cytochromes P450.

**Results:** A catalase-related hemoprotein in the coral *Capnella imbricata* converts 8*R*-hydroperoxy-eicosatetraenoic acid in a P450-type reaction to short-chain aldehydes.

**Conclusion:** A catalase-related hydroperoxide lyase is identified in Animalia.

**Significance:** The catalase-related hemoprotein has the catalytic competence of a P450.

In corals a catalase-lipoxygenase fusion protein transforms arachidonic acid to the allene oxide 8*R*,9-epoxy-5,9,11,14-eicosatetraenoic acid from which arise cyclopentenones such as the prostanoid-related clavulones. Recently we cloned two catalase-lipoxygenase fusion protein genes (*a* and *b*) from the coral *Capnella imbricata*, form *a* being an allene oxide synthase and form *b* giving uncharacterized polar products (Löhela, H., Teder, T., Töldsepp, K., Ekins, M., and Samel, N. (2014) *PLoS ONE* 9, e89215). Here, using HPLC-UV, LC-MS, and NMR methods, we identify a novel activity of fusion protein *b*, establishing its role in cleaving the lipoxygenase product 8*R*-hydroperoxy-eicosatetraenoic acid into the short-chain aldehydes (5*Z*)-8-oxo-octanoic acid and (3*Z*,6*Z*)-dodecadienal; these primary products readily isomerize in an aqueous medium to the corresponding 6*E*- and 2*E*,6*Z* derivatives. This type of enzymatic cleavage, splitting the carbon chain within the conjugated diene of the hydroperoxide substrate, is known only in plant cytochrome P450 hydroperoxide lyases. In mechanistic studies using <sup>18</sup>O-labeled substrate and incubations in H<sub>2</sub><sup>18</sup>O, we established synthesis of the C8-oxo acid and C12 aldehyde with the retention of the hydroperoxy oxygens, consistent with synthesis of a short-lived hemiacetal intermediate that breaks down spontaneously into the two aldehydes. Taken together with our initial studies indicating differing gene regulation of the allene oxide synthase and the newly identified catalase-related hydroperoxide lyase and given the role of aldehydes in plant defense, this work uncovers a potential pathway in coral stress signaling and a novel enzymatic activity in the animal kingdom.

Lipid mediator biosynthesis commonly involves the dioxygenation of a fatty acid followed by a cytochrome P450-catalyzed rearrangement of the resulting fatty acid peroxide in the next step of the pathway. In higher animals the cyclooxygenases are so coupled with thromboxane synthase (cytochrome P450 CYP5) or prostacyclin synthase (CYP8), thereby producing important mediators of vascular homeostasis (1). In plants, the pair of enzymes is usually a lipoxygenase (LOX),<sup>2</sup> forming a fatty acid hydroperoxide, and a member of the P450 CYP74 family with allene oxide synthase (AOS), divinyl ether synthase, or hydroperoxide lyase (HPL) activity (2, 3). These enzymes give rise to products including the plant hormone jasmonic acid via AOS and mediators of plant defense via the HPL (4). In fungi there are many examples of a single participating gene encoding a two-domain protein comprised of an N-terminal heme dioxygenase and a C-terminal cytochrome P450 (5–7). The resulting oxylipin products act as hormone-like signals modulating asexual and sexual spore development and in the production of toxins (7, 8).

Certain lower animals, best studied in corals, express a different type of fusion protein that consists of an N-terminal catalase-related hemoprotein coupled to a C-terminal LOX domain (9, 10). The prototypical enzyme of this type is the cAOS-LOX fusion protein, which dioxygenates arachidonic acid to an 8*R*-hydroperoxyeicosatetraenoic acid (8*R*-HpETE) intermediate followed by its conversion to an allene oxide by the cAOS domain (11). Although the plant AOS and cAOS catalyze similar reactions, the enzymes are structurally unrelated (12–14). The highly labile allene oxide products of both enzyme types readily break down to stable end products,  $\alpha$ -ketol and cyclopentenone (6). Moreover, despite the structural relatedness to catalase, cAOS lacks the capability to catalyze the decomposition of hydrogen peroxide to water and molecular oxygen (14, 15).

\* This work was supported, in whole or in part, by National Institutes of Health Grant GM-074888 (to A. R. B.). This work was also supported by the Institutional Research Funding IUT19–9 of the Estonian Ministry of Education and Research and the Estonian Science Foundation Grant 9410 (both to N. S.). The authors declare that they have no conflicts of interest with the contents of this article.

<sup>1</sup> To whom the correspondence may be addressed: Dept. of Chemistry, Tallinn University of Technology, 12618 Tallinn, Estonia. Tel.: 372-620-4376; Fax: 372-620-2828; E-mail: nigulas.samel@ttu.ee.

<sup>2</sup> The abbreviations used are: LOX, lipoxygenase; AA, arachidonic acid; AOS, allene oxide synthase; cAOS, catalase-related AOS; HPL, hydroperoxide lyase; cHPL, catalase-related HPL; 8*R*-H(p)ETE, 8*R*-hydro(pero)xyeicosatetraenoic acid; RP-HPLC, reversed phase HPLC; SP-HPLC, straight phase HPLC.

## Catalase-related Fatty Acid Hydroperoxide Lyase

In our recent study of the soft coral *Capnella imbricata* we cloned two highly homologous catalase-lipoxygenase fusion proteins (designated **a** and **b**) with 88% of amino acid identity (16). Although the catalytically important amino acids of catalase-related and lipoxygenase domains were conserved, the biosynthesis with [ $1\text{-}^{14}\text{C}$ ]arachidonic acid led to the formation of different products. Although fusion protein **a** catalyzed the formation of an  $\alpha$ -ketol and cyclopentenone stable end products and thereby can be designated as a cAOS-LOX, incubation with fusion protein **b** gave rise to unknown polar compounds (16). Herein we present the identification of short-chain compounds formed by the catalase-related hemoprotein **b** and thereby characterize a fatty acid hydroperoxide lyase pathway in coral arachidonic acid metabolism.

### Experimental Procedures

**Materials**—Arachidonic acid (AA) was purchased from NuChek Prep Inc. (Elysian, MN). 8R-HpETE was synthesized using the *Plexaura homomalla* 8R-lipoxygenase domain of the cAOS-LOX fusion protein, expressed in *Escherichia coli* (11). The  $^{18}\text{O}_2$ -8R-HpETE was prepared from AA by *P. homomalla* 8R-LOX under an  $^{18}\text{O}_2$  (Isotech (Miami, OH)) atmosphere in a degassed buffer (50 mM Tris, pH 8.0). The  $^{18}\text{O}$ -labeled water was purchased from the Mound Facility (Miamisburg, OH). Only HPLC grade solvents were used.

**Cloning and Expression of Fusion Protein **b** and the Catalase-related Domain**—The ORF of fusion protein **b** (GenBank<sup>TM</sup> accession number KF000374) with terminal NheI restriction sites and with an N-terminal His<sub>6</sub> tag was PCR-amplified from the fusion protein **b** construct (16) using forward (5'-ATT-CATATGATGGTTTGGAAAAATTTGGTTACG-3') and reverse (5'-CAGCTAGCCTAGATTGCAGTTCCG-3') primers. Subsequently, the ORF of the catalase-related domain with a stop codon and C-terminal His<sub>4</sub> tag was PCR-amplified from fusion protein **b** sequence using forward (5'-ATTCATATGATGGTTTGGAAAAATTTGGTTACG-3') and reverse (5'-ATAGCTAGCTTAGTGATGGTGATGGTTCTGTCCTGTTGGAACCAGAG-3') primers with NdeI and NheI restriction sites, respectively. The amplicons of fusion protein **b** and the catalase-related domain were cloned into the pET11a expression vector (Stratagene) and sequenced. The His-tagged fusion protein **b** and catalase-related domain were expressed in *E. coli* BL21(DE3) cells (Novagen) in a Terrific Broth medium at 20 °C overnight and purified as described previously (17). The protein fractions were dialyzed against an ice-cold 50 mM Tris (pH 8.0) buffer containing 100 mM NaCl by slowly stirring overnight at 4 °C. Purified proteins were stored at -80 °C for further use. Proteins were quantified based on the absorbance at 406 nm ( $\epsilon \sim 100,000 \text{ M}^{-1} \text{ cm}^{-1}$ ) characteristic for hemoproteins.

**Chiral analysis of *C. imbricata* Fusion Protein **b**-derived 8-HpETE Intermediate**—Incubations with 5 nM fusion protein **b** were performed at room temperature using 100  $\mu\text{M}$  AA in a 50 mM Tris (pH 8.0) buffer containing 100 mM NaCl and 1 mM CaCl<sub>2</sub> in the presence of the reducing agent SnCl<sub>2</sub> to reduce the LOX-catalyzed 8-HpETEs *in situ*. Incubations with *Gersemia fruticosa* 8R-LOX were performed in parallel. Individual LOX products were extracted with EtOAc, and the corresponding methyl esters were prepared using diazomethane. LOX prod-

ucts were isolated on SP-HPLC using a Phenomenex silica 5- $\mu\text{m}$  column (0.46  $\times$  25 cm) with a hexane/isopropyl alcohol solvent system (isocratic: 100:2 by volume) at a flow rate of 1 ml/min at 235 nm. Methyl esters of 8-HETE were analyzed on a Chiralcel OD-H (0.46  $\times$  25 cm) column at a flow rate of 1 ml/min at 235 nm using the same solvent system as described previously. The methylated *C. imbricata* LOX product was co-chromatographed with the methyl esters of  $\pm$ 8-HETE standard (Cayman Chemical Co.), and the 8R-HETE reference by *G. fruticosa* 8R-LOX (10) was used to determine the stereoconfiguration of 8-HETE formed by the LOX domain of the *C. imbricata* fusion protein **b**.

**Incubations with Fusion Protein **b** and Catalase-related Domain**—Incubations with 5 nM fusion protein **b** were conducted at room temperature using 100  $\mu\text{M}$  AA in a 50 mM Tris (pH 8.0) buffer containing 100 mM NaCl and 1 mM CaCl<sub>2</sub> in a quartz cuvette. The change in the absorbance was recorded by repetitive scanning (200–350 nm) using a Lambda-35 UV-visible spectrometer (PerkinElmer Life Sciences). Alternative substrates, eicosapentaenoic acid (20:5 $\omega$ 3), docosahexaenoic acid (22:6 $\omega$ 3), and 5,8,11-eicosatrienoic acid (20:3 $\omega$ 9) (Cayman Chemical Co.), were tested in parallel. Identical incubations with 5 nM catalase-related domain (the presence of CaCl<sub>2</sub> in the incubation is not essential) were performed using 100  $\mu\text{M}$  8R-HpETE as a substrate, and the disappearance of a conjugated diene chromophore ( $\epsilon \sim 25,000 \text{ M}^{-1} \text{ cm}^{-1}$ ) was recorded at 235 nm. The substrate specificities with 8RS-, 11RS-, and 11R-HpETE were examined in parallel.

To analyze the primary products formed, reactions with 8R-HpETE and the catalase-related domain were stopped with the addition of the reducing agent NaBH<sub>4</sub> (0.5 mg of NaBH<sub>4</sub> per 1 ml of buffer). The reaction was acidified down to pH 4 and loaded on a 1-cc Oasis HLB cartridge (Waters), eluted with 1 ml of MeOH, and stored at -80 °C for further analysis. Products were taken to dryness and dissolved in a corresponding column solvent before the HPLC analyses.

To analyze the oxygen incorporation from the substrate, incubations with 0.3 mM  $^{18}\text{O}_2$ -8R-HpETE and 24  $\mu\text{M}$  catalase-related domain were performed in a 1-ml ice-cold incubation buffer either for 30 s or for 2 min on ice. In addition, reactions with 24  $\mu\text{M}$  catalase domain and 2 mM 8R-HpETE in a 0.2-ml ice-cold buffer (50 mM Tris (pH 8.0), 100 mM NaCl) containing 0.1 ml H<sub>2</sub><sup>18</sup>O were carried out for 30 s on ice. Control reactions with the unlabeled substrate and water were conducted in parallel. All reactions were stopped by adding NaBH<sub>4</sub>.

**Carbon Monoxide Binding of Ferrous catalase-related Domain**—The ferrous state of the catalase-related domain of fusion protein **b** was generated by the addition of sodium dithionite into a 1-ml quartz cuvette containing 1  $\mu\text{M}$  ferric catalase-related domain in the incubation buffer. A ferrous-CO complex was prepared by bubbling CO gas into the cuvette for 2 min. The change in the chromophore of the Soret band (406 nm; ferric cHPL) to a ferrous-CO complex was observed using UV-visible spectrometer scanning at 200–700 nm.

**HPLC Analyses**—Non-reduced and NaBH<sub>4</sub>-reduced products were analyzed by RP-HPLC using a C18 Waters Symmetry 5- $\mu\text{m}$  column (46  $\times$  250 mm) with a CH<sub>3</sub>CN/H<sub>2</sub>O/glacial acetic acid solvent system (gradient: 20:80:0.01 to 80:20:0.01 by

volume for 30 min; isocratic: 80:20:0.01 by volume for 10 min) at a flow rate of 1 ml/min. UV signals at 205, 220, 235, and 270 nm were recorded using an Agilent 1100 series diode array detector. For the  $^1\text{H}$  NMR analysis, products formed from 2 mg of substrate were extracted on a 6-cc Agilent Bond Elut C18 column and isolated on RP-HPLC using the same solvent system as described previously. Additional purification was performed on SP-HPLC using a Thomson silica 5- $\mu\text{m}$  column (4.6  $\times$  250 mm) with a hexane/isopropyl alcohol/glacial acetic acid column solvent (100:3:0.01 and 100:10:0.01 by volume for polar and less polar compounds, respectively) at a flow rate of 1 ml/min. Isolated products were dissolved in MeOH and stored at  $-80^\circ\text{C}$  until further analyses.

**RP-HPLC-MS and NMR Analyses**—Products formed from 8R-HpETE by catalase domain were separated on RP-HPLC using a Kinetex C18 2.6- $\mu\text{m}$  column (3  $\times$  100 mm) with  $\text{CH}_3\text{CN}/\text{H}_2\text{O}/\text{HAc}$  (45:55:0.01, by volume) at 0.4 ml/min, and molecular weights were established from the M-H anions measured by negative ion electrospray LTQ1 iontrap LC-MS instrument.

The products formed from  $^{18}\text{O}$ -labeled 8R-HpETE by the catalase-related domain were eluted on RP-HPLC/MS using a Kinetex C18 2.6- $\mu\text{m}$  (3  $\times$  100 mm) column with a MeOH/ $\text{H}_2\text{O}/\text{HAc}$  solvent system containing 10 mM  $\text{NH}_4\text{OAc}$ , 0.1% AcOH, and 100  $\mu\text{M}$   $\text{AgBF}_4$  (gradient: 60:40:0.01 to 90:10:0.01 (MeOH/ $\text{H}_2\text{O}/\text{HAc}$ ) by volume with a flow rate of 0.2 ml/min for 5 min; isocratic: 90:10:0.01 by volume with a flow rate of 0.3 ml/min). The molecular weights were established from the formed silver adducts using silver coordination on double bonds and the M-H $^+$  cation measured by positive ion electrospray Quantum3 LC-MS instrument.

$^1\text{H}$  NMR and  $^1\text{H}$ ,  $^1\text{H}$  COSY NMR spectra were recorded on a Bruker 600-MHz spectrometer at 298 K. The parts/million values are reported relative to residual non-deuterated  $\text{C}_6\text{D}_6$  ( $\delta = 7.16$ ) and  $\text{CDCl}_3$  ( $\delta = 7.24$ ) for non-reduced and  $\text{NaBH}_4$ -reduced products, respectively. All spectra were analyzed on TopSpin 3.0 software (Bruker).

## Results

**Heterologous Expression of a Novel Catalase-Lipoxygenase Fusion Protein**—The *C. imbricata* catalase-lipoxygenase fusion cDNA including an N-terminal His tag was cloned into the expression vector pET11a, and the 122-kDa protein was expressed in *E. coli* BL21(DE3) with a 1-mg yield of active protein per liter under the conditions described under “Experimental Procedures.” The catalase-domain (43 kDa) alone was expressed similarly, obtaining the same yield and activity (Fig. 1). The UV-visible spectrum shows the main Soret band at 406 nm, typical of a high spin ferric catalase (Fig. 1). The absorbance shifted to 427 nm in the CO complex of the dithionite-reduced (ferrous) enzyme, a value close to the reported lambda max of the *P. homomalla* CO complex of ferrous-cAOS (427 nm) (18, 19).

**Characterization of the Catalytic Specificity of the LOX Domain**—The 8-HpETE formed by *C. imbricata* cHPL-LOX was chromatographed on a Chiralcel OD-H chiral column as the HETE methyl ester derivative as described under “Experimental Procedures.” The retention time of the methyl ester of

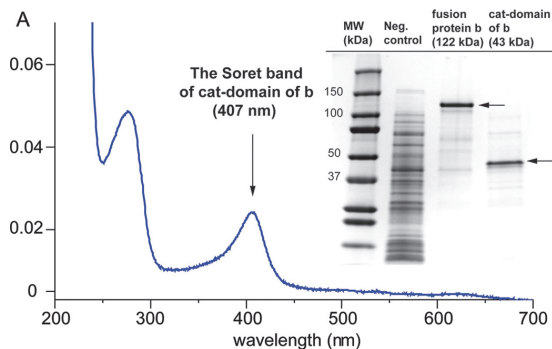


**FIGURE 1. The UV-visible spectrum of catalase-related domain of fusion protein **b** and the SDS-PAGE gel image of expressed fusion protein **b** and catalase domain.** *cat-domain of b*, the catalase-related domain of fusion protein **b**.

8-HETE at 15 min corresponds to the 8R enantiomer formed by *G. fruticosa* 8R-LOX. The chromatogram of the racemic 8-HETE standard analyzed on chiral SP-HPLC appeared in two peaks, the first peak being 8R and the second peak 8S (10), with retention times at 15 and 18 min, respectively. The methyl ester of 8-HETE co-chromatographed with the racemic 8-HETE standard resulted in an increase of the first peak (data not shown). Therefore, co-elution of the *C. imbricata* fusion protein **b**-derived 8-HETE with the references of 8R enantiomer confirms the specificity of the 8R-LOX domain.

**HPLC Analyses of Products of the Catalase-related Domain**—Incubations of 8R-HpETE with the His-tagged fusion protein **b** or its catalase-only domain resulted in the disappearance of the conjugated diene chromophore of 8R-HpETE and the formation of end products with weak or negligible UV absorbance (Fig. 2). In addition, *C. imbricata* fusion protein **b** converts the substrate analogue 5,8,11-eicosatrienoic acid and naturally occurring eicosapentaenoic acid and docosahexaenoic acid similarly to AA (data not shown). Among arachidonate-derived substrates, the expressed catalase-related domain was specific for 8R-HpETE and did not measurably metabolize 8RS-HpETE (8S being inhibitory) or 11R- and 11RS-HpETE. The  $k_{\text{cat}}$  and  $K_m$  of cHPL with 8R-HpETE were determined as  $133 \pm 5 \text{ s}^{-1}$  and  $3.8 \pm 0.5 \mu\text{M}$ , respectively, with a  $k_{\text{cat}}/K_m$  value of  $35 \mu\text{M}^{-1} \text{ s}^{-1}$ .

RP-HPLC analysis of the products from 8R-HpETE consistently showed the appearance of two very broad UV-205-nm absorbing areas on the chromatogram followed in both cases by a sharp 220-nm peak (Fig. 3A). It became apparent (as explained below) that the primary enzymatic products were represented by the exceptionally broad peaks labeled **1** and **2** on Fig. 3A and that the sharp peaks labeled **3** and **4** eluting at  $\sim 8$  and 37 min were actually formed via non-enzymatic isomerization of **1** and **2**, respectively. It was evident at this stage that the catalase domain exhibited a novel activity as no allene oxide-derived  $\alpha$ -ketol or cyclopentenone was detected. It was also established that the products were formed by the chain cleavage of 8R-HpETE because after incubation and extraction of an incubation of  $[1-^{14}\text{C}]$ -AA with fusion protein **b**, the  $^{14}\text{C}$  label was retained only in the early eluting product **3**, and product **4** was unlabeled (16).

## Catalase-related Fatty Acid Hydroperoxide Lyase

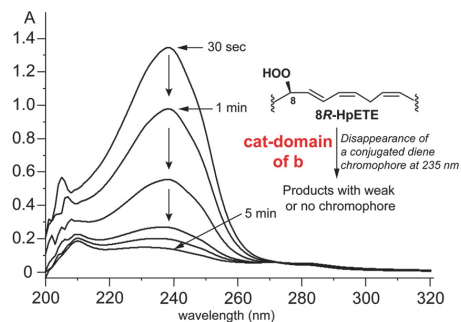


**FIGURE 2. Repetitive UV scans illustrating the transformation of 8R-HpETE by the catalase-related domain of *C. imbricata* fusion protein **b**.** The transformation is associated with the disappearance of the conjugated diene chromophore of 8R-HpETE and gives a product(s) with weak or no chromophore. *cat-domain* of **b**, the catalase-related domain of fusion protein **b**.

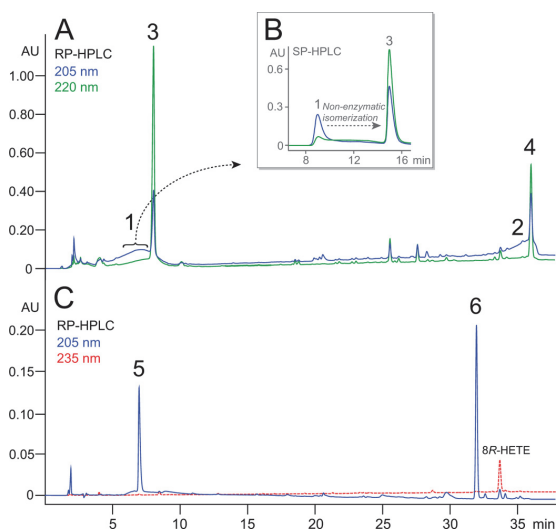


**FIGURE 3. HPLC analyses of products of the catalase domain of **b** reacting with 8R-HpETE.** **A**, RP-HPLC chromatogram of the product profile monitored at 205 nm (blue line, showing broad peaks **1** and **2**) and 235 nm (green line, sharp peaks of products **3** and **4**). **B**, inset, SP-HPLC chromatogram illustrating the non-enzymatic isomerization of isolated product **1** to product **3**. **C**, RP-HPLC chromatogram of the products of *in situ* NaBH<sub>4</sub> reduction of the enzymatic incubation, producing **5** and **6** (blue line) as alcohol derivatives of products **1** and **2**, respectively, with 8R-HETE (reduced substrate) eluting at 34 min and detected at 235 nm (red line). The RP-HPLC analyses used a C18 Waters Symmetry 5- $\mu$ m column (4.6  $\times$  250 mm) at a flow rate of 1 ml/min with a solvent gradient of CH<sub>3</sub>CN/H<sub>2</sub>O/glacial acetic acid in the proportions 20:80:0.01 to 80:20:0.01 (by volume) over 30 min then held isocratically for 10 min. UV signals at 205, 220, 235, and 270 nm were recorded using an Agilent 1100 series diode array detector. The SP-HPLC in panel **B** used a Thomson silica 5- $\mu$ m column (4.6  $\times$  250 mm) with hexane/isopropyl alcohol/glacial acetic acid solvent (100:10:0.01, by volume) and a flow rate of 1 ml/min. AU, absorbance units.

Once it became apparent that the broad peaks **1** and **2** were a consistent feature of the product profile, product **1** was collected from the initial RP-HPLC run and re-chromatographed on SP-HPLC, (Fig. 3B). This clearly showed that product **1** was converting to **3** and, indeed, the elevated baseline between the peaks reflected this transformation in progress (Fig. 3B). Initial

**TABLE 1**

**<sup>1</sup>H NMR chemical shifts ( $\delta$ ) and coupling constants (Hz) of C8-oxo acid (product **3**)**

NMR analysis was conducted using C<sub>6</sub>D<sub>6</sub> solvent.

Hydrogens	Chemical shift ( $\delta$ )	Coupling constant (Hz)	Multiplicity	Number of protons
H8	9.27	$J_{8,7} = 7.6$	d	1
H7	5.81	$J_{7,6} = 15.6$ (trans) $J_{7,8} = 7.6$	dd	1
H6	5.89	$J_{6,5} = 6.5$ $J_{6,7} = 15.6$ (trans)	dt	1
H5	1.52	$J_{5,4} = 14.9$ $J_{5,6} = 7.2$	dd	2
H4	0.88	$J_{4,3} = 7.8$ $J_{4,5} = 15.4$	m	2
H3	1.18	$J_{3,2} = 15.5$ $J_{3,4} = 7.7$	m	2
H2	1.85	$J_{3,4} = 14.6$	t	2

characterization of the stable products **3** and **4** showed that they each displayed a conjugated enone chromophore (lambda max 225 nm in acetonitrile). The facile isomerization of **1** and **2** would be readily explained by a double bond isomerization to form the conjugated enone systems of **3** and **4**. To prevent this from occurring, an incubation of 8R-HpETE with the catalase domain was terminated by the addition of NaBH<sub>4</sub> *in situ*, and the resulting products were analyzed by RP-HPLC (Fig. 3C); this revealed two new products, designated **5** and **6**, with stable chromatographic characteristics and displaying only 205-nm UV absorbance.

**LC-MS and NMR Analyses**—Negative ion electrospray LC-MS analysis of product **3** gave an M-1 ion at *m/z* 155, corresponding to the predicted mass of an oxo-octenoic acid, whereas product **4** was undetectable. Product **3** was identified by NMR (Table 1). The doublet at 9.27 ppm (H8) represents the C-8 aldehydic proton, which is coupled to H7 at 5.81 ppm with a  $J_{5,6}$  coupling of 15.6 Hz to H6 (5.89 ppm) defining the 6,7-trans double bond and the conjugated enone system (Fig. 4A). These data and the remaining signals established the structure of **3** as (6*E*)-8-oxo-octenoic acid. Due to volatility and solubility issues, the purification of product **4** for NMR analysis was unsuccessful, and its structure was deduced as the corresponding conjugated C<sub>12</sub> aldehyde, 1-oxo-2*E*,6*Z*-dodecene, from its UV spectral characteristics and by silver-coordinated LC-MS and NMR analyses of the corresponding C<sub>12</sub> NaBH<sub>4</sub>-reduced fragment.

**Identification of Products 5 and 6**—The NaBH<sub>4</sub>-reduced products **5** and **6** (Fig. 3C) were identified by NMR (Table 2). In the spectrum of product **5** (Table 2, left), the triplet at 3.64 ppm had an area of two, representing the geminal C-8 hydrogens, and indicating a primary alcohol. The same applies to the hydroxyl of **6** (H-1 at 3.64 ppm; Table 2, right). Most significantly, in each case the primary alcohols were coupled to a CH<sub>2</sub> moiety, which in turn is coupled to a *cis* double bond (10.9 Hz; *cis*); Fig. 4B. Together with the rest of the NMR data, the structures of **5** and **6** were thus established as (5*Z*)-8-hydroxy-octenoic acid and (3*Z*,6*Z*)-dodecadien-1-ol, respectively. It follows that the primary products of the catalase domain detected as the broad peaks at 205 nm, products **1** and **2**, were the corresponding aldehydes, (5*Z*)-8-oxo-octenoic acid and (3*Z*,6*Z*)-1-oxo-dodecadien-1-ol. The results establish that the *C. imbricata* catalase domain



of fusion protein **b** displays a novel hydroperoxide lyase activity and that it can be designated as a cHPL, catalase-related hydroperoxide lyase.

**Isotopic Analyses of Products Formed by cHPL**—Incubations with  $^{18}\text{O}_2$ -labeled 8*R*-HpETE were conducted to define the oxygen incorporation in products and describe the reaction mechanism of cHPL. As aldehydes readily exchange oxygen with water, 30-s incubations with  $^{18}\text{O}_2$ -labeled 8*R*-HpETE and cHPL were conducted on ice, and the primary aldehydes were analyzed after *in situ* reduction with  $\text{NaBH}_4$  to the corresponding alcohols. The incorporation of  $^{18}\text{O}$  in the C8-hydroxy acid and C12-alcohol was determined by LC-MS analyses using a

silver coordination methodology that produces ionization of any alkene-containing molecule (20). The two isotopes of silver (107 and 109) were almost equally represented, giving doublets of ions for the silver adducts of (5*Z*)-8-hydroxy acid and (3*Z*,6*Z*)-dodecadien-1-ol at 265/267 and 289/291, respectively, and 267/269 and 291/293 for the corresponding  $^{18}\text{O}$ -labeled ions. Additional ions were observed for the ammonium adducts ( $[\text{M}+18]^+$ ) with the carboxyl of the C8-hydroxy acid with predicted  $m/z$  for the unlabeled and  $^{18}\text{O}$ -labeled species of 176 and 178, respectively.

LC-MS analyses revealed that incubations with  $^{18}\text{O}$ -labeled 8*R*-HpETE resulted in the formation of  $^{18}\text{O}$ -incorporated C8-hydroxy acid (having  $m/z$  of 267/269, respective to silver adducts, and  $m/z$  of 178, respective to the  $\text{NH}_4^+$  adduct) (Fig. 4C) and C12-alcohol ( $m/z$  of 291/293 respective to silver adducts) (Fig. 5D). The C8-hydroxy acid and C12-alcohol

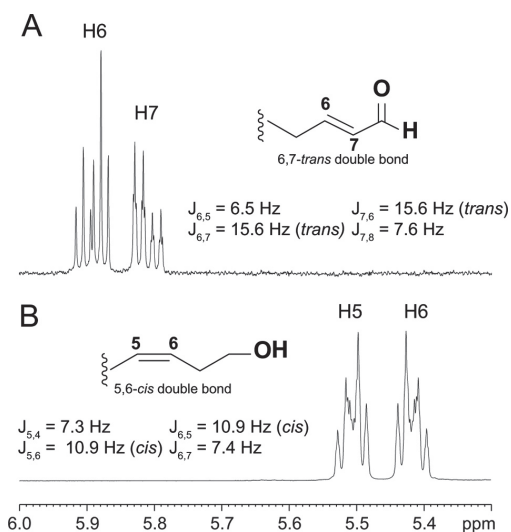


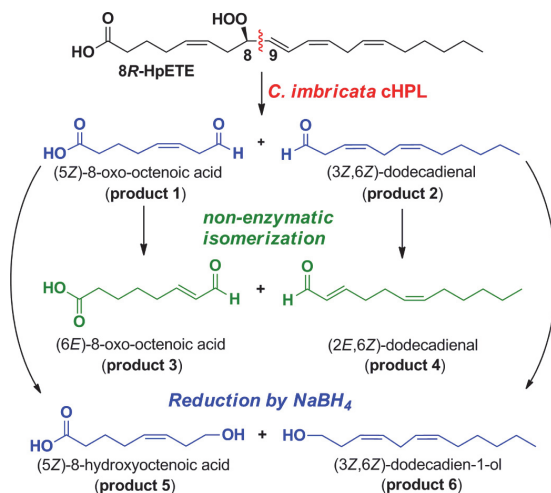
FIGURE 4.  $^1\text{H}$  NMR one-dimensional spectra of double bond region of (6*E*)-8-oxo-octenoic acid (A) and (5*Z*)-8-hydroxy acid (B). Coupling constants between H6 and H7 (A) and H5 and H6 (B) describe the stereo configuration of the corresponding double bond. The (6*E*)-8-oxo-octenoic acid (A) represents isomerized product from primary (6*E*)-8-oxo-octenoic acid, which is analyzed as C8-hydroxy acid derivative (B). C8-oxo acid (A) and C8-hydroxy acid (B) were analyzed in  $\text{C}_6\text{D}_6$  and  $\text{CDCl}_3$  solvents, respectively.

TABLE 2

$^1\text{H}$  NMR chemical shifts ( $\delta$ ) and coupling constants (Hz) of C12-hydroxy acid (left) and C12-alcohol (right)

NMR analysis was conducted using a  $\text{CDCl}_3$  solvent (left and right).

C8-hydroxy acid (product 5)					C12 alcohol (product 6)				
Hydrogens	Chemical shift ( $\delta$ )	Coupling constant (Hz)	Multiplicity	Number of protons	Hydrogens	Chemical shift ( $\delta$ )	Coupling constant (Hz)	Multiplicity	Number of protons
H8	3.64	$J_{8,7} = 12.9$	t	2	H12	0.87	$J_{12,11} = 6.7$	t	3
H7	2.31	$J_{7,6} = 6.8$	q	2	H9	1.35	$J_{9,8} = 7.1$	m	2
H6	5.42	$J_{6,5} = 10.9$ (cis)	m	1	H8	2.03	$J_{8,7} = 7.3$	q	2
H5	5.51	$J_{6,7} = 7.4$	m	1	H7	5.38	$J_{8,9} = 7.2$	m	1
H4	2.13	$J_{5,4} = 7.3$	q	2	H6	5.31	$J_{7,6} = 10.9$ (cis)	dt	1
H3	1.71	$J_{5,6} = 10.9$ (cis)	m	2	H5	2.81	$J_{6,7} = 7.3$	t	2
H2	2.35	$J_{4,3} = 14.6$	t	2	H4	5.52	$J_{7,8} = 10.6$ (cis)	dt	1
		$J_{4,5} = 7.3$			H3	5.38	$J_{6,5} = 7.1$	m	1
		$J_{3,2} = 7.3$			H2	2.43	$J_{5,6} = 7.3$	q	2
		$J_{3,4} = 14.7$			H1	3.64	$J_{5,4} = 7.3$	t	2
		$J_{3,2} = 14.6$					$J_{4,5} = 7.4$		
							$J_{4,3} = 10.7$ (cis)		
							$J_{3,4} = 10.7$ (cis)		
							$J_{3,2} = 7.3$		
							$J_{2,1} = 13.4$		
							$J_{2,3} = 6.8$		
							$J_{1,2} = 6.5$		



SCHEME 1. The representation of product formation by cHPL. Primary products (product 1 and 2; blue) were identified as alcohol derivatives (product 5 and 6; blue). The secondary products (isomerized; product 3 and 4) are presented as green.

## Catalase-related Fatty Acid Hydroperoxide Lyase

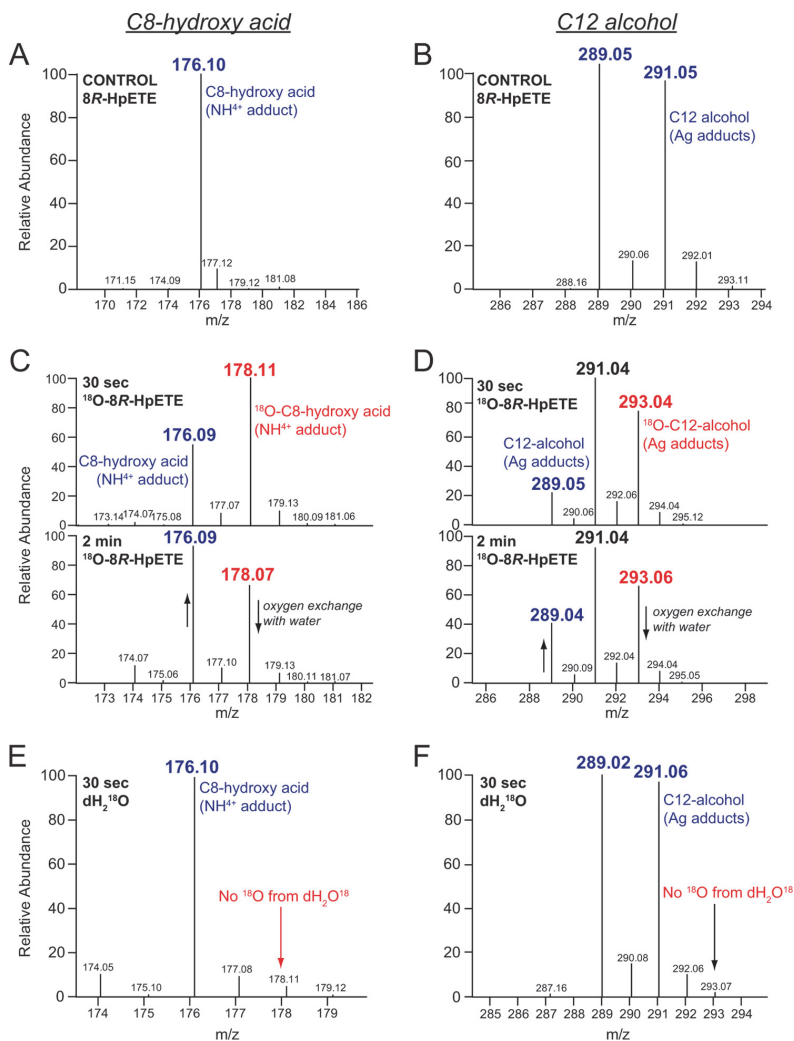


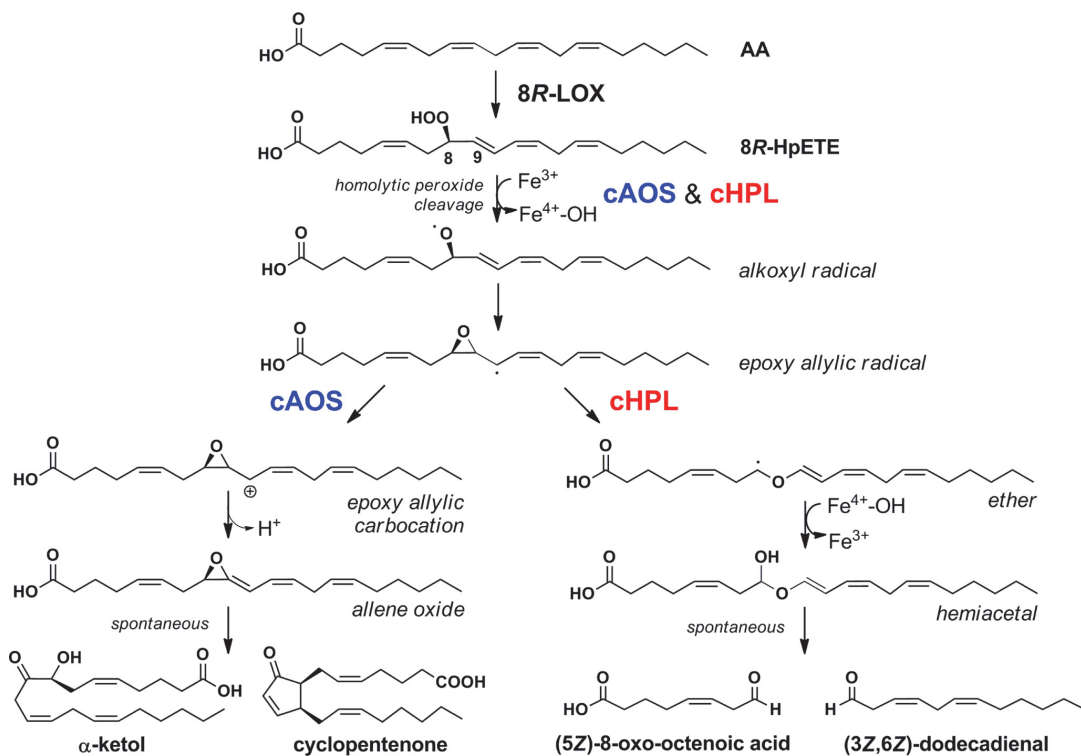
FIGURE 5. LC-MS analysis of  $^{18}\text{O}$  incorporation in the  $\text{NaBH}_4$ -reduced products of *C. imbricata* cHPL. The left panels illustrate the  $\text{NH}_4^+$  adduct ions of the C8-hydroxy acid (panels A, C, and E) and the right panels show the doublet of  $\text{Ag}^+$  adduct ions of the C12 alcohol (panels B, D, and F). A and B, the ion profiles from 30-s incubation of cHPL with unlabeled 8R-HpETE. C and D, after incubation of cHPL with  $^{18}\text{O}$ -labeled 8R-HpETE for 30 s or 2 min, illustrating  $^{18}\text{O}$  incorporation and the partial loss of  $^{18}\text{O}$  in the 2 min incubation. E and F, the ion profiles from the incubation of cHPL with unlabeled 8R-HpETE in the presence of  $^{18}\text{O}$ -labeled water. For clarity, only  $\text{NH}_4^+$  adducts of the C8-hydroxy acid are shown. The  $^{16}\text{O}$ - and  $^{18}\text{O}$ -containing products are presented as blue and red, respectively.

formed in a  $\text{H}_2^{18}\text{O}$ -containing buffer (Fig. 5, E and F, respectively) did not contain any oxygen-18 isotope and were identical to the control incubations (Fig. 5, A and B, respectively). The altered ratios of  $^{16}\text{O}$  and  $^{18}\text{O}$  in C8-hydroxy acid and C12-alcohol after longer incubation (2 min instead of 30 s) illustrate the time dependence in oxygen exchange between the aldehydes and water (Figs. 5C and 4D). These results establish that the hydroperoxy oxygens of 8R-HpETE are retained in the two aldehydic fragments, a mechanism consistent with the conversion of 8R-HpETE to a hemiacetal derivative that spontaneously breaks down to the two-chain cleavage products (21).

## Discussion

Currently, although individual lipoxygenases have been described in corals (22–25), only 8R-LOX seems to be associated with a catalase-related/LOX fusion protein (9, 10, 16). The structural analysis of the *P. homomalla* cAOS domain of the cAOS-LOX fusion protein revealed that conservation of the catalase core structure (14) and the most significant catalase-related residues are also present in cHPL, thus expanding the diversity of heme-containing catalase-related enzymes in the fatty acid hydroperoxide metabolism. Illustrating the independence of both domains, the separately

## Catalase-related Fatty Acid Hydroperoxide Lyase



expressed *P. homomalla* AOS-LOX domains each retained activity (11), and a similar functional independence of the two domains of the cHPL-LOX was shown here. The covalent linkage of cHPL with 8R-LOX probably helps to target the fusion protein into membranes, assuring the close proximity of the component domains to the newly released arachidonic acid substrate, as demonstrated with cAOS-LOX (26).

We determined the catalytic efficiency ( $k_{\text{cat}}/K_m$ ) of the *C. imbricata* cHPL as  $35 \mu\text{M}^{-1} \text{s}^{-1}$ , which is similar to the *P. homomalla* cAOS,  $31 \mu\text{M}^{-1} \text{s}^{-1}$  (11). The catalytic efficiency of the plant cytochrome P450 HPL (CYP74) can be highly variable, depending on the inclusion of detergents. For example, for a *Medicago truncatula* CYP74 HPL with its optimal substrate 13S-hydroperoxy-C18:3 $\omega$ 3, the  $k_{\text{cat}}/K_m$  varied from 3 to  $151 \mu\text{M}^{-1} \text{s}^{-1}$  in the presence and absence of detergent, respectively (27). Although the enzymatic efficiency of HPLs are comparable, the turnover numbers reported for the CYP74 HPLs are an order of magnitude higher than for the *C. imbricata* cHPL (28–31).

**Reaction Mechanism of cHPL**—Our evidence indicates that the coral cHPL catalyzes the C8-oxo acid and C12-aldehyde formation from 8R-HpETE in a route preceded by cytochrome P450 HPL enzymes. It is generally agreed that plant P450 CYP74 family enzymes homolytically cleave the fatty acid hydroperoxide moiety to form an epoxyallylic carbon radical intermediate from which a number of biosynthetic outcomes

are known (3). These include allene oxide synthase and divinyl ether synthase transformations (2, 3, 32). In the third possibility, the HPL route, the rearrangement leads to a covalently complete yet unstable final product, a full-length fatty acid hemiacetal, which through spontaneous decomposition gives the two short-chain aldehydic products (21, 33). The equivalent pathway for the coral cHPL is illustrated in Scheme 2. The ferric cHPL enzyme catalyzes a homolytic cleavage of the 8R-hydroperoxy group with oxidation of the heme to Compound II ( $\text{Fe}^{4+}\text{-OH}$ ). The fatty acid alkoxy radical cyclizes to an epoxy allylic radical. At this point the steps promoted by cAOS or cHPL diverge. cAOS stabilizes the carbocation formation and catalyzes the hydrogen abstraction, which results in the formation of allene oxide (Scheme 2, left side). cHPL stabilizes the epoxy allylic radical and initiates the cleavage of C8-C9-bond in the epoxy group, which results in an allylic ether radical formation. The oxygen rebound from Compound II gives rise to a hemiacetal intermediate. Our isotopic analysis and results by Grechkin and co-workers (21, 33) clearly demonstrate that water is not involved in this process and that both of the original hydroperoxide oxygens are retained in the products. Notably, the chain cleavage in the P450 and cHPL type of fatty acid hydroperoxide lyase occurs within the original pentadiene of the fatty acid hydroperoxide, between C8 and C9 in the case of coral cHPL.

**Technical Challenges in the HPLC Analysis of 3Z-Aldehydes**—In our study we observed exceptionally adverse chromatographic behavior of the two primary cHPL products,

## Catalase-related Fatty Acid Hydroperoxide Lyase

each containing an aldehydic moiety with a 3Z double bond. On RP-HPLC each primary product ran as an abnormal broad band rather than as a distinct peak (Fig. 3), and poor performance was observed also on SP-HPLC (Fig. 3B). Although we could attribute this anomalous performance partly to isomerization to the conjugated enal (the corresponding 2E-aldehydic isomer), our impression is that this is not the only issue. The broad bands on RP-HPLC do not show the characteristic enal chromophore of the 2E-aldehydes, suggesting that some adverse interaction of the 3Z-aldehydes occurs with the HPLC solvent and stationary phase. One of us has prior experience with the HPLC of an authentic sample of a plant CYP74B lyase product (3Z-non-enal) (31), and the same phenomenon was evident, suggesting it is general to the 3Z-aldehydes. As volatile molecules, 3Z-aldehydes are commonly detected among short-chain fragments of fatty acids, and there is very substantial literature on their analysis. However, the chromatographic analyses are typically restricted to gas chromatography in which the chromatographic behavior is quite normal. To the best of our knowledge the adverse HPLC characteristics of the 3Z-aldehydes have not been generally recognized or reported.

**A Contrasting Route to Fatty Acid Chain Cleavage**—The coral cHPL is unique in the animal kingdom. The mechanism and products of transformation are distinct from unrelated enzymatic and non-enzymatic lyase reactions that produce chain cleavage between the hydroperoxide-bearing carbon and the CH<sub>2</sub> moiety in the  $\alpha$  position outside the original penta-diene. To give an example of the latter involving the identical fatty acid hydroperoxide substrate, 8R-HpETE, whereas cHPL gives rise to C8 and C12 aldehydes, there is an uncharacterized lyase activity in starfish oocytes that cleaves the carbon chain between C7 and C8, producing a C7-aldehyde acid and C13 aldehyde (34). Non-enzymatic transformation by free heme favors a similar pathway (e.g. Refs. 35 and 36). This alternative type of lyase reaction is known to be initiated by LOX enzymes and is facilitated under anaerobic conditions (37, 38). Examples include the reactions of porcine leukocyte 12-LOX (39) and rabbit leukocytes (40) and the lipoxygenase-lyase pathway in the moss *Physcomitrella patens* (41).

**Biological Significance of HPL Metabolism**—The AA-derived C8-oxo acid and C12-aldehyde with their isomerized derivatives are potential biologically active signal mediators in corals. In plants, the HPL-derived green leaf volatiles are shown as mediators in abiotic and biotic stress (42). The (3Z)-hexenal and 12-oxo-*cis*-dodecenoic acid formed by 13-HPL have the capability to isomerize non-enzymatically (43) or by the isomerases (44, 45) to biologically active forms, 2E-hexenal and 12-oxo-*trans*-dodecenoic acid (also known as traumatin), respectively. Traumatin plays an important role in plant wound healing (46), and 2(E)-hexenal induces the expression of HPL, AOS, LOX (47, 48), and other stress genes in plants (49). Moreover, the electrophilic  $\alpha,\beta$ -unsaturated carbonyl group of aldehydes might interact with nucleophiles in biological systems (50, 51), and in plants, antimicrobial properties of oxylipins including 2(E)-hexenal have been presented by Prost *et al.* (52).

As mentioned in the Introduction, our previous studies detected what we termed the “unknown polar compounds” in *C. imbricata* that were identified here as aldehydic products of

the cHPL-LOX. These products and the gene expression of the cHPL-LOX were measurable in coral samples under baseline conditions and after wounding (16) and thermal-induced stress (a change in sea water temperature from 23 °C to 28 °C or 31 °C) (53). In contrast to the increased gene expression of the cAOS-LOX fusion protein induced both by wounding and thermal stress, the gene expression of the cHPL-LOX was stable during these test conditions. There are few possible interpretations of this apparent lack of enhancement of the cHPL-LOX activity; (i) in contrast to its plant counterpart, the cHPL may not be involved in a response to mechanical injury, and (ii) given that plant oxylipin synthesis is activated within seconds or a few minutes of wounding (54, 55), a short-lived increase in the cHPL-LOX products may occur immediately after wounding, which has not been analyzed (16, 53). Activation of the plant HPL pathway is associated with changes in the expression of other defense genes (47, 49, 56), and equivalent experiments to explore effects of the coral lyase products are required to elucidate the role of cHPL-LOX pathway.

**Author Contributions**—T. T., H. L., A. R. B., and N. S. designed the study and wrote the paper. H. L. and T. T. cloned the constructs, and T. T. performed the experiments. MS experiments and analysis were conducted by T. T. and W. M. C. NMR analysis was conducted by T. T. and W. E. B. All authors reviewed the results and approved the final version of the manuscript.

## References

1. Tanabe, T., and Ullrich, V. (1995) Prostacyclin and thromboxane syntheses. *J. Lipid Mediat. Cell Signal.* **12**, 243–255
2. Grechkin, A. N. (2002) Hydroperoxide lyase and divinyl ether synthase. *Prostaglandins Other Lipid Mediat.* **68**, 457–470
3. Brash, A. R. (2009) Mechanistic aspects of CYP74 allene oxide synthases and related cytochrome P450 enzymes. *Phytochemistry* **70**, 1522–1531
4. Feussner, I., and Wasternack, C. (2002) The lipoxygenase pathway. *Annu. Rev. Plant Biol.* **53**, 275–297
5. Garscha, U., Jernerén, F., Chung, D., Keller, N. P., Hamberg, M., and Oliw, E. H. (2007) Identification of dioxygenases required for *Aspergillus* development: studies of products, stereochemistry, and the reaction mechanism. *J. Biol. Chem.* **282**, 34707–34718
6. Hoffmann, I., Jernerén, F., and Oliw, E. H. (2013) Expression of fusion proteins of *Aspergillus terreus* reveals a novel allene oxide synthase. *J. Biol. Chem.* **288**, 11459–11469
7. Brodhun, F., and Feussner, I. (2011) Oxylipins in fungi. *FEBS J.* **278**, 1047–1063
8. Tsiatsigiannis, D. I., and Keller, N. P. (2007) Oxylipins as developmental and host-fungal communication signals. *Trends Microbiol.* **15**, 109–118
9. Koljak, R., Boutaud, O., Shieh, B. H., Samel, N., and Brash, A. R. (1997) Identification of a naturally occurring peroxidase-lipoxygenase fusion protein. *Science* **277**, 1994–1996
10. Löhelaid, H., Järving, R., Valmsen, K., Varvas, K., Kreen, M., Järving, I., and Samel, N. (2008) Identification of a functional allene oxide synthase-lipoxygenase fusion protein in the soft coral *Gersemia fruticosa* suggests the generality of this pathway in octocorals. *Biochim. Biophys. Acta* **1780**, 315–321
11. Boutaud, O., and Brash, A. R. (1999) Purification and catalytic activities of the two domains of the allene oxide synthase-lipoxygenase fusion protein of the coral *Plexaura homomalla*. *J. Biol. Chem.* **274**, 33764–33770
12. Lee, D. S., Nioche, P., Hamberg, M., and Raman, C. S. (2008) Structural insights into the evolutionary paths of oxylipin biosynthetic enzymes. *Nature* **455**, 363–368
13. Li, L., Chang, Z., Pan, Z., Fu, Z. Q., and Wang, X. (2008) Modes of heme binding and substrate access for cytochrome P450 CYP74A revealed by

- crystal structures of allene oxide synthase. *Proc. Natl. Acad. Sci. U.S.A.* **105**, 13883–13888
14. Oldham, M. L., Brash, A. R., and Newcomer, M. E. (2005) The structure of coral allene oxide synthase reveals a catalase adapted for metabolism of a fatty acid hydroperoxide. *Proc. Natl. Acad. Sci. U.S.A.* **102**, 297–302
  15. Tosha, T., Uchida, T., Brash, A. R., and Kitagawa, T. (2006) On the relationship of coral allene oxide synthase to catalase: a single active site mutation that induces catalase activity in coral allene oxide synthase. *J. Biol. Chem.* **281**, 12610–12617
  16. Löhelaid, H., Teder, T., Töldsepp, K., Ekins, M., and Samel, N. (2014) Up-regulated expression of AOS-LOXa and increased eicosanoid synthesis in response to coral wounding. *PLoS ONE* **9**, e89215
  17. Brash, A. R., Niraula, N. P., Boeglin, W. E., and Mashhadi, Z. (2014) An ancient relative of cyclooxygenase in cyanobacteria is a linoleate 10S-dioxygenase that works in tandem with a catalase-related protein with specific 10S-hydroperoxide lyase activity. *J. Biol. Chem.* **289**, 13101–13111
  18. Abraham, B. D., Sono, M., Boutaud, O., Shriner, A., Dawson, J. H., Brash, A. R., and Gaffney, B. J. (2001) Characterization of the coral allene oxide synthase active site with UV-visible absorption, magnetic circular dichroism, and electron paramagnetic resonance spectroscopy: evidence for tyrosinate ligation to the ferric enzyme heme iron. *Biochemistry* **40**, 2251–2259
  19. Bandara, D. M., Sono, M., Bruce, G. S., Brash, A. R., and Dawson, J. H. (2011) Coordination modes of tyrosinate-ligated catalase-type heme enzymes: magnetic circular dichroism studies of *Plexaura homomalla* allene oxide synthase, *Mycobacterium avium* ssp. paratuberculosis protein-2744c, and bovine liver catalase in their ferric and ferrous states. *J. Inorg. Biochem.* **105**, 1786–1794
  20. Havrilla, M. C., and Hachey, D. L. P., N. A. (2000) Coordination ( $\text{Ag}^+$ ) ion spray-mass spectrometry of peroxidation products of cholesterol linoleate and cholesterol arachidonate: high-performance liquid chromatography-mass spectrometry analysis of peroxide products from polyunsaturated lipid autoxidation. *J. Am. Chem. Soc.* **122**, 8042–8055
  21. Grechkin, A. N., and Hamberg, M. (2004) The “heterolytic hydroperoxide lyase” is an isomerase producing a short-lived fatty acid hemiacetal. *Biochim. Biophys. Acta* **1636**, 47–58
  22. Eek, P., Järving, R., Järving, I., Gilbert, N. C., Newcomer, M. E., and Samel, N. (2012) Structure of a calcium-dependent 11R-lipoxygenase suggests a mechanism for  $\text{Ca}^{2+}$  regulation. *J. Biol. Chem.* **287**, 22377–22386
  23. Mortimer, M., Järving, R., Brash, A. R., Samel, N., and Järving, I. (2006) Identification and characterization of an arachidonate 11R-lipoxygenase. *Arch. Biochem. Biophys.* **445**, 147–155
  24. Järving, R., Löökene, A., Kurg, R., Siimon, L., Järving, I., and Samel, N. (2012) Activation of 11R-lipoxygenase is fully  $\text{Ca}^{2+}$ -dependent and controlled by the phospholipid composition of the target membrane. *Biochemistry* **51**, 3310–3320
  25. Brash, A. R., Boeglin, W. E., Chang, M. S., and Shieh, B. H. (1996) Purification and molecular cloning of an 8R-lipoxygenase from the coral *Plexaura homomalla* reveal the related primary structures of R- and S-lipoxygenases. *J. Biol. Chem.* **271**, 20949–20957
  26. Gilbert, N. C., Niebuhr, M., Tsuruta, H., Bordelon, T., Ridderbusch, O., Dassey, A., Brash, A. R., Bartlett, S. G., and Newcomer, M. E. (2008) A covalent linker allows for membrane targeting of an oxylipin biosynthetic complex. *Biochemistry* **47**, 10665–10676
  27. Hughes, R. K., Yousafzai, F. K., Ashton, R., Chechetkin, I. R., Fairhurst, S. A., Hamberg, M., and Casey, R. (2008) Evidence for communality in the primary determinants of CYP74 catalysis and of structural similarities between CYP74 and classical mammalian P450 enzymes. *Proteins* **72**, 1199–1211
  28. Noordermeer, M. A., Van Dijken, A. J., Smeekens, S. C., Veldink, G. A., and Vliegthart, J. F. (2000) Characterization of three cloned and expressed 13-hydroperoxide lyase isoenzymes from alfalfa with unusual N-terminal sequences and different enzyme kinetics. *Eur. J. Biochem.* **267**, 2473–2482
  29. Matsui, K., Ujita, C., Fujimoto, S., Wilkinson, J., Hiatt, B., Knauf, V., Kajiwara, T., and Feussner, I. (2000) Fatty acid 9- and 13-hydroperoxide lyases from cucumber. *FEBS Lett.* **481**, 183–188
  30. Matsui, K., Miyahara, C., Wilkinson, J., Hiatt, B., Knauf, V., and Kajiwara, T. (2000) Fatty acid hydroperoxide lyase in tomato fruits: cloning and properties of a recombinant enzyme expressed in *Escherichia coli*. *Biosci. Biotechnol. Biochem.* **64**, 1189–1196
  31. Tijet, N., Schneider, C., Muller, B. L., and Brash, A. R. (2001) Biogenesis of volatile aldehydes from fatty acid hydroperoxides: molecular cloning of a hydroperoxide lyase (CYP74C) with specificity for both the 9- and 13-hydroperoxides of linoleic and linolenic acids. *Arch. Biochem. Biophys.* **386**, 281–289
  32. Hamberg, M. (1989) Fatty acid allene oxides. *J. Am. Oil Chem. Soc.* **66**, 1445–1449
  33. Grechkin, A. N., Brühlmann, F., Mukhtarova, L. S., Gogolev, Y. V., and Hamberg, M. (2006) Hydroperoxide lyases (CYP74C and CYP74B) catalyze the homolytic isomerization of fatty acid hydroperoxides into hemiacetals. *Biochim. Biophys. Acta* **1761**, 1419–1428
  34. Brash, A. R., Hughes, M. A., Hawkins, D. J., Boeglin, W. E., Song, W. C., and Meijer, L. (1991) Allene oxide and aldehyde biosynthesis in starfish oocytes. *J. Biol. Chem.* **266**, 22926–22931
  35. Gardner, H. W. (1989) Oxygen radical chemistry of polyunsaturated fatty acids. *Free Radic. Biol. Med.* **7**, 65–86
  36. Labeque, R., and Marnett, L. J. (1988) Reaction of hematin with allylic fatty acid hydroperoxides: identification of products and implications for pathways of hydroperoxide-dependent epoxidation of 7,8-dihydroxy-7,8-dihydrobenzo[a]pyrene. *Biochemistry* **27**, 7060–7070
  37. Garssen, G. J., Vliegthart, J. F., and Boldingh, J. (1971) An anaerobic reaction between lipoxygenase, linoleic acid, and its hydroperoxides. *Biochem. J.* **122**, 327–332
  38. Garssen, G. J., Vliegthart, J. F., and Boldingh, J. (1972) The origin and structures of dimeric fatty acids from the anaerobic reaction between soya-bean lipoxygenase, linoleic acid, and its hydroperoxide. *Biochem. J.* **130**, 435–442
  39. Glasgow, W. C., Harris, T. M., and Brash, A. R. (1986) A short-chain aldehyde is a major lipoxygenase product in arachidonic acid-stimulated porcine leukocytes. *J. Biol. Chem.* **261**, 200–204
  40. Lam, B. K., Linh, Y. L., Ho, H. Y., and Wong, P. Y. (1987) Hydroperoxide lyase in rabbit leukocytes: conversion of 15-hydroperoxyeicosatetraenoic acid to 15-keto-pentadeca-5,8,11,13-tetraenoic acid. *Biochem. Biophys. Res. Commun.* **149**, 1111–1117
  41. Wichard, T., Göbel, C., Feussner, I., and Pohnert, G. (2004) Unprecedented lipoxygenase/hydroperoxide lyase pathways in the moss *Physcomitrella patens*. *Angew. Chem. Int. Ed. Engl.* **44**, 158–161
  42. Matsui, K. (2006) Green leaf volatiles: hydroperoxide lyase pathway of oxylipin metabolism. *Curr. Opin. Plant Biol.* **9**, 274–280
  43. Noordermeer, M. A., Van Der Goot, W., Van Kooij, A. J., Veldsink, J. W., Veldink, G. A., and Vliegthart, J. F. (2002) Development of a biocatalytic process for the production of C6-aldehydes from vegetable oils by soybean lipoxygenase and recombinant hydroperoxide lyase. *J. Agric. Food Chem.* **50**, 4270–4274
  44. Noordermeer, M. A., Veldink, G. A., and Vliegthart, J. F. (1999) Alfalfa contains substantial 9-hydroperoxide lyase activity and a 3Z:2E-enal isomerase. *FEBS Lett.* **443**, 201–204
  45. Takamura, H., and Gardner, H. W. (1996) Oxygenation of (3Z)-alkenal to (2E)-4-hydroxy-2-alkenal in soybean seed (*Glycine max* L.). *Biochim. Biophys. Acta* **1303**, 83–91
  46. Zimmerman, D. C., and Coudron, C. A. (1979) Identification of traumatin, a wound hormone, as 12-oxo-trans-10-dodecenoic acid. *Plant Physiol.* **63**, 536–541
  47. Bate, N. J., and Rothstein, S. J. (1998) C6-volatiles derived from the lipoxygenase pathway induce a subset of defense-related genes. *Plant J.* **16**, 561–569
  48. Gomi, K., Yamasaki, Y., Yamamoto, H., and Akimitsu, K. (2003) Characterization of a hydroperoxide lyase gene and effect of C6-volatiles on expression of genes of the oxylipin metabolism in citrus. *J. Plant Physiol.* **160**, 1219–1231
  49. Kishimoto, K., Matsui, K., Ozawa, R., and Takabayashi, J. (2005) Volatile C6-aldehydes and Allo-ocimene activate defense genes and induce resistance against *Botrytis cinerea* in *Arabidopsis thaliana*. *Plant Cell Physiol.* **46**, 1093–1102
  50. Farmer, E. E., and Davoine, C. (2007) Reactive electrophile species. *Curr. Opin. Plant Biol.* **10**, 380–386

## Catalase-related Fatty Acid Hydroperoxide Lyase

51. Mueller, M. J., and Berger, S. (2009) Reactive electrophilic oxylipins: pattern recognition and signalling. *Phytochemistry* **70**, 1511–1521
52. Prost, I., Dhondt, S., Rothe, G., Vicente, J., Rodriguez, M. J., Kift, N., Carbonne, F., Griffiths, G., Esquerré-Tugayé, M. T., Rosahl, S., Castresana, C., Hamberg, M., and Fournier, J. (2005) Evaluation of the antimicrobial activities of plant oxylipins supports their involvement in defense against pathogens. *Plant Physiol.* **139**, 1902–1913
53. Löhelaid, H., Teder, T., and Samel, N. (2015) Lipoxygenase-allene oxide synthase pathway in octocoral thermal stress response. *Coral Reefs* **34**, 143–154
54. D'Auria, J. C., Pichersky, E., Schaub, A., Hansel, A., and Gershenzon, J. (2007) Characterization of a BAHD acyltransferase responsible for producing the green leaf volatile (Z)-3-hexen-1-yl acetate in *Arabidopsis thaliana*. *Plant J.* **49**, 194–207
55. Glauser, G., Dubugnon, L., Mousavi, S. A., Rudaz, S., Wolfender, J. L., and Farmer, E. E. (2009) Velocity estimates for signal propagation leading to systemic jasmonic acid accumulation in wounded *Arabidopsis*. *J. Biol. Chem.* **284**, 34506–34513
56. Bate, N. J., Sivasankar, S., Moxon, C., Riley, J. M., Thompson, J. E., and Rothstein, S. J. (1998) Molecular characterization of an *Arabidopsis* gene encoding hydroperoxide lyase, a cytochrome P-450 that is wound inducible. *Plant Physiol.* **117**, 1393–1400

## PUBLICATION II

T. Teder, H. Lõhelaid, N. Samel

**Structural and functional insights into the reaction specificity of catalase-related hydroperoxide lyase: A shift from lyase activity to allene oxide synthase by site-directed mutagenesis**

*PLoS One* 12 (2017) e0185291





RESEARCH ARTICLE

# Structural and functional insights into the reaction specificity of catalase-related hydroperoxide lyase: A shift from lyase activity to allene oxide synthase by site-directed mutagenesis

Tarvi Teder, Helike Löhelaid, Nigulas Samel\*

Department of Chemistry and Biotechnology, Tallinn University of Technology, Tallinn, Estonia

\* [nigulas.samel@ttu.ee](mailto:nigulas.samel@ttu.ee)



**OPEN ACCESS**

**Citation:** Teder T, Löhelaid H, Samel N (2017) Structural and functional insights into the reaction specificity of catalase-related hydroperoxide lyase: A shift from lyase activity to allene oxide synthase by site-directed mutagenesis. PLoS ONE 12(9): e0185291. <https://doi.org/10.1371/journal.pone.0185291>

**Editor:** Claudio M. Soares, Universidade Nova de Lisboa Instituto de Tecnologia Química e Biológica, PORTUGAL

**Received:** July 17, 2017

**Accepted:** September 8, 2017

**Published:** September 27, 2017

**Copyright:** © 2017 Teder et al. This is an open access article distributed under the terms of the [Creative Commons Attribution License](https://creativecommons.org/licenses/by/4.0/), which permits unrestricted use, distribution, and reproduction in any medium, provided the original author and source are credited.

**Data Availability Statement:** All relevant data are within the paper and its Supporting Information files.

**Funding:** This work was supported by the Institutional Research Funding IUT19-9 of the Estonian Ministry of Education and Research and the Estonian Science Foundation Grant 9410 (both to NS). The funders had no role in study design,

## Abstract

Two highly identical fusion proteins, an allene oxide synthase-lipoxygenase (AOS-LOX) and a hydroperoxide lyase-lipoxygenase (HPL-LOX), were identified in the soft coral *Capnella imbricata*. Both enzymes initially catalyze the formation of 8*R*-hydroperoxy-eicosate-traenoic acid (8*R*-HpETE) from arachidonic acid by the C-terminal lipoxygenase (LOX) domain. Despite the fact that the defined catalytically important residues of N-terminal catalase-related allene oxide synthase (cAOS) domain are also conserved in *C. imbricata* hydroperoxide lyase (cHPL), their reaction specificities differ. In the present study, we tested which of the amino acid substitutions around the active site of cHPL are responsible for a control in the reaction specificity. The possible candidates were determined via comparative sequence and structural analysis of the substrate channel and the heme region of coral cAOSs and *C. imbricata* cHPL. The amino acid replacements in cHPL—R56G, ME59-60LK, P65A, F150L, YS176-177NL, I357V, and SSSAGE155-160PVKEGD—with the corresponding residues of cAOS were conducted by site-directed mutagenesis. Although all these mutations influenced the catalytic efficiency of cHPL, only F150L and YS176-177NL substitutions caused a shift in the reaction specificity from HPL to AOS. The docking analysis of *P. homomalla* cAOS with 8*R*-HpETE substrate revealed that the Leu150 of cAOS interacts with the C5-C6 double bond and the Leu177 with the hydrophobic tail of 8*R*-HpETE. We propose that the corresponding residues in cHPL, Phe150 and Ser177, are involved in a proper coordination of the epoxy allylic radical intermediate necessary for aldehyde formation in the hydroperoxide lyase reaction.

## Introduction

Oxylipins are oxidized polyunsaturated fatty acids and their biosynthesis can be divided into two main steps [1]. Firstly, a molecular oxygen is introduced to a polyunsaturated fatty acid

data collection and analysis, decision to publish, or preparation of the manuscript.

**Competing interests:** The authors have declared that no competing interests exist.

**Abbreviations:** AA, arachidonic acid; AO, allene oxide; cAOS, catalase-related allene oxide synthase; cHPL, catalase-related hydroperoxide lyase; HpETE, hydroperoxy-eicosatetraenoic acid; LOX, lipoxygenase; wt, wild-type.

substrate by a dioxygenase resulting in the formation of a primary oxylipin (fatty acid hydroperoxide) [2,3]. Secondly, the rearrangement of oxygens or the modification of a functional group of a primary oxylipin is catalyzed by various enzymes, mostly related to the cytochrome P450 superfamily [4]. In animals, thromboxane synthase (CYP5) or prostacyclin synthase (CYP8) are responsible for the synthesis of the corresponding lipid mediators from cyclooxygenase-derived endoperoxides [5]. In plants, lipoxygenase-derived fatty acid hydroperoxides are mainly converted by different members of the cytochrome P450 CYP74 family [6]. For example, allene oxide synthase (AOS) pathway is involved in the synthesis of an important plant stress hormone, jasmonic acid [7], and hydroperoxide lyase (HPL) gives rise to short-chain aldehydes with antifungal and -bacterial properties [8].

In soft corals (*Cnidaria*, *Animalia*), a lipoxygenase (LOX) and an allene oxide synthase (AOS) are encoded as a single fusion protein having the ability to catalyze two sequential reactions [9,10]. Recently, in the soft coral *Capnella imbricata*, an AOS-LOX fusion protein was identified in parallel with another fusion protein, a hydroperoxide lyase-lipoxygenase (HPL-LOX) [11]. The C-terminal LOX domain of both fusion proteins initially converts arachidonic acid (AA) to 8*R*-hydroperoxy-eicosatetraenoic acid (8*R*-HpETE) while the reaction specificities of N-terminal catalase-related AOS (cAOS) and HPL (cHPL) domains differ [12]. The cAOS domain synthesizes an unstable allene-8,9-epoxide (AO), detected as its stable hydrolysis products,  $\alpha$ -ketol and cyclopentenone, whereas the cHPL domain produces short-chain aldehydes, 8-oxo-(6*E*)-octenoic acid (C8-oxo acid) and (3*Z*,6*Z*)-dodecadialenal (C12 aldehyde) (Fig 1) [12]. Previously, we have shown that the gene expression and eicosanoid synthesis of *C. imbricata* cAOS-LOX increased in response to abiotic stressors like mechanical injury [11] and elevated water temperature [13] while the biological role of cHPL-LOX remained elusive.

Despite the fact that allene oxides are also formed by plant and fungal cytochrome P450s [15–17], these enzymes are not structurally related to coral cAOS [18]. Instead, the crystal structure of *Plexaura homomalla* cAOS revealed a similar core structure to catalase. Moreover, the heme coordinating residues, R64, R102, R360; the distal heme residues, H67, T66, N137; and the proximal heme ligand, Y353 of cAOS, are identical to the corresponding residues of catalase [18]. Despite these similarities between cAOS and catalase, the former is not able to scavenge hydrogen peroxide (H<sub>2</sub>O<sub>2</sub>) [18].

The structural comparison of highly conserved cAOS and cHPL domains revealed some variations in the substrate channel and the heme region. In the present study, using *in silico* modelling and mutational analysis we attempted to find out which of these substitutions were responsible in the cHPL-specific reaction.

## Materials and methods

### Materials

AA, [1-<sup>14</sup>C]-labeled AA and H<sub>2</sub>O<sub>2</sub> were purchased from Cayman Chemical Co., GE Healthcare and Merck, respectively. 8*R*-HpETE and [1-<sup>14</sup>C]-labeled 8*R*-HpETE were synthesized using the *C. imbricata* 8*R*-lipoxygenase domain of the cHPL-LOX fusion protein, expressed in *Escherichia coli*. Only HPLC grade solvents (Sigma-Aldrich) were used. All the other reagents were purchased from Merck.

### Sequence and structural analysis of coral cAOS and cHPL

Amino acid sequences were aligned using MegAlign software (DNASTar 7.1). 3D models of cHPL and its mutants were prepared based on the *P. homomalla* cAOS (PDB code: 1u5u) and cAOS-LOX (PDB code: 3dy5) crystal structures using CPHmodels 3.2 server [19]. The high

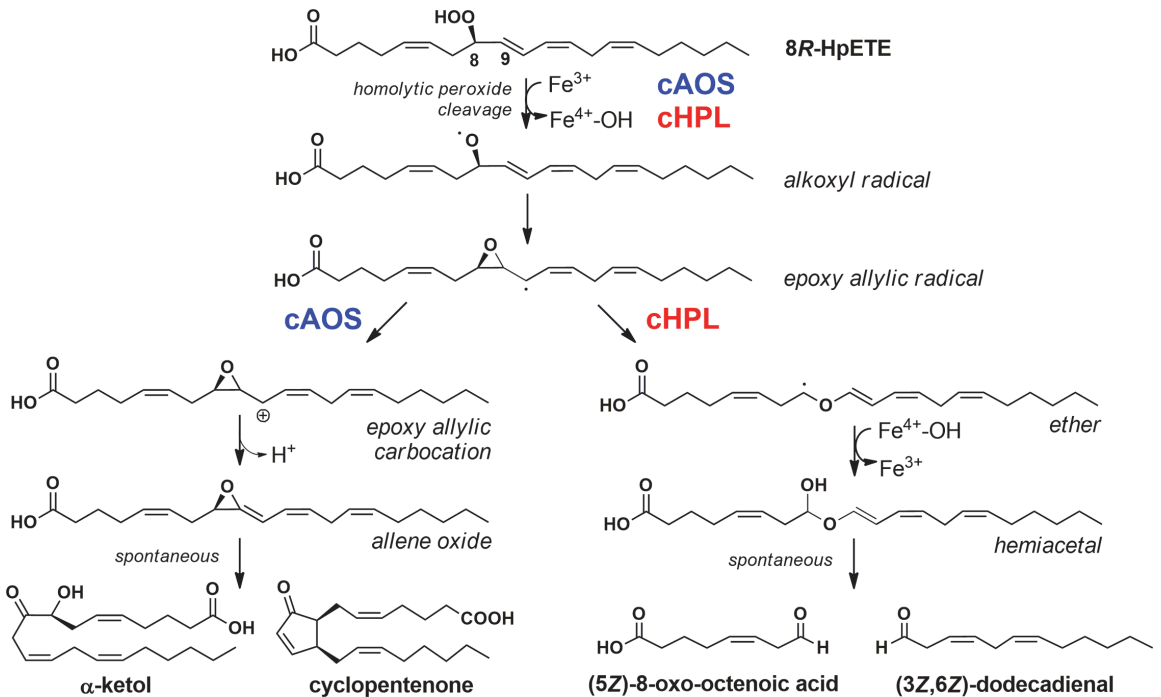


**Fig 1. Two parallel 8R-HpETE-dependent pathways in the soft coral *C. imbricata*.** Highly identical cAOS and cHPL domains both catalyze the formation of an epoxy allylic radical intermediate but the next steps in the corresponding reactions differ. The accepted way in presenting cAOS reaction is via a carbocation intermediate while cHPL reaction can be described by using a radical pathway [14].

<https://doi.org/10.1371/journal.pone.0185291.g001>

sequence identity between the template and targets around 83% (S1A Fig) and the sufficient resolution of X-ray structures, 2.0 Å and 3.5 Å for *P. homomalla* cAOS and cAOS-LOX, respectively, were preconditions for the homology models with a good quality. As the protein crystals were grown around pH 6, the obtained models also contained positively charged Lys and Arg, and negatively charged Glu and Asp residues [18]. The surface area and the volume of binding pockets of proteins were calculated using CASTp server and are presented as Å<sup>2</sup> and Å<sup>3</sup>, respectively [20]. The docking of *P. homomalla* cAOS with two ligands, 8R-HpETE or AO, was conducted using the Swissdock tool [21]. The carboxy groups of fatty acids are negatively charged at a pH greater than 4.5, however, identical docking results were obtained with either charged or neutral ligands. Protein structures were visualized using UCSF Chimera (1.10.1) software [22].

### Preparation of expression constructs

The R56G (Arg56 in cHPL; Gly56 in cAOS), P65A, ME59-60LK, F150L, YS176-177NL, I357V mutations were inserted into the cHPL-His<sub>4</sub>+pET11a construct [12] by using the whole plasmid PCR method [23]. Complementary primers for the site-directed mutagenesis with the silent mutations for the restriction analysis are presented in S1 Table. The PVKEGD fragment was PCR-amplified from the His<sub>6</sub>-cAOS-LOX sequence [11] by specific forward- and reverse

primers (S1 Table) with *Xho*I and *Psi*I restriction sites, respectively. For the SSSAGE155-160PVKEGD replacement, the *Xho*I restriction site was introduced to the cHPL-His<sub>4</sub>+pET11a construct by using the whole plasmid PCR method as described above. The SSSAGE fragment in the cHPL sequence was replaced with the PVKEGD fragment from the cAOS sequence. The ORF of the 8R-LOX domain with an N-terminal His<sub>6</sub>-tag was PCR-amplified from the His<sub>6</sub>-cHPL-LOX sequence [11] and cloned into the pET11a expression vector (Stratagene). Similarly, the *C. imbricata* cAOS-H4 domain was PCR-amplified from the His<sub>6</sub>-cAOS-LOX sequence and cloned into the same expression vector. The cAOS L150F construct was derived from the cAOS-H4 sequence by using the whole plasmid PCR method as described above. The primers for His<sub>6</sub>-8R-LOX, cAOS-H4, and cAOS L150F used in PCR are presented in S1 Table. All the mutations were screened by restriction analysis and all the prepared constructs were sequenced (Agowa, Germany).

### Expression and purification of cHPL mutants

Expression vectors were transformed into *E. coli* BL21(DE3) cells (Novagen) and the expression at OD<sub>600</sub> = 0.7–0.8 was induced with 1-thio-β-D-galactopyranoside (IPTG; final concentration at 0.4 mM). Most of the mutants were expressed in 300 mL of Terrific Broth (TB) medium at 15°C overnight. The cAOS L150F and cHPL SSSAGE155-160PVKEGD were expressed in 1.2 and 2.4 L of TB medium, respectively, at 10°C for 3 days. The *C. imbricata* 8R-LOX and cAOS-H4 domains were expressed in 300 mL and 3 L of TB medium, respectively, at 10°C overnight. All the cultures were harvested and stored at -80°C. The cell pellets were resuspended in a 20 mM Tris (pH 8.0) buffer containing 100 μM phenylmethylsulfonyl fluoride, 0.2% Tergitol NP-40 (Sigma-Aldrich) and 1 mg/mL of lysozyme (Sigma-Aldrich), and sonicated using a Torbeo 36810-series ultrasonic cell disruptor (Cole Parmer). The proteins recovered in the 40 000 × g supernatant of sonicated cells were loaded on the nickel-NTA column (0.5 ml of bed volume, Sigma-Aldrich) equilibrated with the loading buffer (20 mM Tris, 300 mM NaCl, pH 8.0). The His-tagged proteins were eluted with the elution buffer (20 mM Tris, 300 mM NaCl, 200 mM imidazole, pH 8.0) and the 0.5 mL fractions were collected and assayed for activity. The positive fractions were dialyzed against a 50 mM Tris (pH 8.0) and 150 mM NaCl buffer by using an OrDial14 regenerated cellulose tubular dialysis membrane (MWCO: 12000–14000 Da; Orange Scientific) by slowly stirring at 4°C overnight. The dialyzed proteins were stored at -80°C for further use. The purity of protein preparations was determined by SDS-PAGE. All the mutants were quantified at 406 nm ( $\epsilon \sim 100\,000\text{ M}^{-1}\text{ cm}^{-1}$ ) characteristic for hemoproteins. The wt cHPL and mutants with a same heme concentration were compared by SDS-PAGE and the relative quantities of heme-free protein were determined by using GeneTools densitometry (Syngene).

### Incubations with the 8R-HpETE substrate

Incubations with each cHPL mutant (10 nM) were performed using 10 μM 8R-HpETE in 50 mM Tris (pH 8.0) buffer containing 100 mM NaCl and 1 mM CaCl<sub>2</sub> in a quartz cuvette with constant stirring at 20°C. The disappearance of a conjugated diene chromophore ( $\epsilon \sim 25\,000\text{ M}^{-1}\text{ cm}^{-1}$ ) at 235 nm was recorded using a 1601 UV-visible spectrometer (Shimadzu). The kinetic measurements were conducted using 5–50 μM 8R-HpETE substrate and the initial reaction velocity was determined from the linear part of the curve. The  $k_{\text{cat}}$  and  $K_{\text{m}}$  values were calculated employing the nonlinear regression analysis of the Michaelis-Menten equation.

Incubations with 20 μM [1-<sup>14</sup>C]-AA-derived 8R-HpETE were performed for the product analysis. The reactions were stopped using a mild reducing agent SnCl<sub>2</sub> (final concentration at

1 mg/mL) and acidified with HCl to pH 3.5. The products were extracted using ethyl acetate, taken to dryness and dissolved in an HPLC eluent prior to further analysis.

### Incubations with the H<sub>2</sub>O<sub>2</sub> substrate

Incubations with 60 nM wt cHPL or selected mutants were conducted using 0.8 mM H<sub>2</sub>O<sub>2</sub> substrate in a 50 mM Tris (pH 8.0) buffer containing 100 mM NaCl and 1 mM CaCl<sub>2</sub> in a cuvette with constant stirring at 20°C. Incubations with the *C. imbricata* cAOS-LOX and the cAOS domain were conducted in parallel. The production of oxygen was measured with the Model 110 Fiber Optic Oxygen Monitor (Instech) and the  $k_{\text{cat}}$  values were determined based on the initial production of oxygen in  $\mu\text{M}/\text{min}$ .

### RP-HPLC-MS analysis of products formed by cHPL mutants

The products were analyzed by RP-HPLC connected to MSMS or radiometric detector by using the same protocol as described previously [11].

### Oligomerization analysis of wild-type cHPL and cHPL mutants

The oligomerization state of 10–15  $\mu\text{g}$  of a cHPL mutant or about 50  $\mu\text{g}$  of wt cHPL was analyzed by size exclusion chromatography using a Superdex 200 Increase 10/300 GL (GE Healthcare) column with a 50 mM Tris (pH 8.0) and 150 mM NaCl buffer at a flow rate of 0.7 mL/min on an ÄKTA FPLC system (GE Healthcare) at 406 and 280 nm. The oligomerization states of the *C. imbricata* cAOS-LOX and the cAOS domain were determined in parallel. The retention times of the analyzed proteins were compared with authentic standards: thyroglobulin (669 kDa), ferritin (440 kDa), aldolase (158 kDa), BSA (67 kDa), ovalbumin (43 kDa), chymotrypsinogen (25 kDa), and ribonuclease A (13.7 kDa).

## Results

### The strategy for site-directed mutagenesis

To determine potential targets for mutational analysis, the residues of *C. imbricata* cHPL and coral cAOSs [9–11] were compared at sequence (Fig 2A) and structure levels (Fig 3A). Seven main differences in the residues located around the heme region, the substrate channel and the substrate entry site were observed as follows: P65A and I357V in the heme region; F150L in the connecting area between the heme and the substrate entry site (Fig 3A); YS176-177NL at the backside of the substrate channel coordinating the tail of the 8R-HpETE substrate (Fig 3A and 3B); R56G, ME59-60LK, and SSSAGE155-160PVKEGD in the active site entrance of the substrate channel. The amino acid pairs, i.e. R56/G56, P65/A65, F150/L150, and I357/V357, are highlighted in the superpositioned cHPL model and the crystal structure of *P. homomalla* cAOS, respectively (Fig 2B). All the presented substitutions in cHPL (Fig 2A) were performed and investigated. In addition, an opposite mutant, cAOS L150F, was prepared in parallel and will be discussed below.

### The coordination of ligands by cAOS and cHPL

Previous docking studies with *P. homomalla* cAOS have been focused only on the distal heme residues, H67 and T66, in regard of the interaction with a hydroperoxide [24]. As the main aim of this study was to determine the differences between the cHPL and cAOS substrate channels, we evaluated all the residues involved in the coordination of the 8R-HpETE substrate or AO.

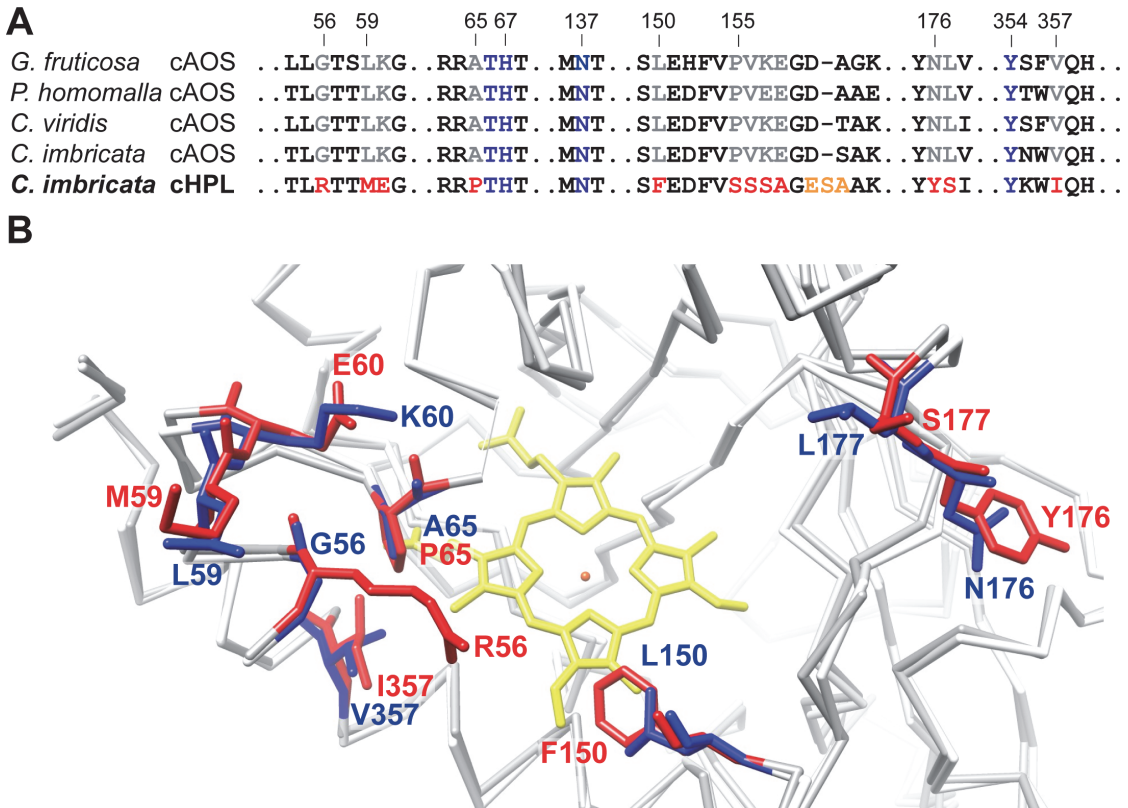


**Fig 2. The differences between the residues of coral cAOSs and *C. imbricata* cHPL.** **A**—alignment of amino acid sequences of coral cAOSs and *C. imbricata* cHPL presenting the conserved (blue) and distinct (grey vs red, respectively) residues in the substrate channel. The following amino acid sequences were compared: *Gersemia fruticosa* cAOS (NCBI ID: EU082210.1); *P. homomalla* cAOS (NCBI ID: AF003692.1); *Clavularia viridis* cAOS (NCBI ID: AB188528.1); *C. imbricata* cAOS (NCBI ID: KF000373.1); *C. imbricata* cHPL (NCBI ID: KF000374.1). **B**—the crystal structure of *P. homomalla* cAOS (blue) superpositioned with the model of *C. imbricata* cHPL (red) highlighting the main differences in the substrate pocket. The difference in the SSSAGE155-160PVKEGD fragments is not shown due to the illustrative purposes. The conserved amino acids between cAOS and cHPL are presented as a white and grey backbone, respectively. The heme is presented in yellow and the heme iron in orange.

<https://doi.org/10.1371/journal.pone.0185291.g002>

The analysis of the X-ray structure of *P. homomalla* cAOS revealed that the negatively charged carboxy group of the 8R-HpETE substrate could be coordinated by the positively charged K107 and/or K60, located at the active site entrance of the substrate channel, and the hydroperoxy group of 8R-HpETE interacted with the catalytically important T66, H67, and N137 near the heme region [18]. These interactions were also observed in our docking analysis of *P. homomalla* cAOS with both ligands, 8R-HpETE and AO. As the length of H-bond should be less than 6 Å for stronger interaction [24], all the interactions determined in this study fulfilled this requirement.

Although the 8R-HpETE substrate was successfully placed inside the substrate channel of *P. homomalla* cAOS and *C. imbricata* cHPL models by the docking tool, the latter model did not give expected interactions between the distal heme residues, T66, H67, and the hydroperoxy group of 8R-HpETE. Docking analyses with individual cHPL mutants and also with the cHPL

domain containing all the substituted residues did not give anticipated interactions either. Therefore, the further analysis was conducted only based on the docking results of *P. homomalla* cAOS.

The distance between the carboxy group of 8R-HpETE and K107 of cAOS was determined as 3.2 Å, while with K60 it was 5.0 Å. This may be indicative to the carboxy head coordination only by K107. The distances of T66, H67 and N137 from the hydroperoxy group of 8R-HpETE were determined as 3.0, 3.3 and 5.0 Å, respectively (Fig 3A and 3B). The weaker interaction between the N137 of cAOS and 8R-HpETE is in correlation with previous mutational studies of *P. homomalla* cAOS which indicated that the N137 was not important in the catalysis *per se*, but may have a supporting role in the substrate binding [25]. The docking with the second ligand, AO, showed that it can be located inside the substrate channel in two different conformations. In the first model, the epoxy group of AO was located closer to T66 and H67 (Fig 3C) with the respective distances of 4.7 and 4.5 Å. In the second model, the epoxy group was rotated 90 degrees away from T66 and H67 (Fig 3D) with distances of 5.5 and 5.2 Å, respectively. The distance between N137 and the epoxy group of AO, 4.6 Å, was the same for both models.

Among all the residues of our interest, the L150 and L177 of *P. homomalla* cAOS were the most proximal ones interacting with the U-shaped ligand (Fig 3). The corresponding residues in cHPL were F150 and S177, respectively. L150 was located near the C5-C7 of 8R-HpETE with the respective distances of 4.9, 3.4, 3.1 Å and was positioned on the opposite side of the hydroperoxy group (Fig 3A). L177 interacted with the hydrophobic tail at the C15-C17 of 8R-HpETE with distances of 3.3, 3.4, 4.0 Å, respectively (Fig 3A). The proximity between L150 and L177 with 8R-HpETE indicate that these residues are involved in the substrate binding and coordination.

### Protein expression and analysis of cHPL mutants

All the expressed mutants were determined to be catalytically active via enzyme assay using the 8R-HpETE substrate. Based on the obtained protein concentrations, the yields of cHPL R56G, ME59-60LK, P65A, YS176-177NL, and I357V mutants were determined to be 250–300 µg of soluble protein per 1 L of TB medium. The yields of wt cHPL, cHPL F150L, wt cAOS, and cAOS L150F were lower, 100, 170, 110, and 140 µg/L, respectively. However, the SSSAGE155-160PVKEGD alteration drastically reduced the yield of the corresponding mutant in the supernatant to 30 µg/L and therefore, size exclusion chromatography was not performed. The yields of wt cHPL and cHPL mutants were much lower compared to those of *P. homomalla* wt cAOS [26]. To estimate the presence of a heme, the protein samples at the same heme concentration were analyzed by SDS-PAGE (Fig 4). The heme content in wt cHPL and cHPL SSSAGE155-160PVKEGD samples was similar as there was no significant differences in the band sizes (Fig 4). The relative amount of heme-free protein in cHPL I357V, P65A, ME59-60LK, YS176-177NL, R56G, F150L, and cAOS L150F samples compared to the wt cHPL were determined as follows: 49%, 46%, 45%, 67%, 64%, 76% and 27%, respectively. In comparison with other samples, cHPL F150L sample contained the highest amount of heme-free protein (Fig 4) which implies notable changes in protein-heme interactions.

To investigate the influence of mutation on the Soret band of cHPL, the λ maxima of prepared mutants and wt enzymes were compared. In the UV spectra analysis, a 1 nm difference of the λ maximum of a heme between *C. imbricata* wt cAOS and cHPL was observed, 407 vs 406 nm, respectively. At the same time, the λ maxima of the N-terminal heme-containing domain and the corresponding fusion proteins were identical. The λ maxima of cHPL R56G and YS176-177NL remained unaltered. For other mutants, slight shifts of the Soret band at

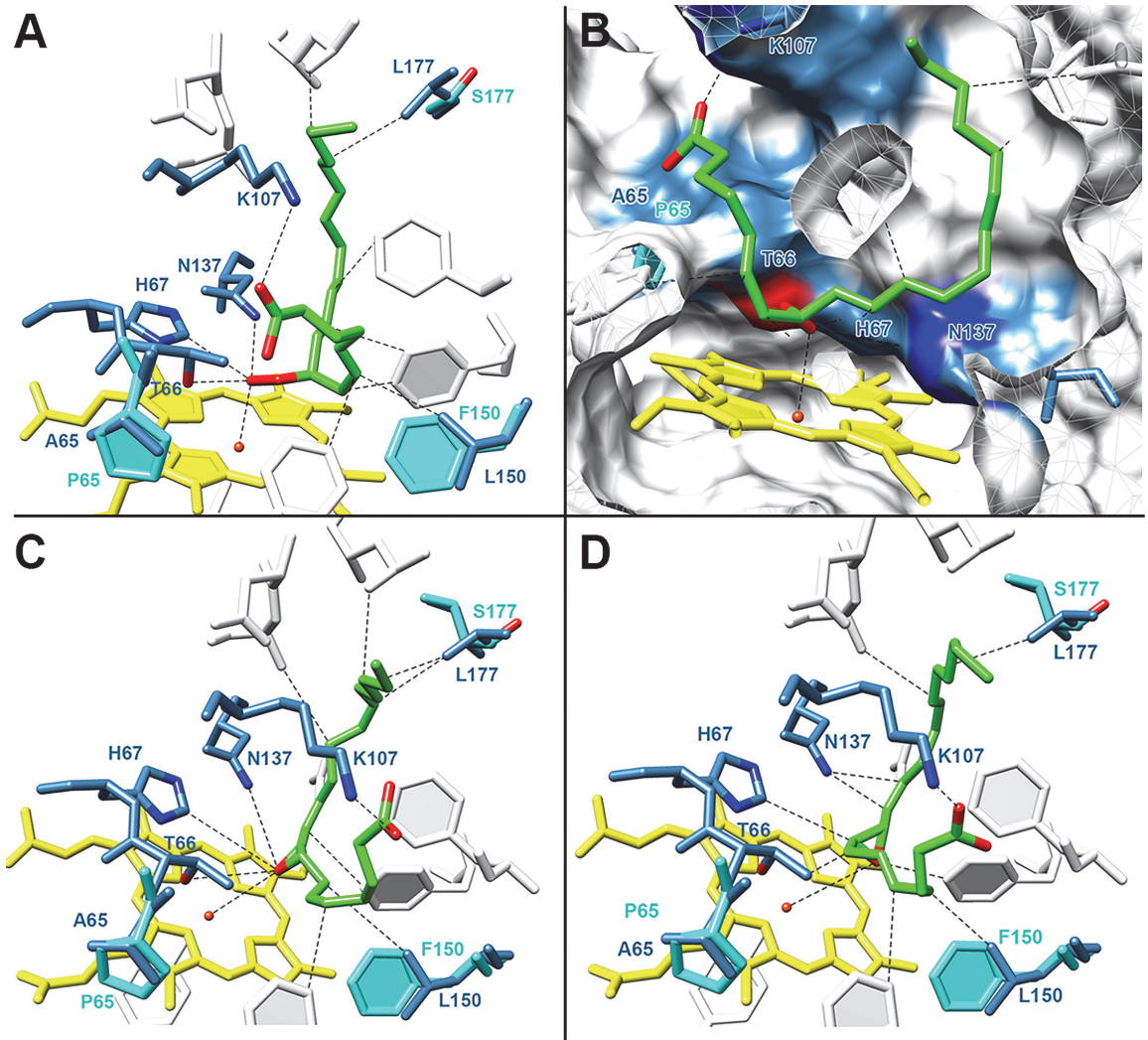


**Fig 3. The docking analysis of *P. homomalla* cAOS with 8F-HpETE and AO.** **A**–8F-HpETE located in the substrate pocket; **B**–the rotated view of 8F-HpETE in the substrate pocket with a hydrophobic surface; **C**–AO in the substrate pocket; **D**–an alternative positioning of AO in the substrate pocket. The colors used in the figure are presented as follows: heme–yellow; heme iron–orange; ligands–green; the interacting residues of *P. homomalla* cAOS–blue; the interacting residues of *C. imbricata* cHPL–cyan; residues supporting the coordination of ligand or heme–gray; oxygen atoms–red; nitrogen atoms–blue. For clarity, the distances between the ligand and selected residues are given in the text.

<https://doi.org/10.1371/journal.pone.0185291.g003>

405–408 nm were detected (data not shown) which can be explained by the small changes in the interactions between the heme, heme coordinating residues, proximal heme ligand, and proximal aromatic residues [27,28]. As there were no significant changes in the Soret bands, we can say that any of the mutations did not affect the conformation of the heme and the oxidation state of the heme iron [29–31].



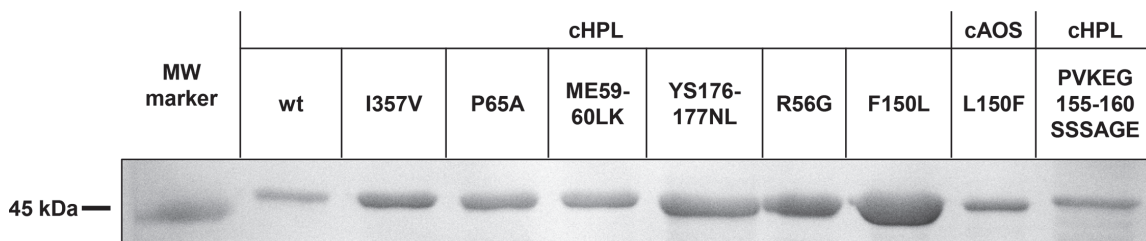


**Fig 4. SDS-PAGE analysis of purified wt cHPL and corresponding mutants.** Protein samples with an equal heme concentration (0.4  $\mu\text{M}$ ) were compared.

<https://doi.org/10.1371/journal.pone.0185291.g004>

Size exclusion chromatography was performed to evaluate the influence of mutations on the oligomeric state of wt cHPL. The wt cHPL and cHPL ME59-60LK, P65A, F150L, and YS176-177NL mutants eluted from the size exclusion column as two peaks (Fig 5A and 5B). The higher early-eluting peak at 8 minutes represents oligomerized proteins with molecular weights at 440–670 kDa and the smaller peak at 16 minutes corresponds to the cHPL monomer at 45 kDa (Fig 5). The isolated monomer and oligomer maintained their oligomerization states after the reinjection on the size exclusion column. In parallel, the cHPL R56G and I357V mutants eluted mostly as monomers (Fig 5C and 5D). Both substitutions, R56G and I357V, are located in the  $\alpha$ -helical part of cAOS which interacts with the LOX domain of the fusion protein [32]. Presumably, G56 and V357 influenced the properties of the corresponding  $\alpha$ -helices and therefore, the oligomerization of the cHPL domain was reduced. In comparison, the *C. imbricata* cHPL-LOX (Fig 5E), the cAOS domain (Fig 5F), cAOS L150F (Fig 5G) and *P. homomalla* cAOS-LOX (S2 Fig) are monomers. However, the cause of the oligomerization of wt cHPL remains unclear.

### The activity of cHPL mutants

The determined  $k_{\text{cat}}$ ,  $K_m$  and  $k_{\text{cat}}/K_m$  values of cHPL mutants with 8R-HpETE substrate are presented in Table 1. The corresponding kinetic parameters of wt cHPL were previously determined and resulted to be: 133.5  $\text{s}^{-1}$ , 3.8  $\mu\text{M}$ , and 35.1  $\text{s}^{-1} \mu\text{M}^{-1}$  [12]. The  $k_{\text{cat}}$  of cHPL F150L, P65A, and I357V mutants were 2-3-fold lower (Table 1) than that of wt cHPL. The major decrease in the  $k_{\text{cat}}$  value, 7.5  $\text{s}^{-1}$ , was detected with the ME59-60LK substitution. In contrast, R56G and YS176-177NL substitutions increased the  $k_{\text{cat}}$  approximately 3- and 2-folds, respectively. In the case of L150F cAOS, the  $k_{\text{cat}}$  was 7-fold lower, than those of wt cAOS and *P. homomalla* cAOS (Table 1). Due to the substrate inhibition of cHPL PVKEGD155-160SSSAGE with 8R-HpETE at higher substrate concentrations, the kinetic measurements were performed only with 5–30  $\mu\text{M}$  8R-HpETE substrate. The determined  $k_{\text{cat}}$  value of cHPL PVKEGD155-160SSSAGE, 52  $\text{s}^{-1}$ , was similar to those of cHPL F150L and P65A (Table 1).

The  $K_m$  values of cHPL F150L, I357V, YS176-177NL, ME59-60LK, PVKEGD155-160SSSAGE were comparable with those of wt cHPL. The remarkable 4- and 5-fold increase in  $K_m$  values was observed with cHPL P65A and R56G, respectively (Table 1). The  $K_m$  value of cAOS L150F was about 6-fold lower than those of wt cAOS and *P. homomalla* cAOS [26]. The elevated  $k_{\text{cat}}$  of cHPL R56G was probably achieved due to the increased accessibility of the substrate channel (S2 Table). However, the replacement of R56 with G56 lowered the affinity between 8R-HpETE substrate and the enzyme which indicates that R56 of wt cHPL is necessary for stronger binding of 8R-HpETE.

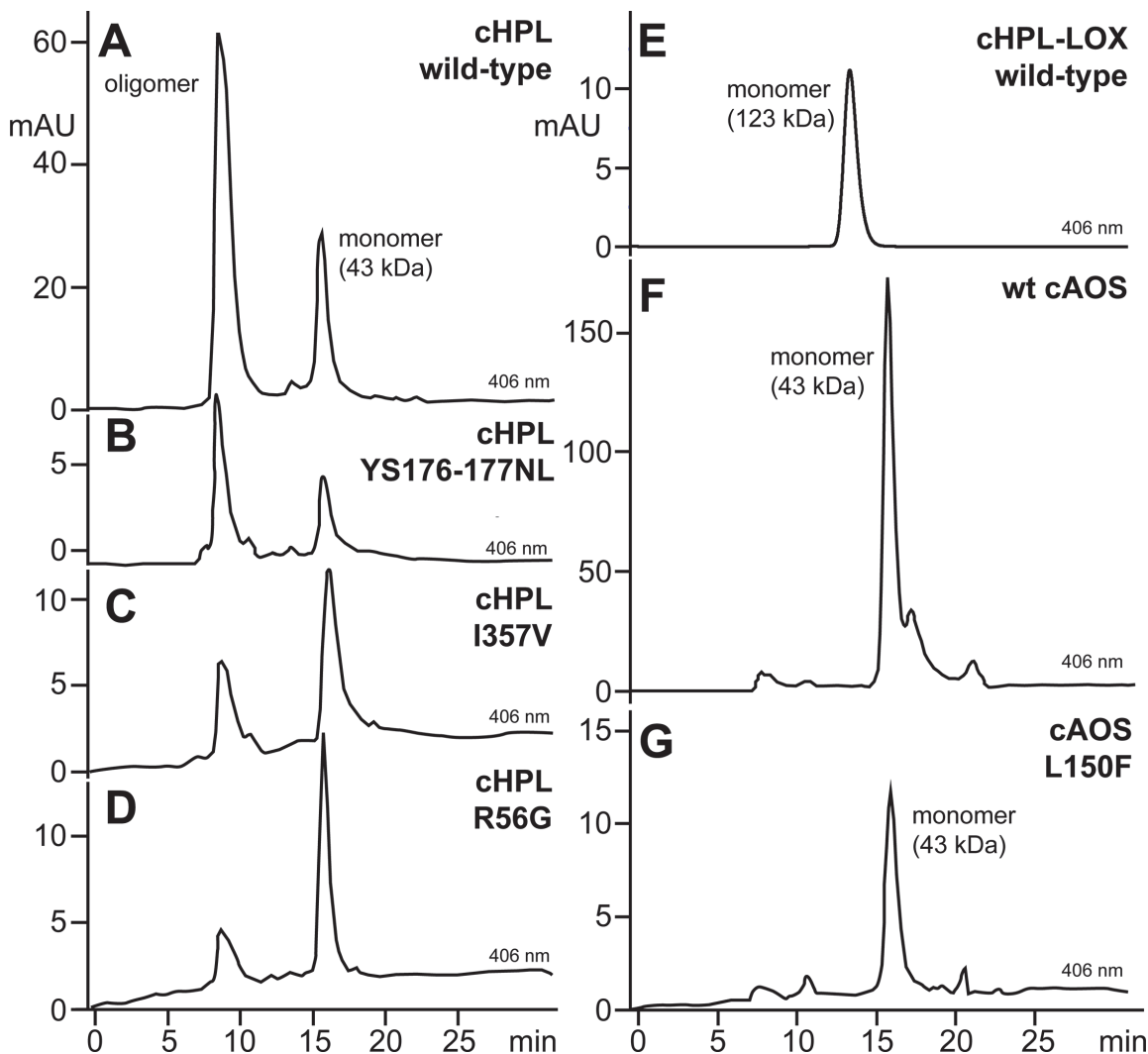


**Fig 5. The oligomerization analysis of *C. imbricata* protein samples.** A—wt cHPL; B—cHPL YS176-177NL. Similar oligomerization states were determined also for cHPL ME59-60LK, P65A, F150L. C—cHPL I357V; D—cHPL R56G; E—wt cHPL-LOX; F—wt cAOS; G—cAOS L150F. Oligomers and monomers of wt cHPL and mutants eluted at 8 and 16 min, respectively.

<https://doi.org/10.1371/journal.pone.0185291.g005>

The catalytic efficiencies ( $k_{cat}/K_m$ ) of cHPL P65A and ME59-60LK were determined to be more than 10-fold lower than the efficiency of the wt enzyme. The  $k_{cat}/K_m$  of cHPL I357V and R56G were about 2-fold lower whereas the catalytic efficiencies of F150L and PVKEGD155-160SSSAGE were comparable with wt cHPL's. The reaction efficiency of cHPL YS176-177NL was about 2-fold higher than that of wt cHPL. The unexpected increase in the efficiency is commented in Discussion. The determined catalytic efficiency of cAOS L150F was in

**Table 1. Kinetic parameters of wt cHPL, wt cAOS and selected mutants with 8R-HpETE and H<sub>2</sub>O<sub>2</sub>.**

Enzyme		8R-HpETE			H <sub>2</sub> O <sub>2</sub>
		k <sub>cat</sub> (s <sup>-1</sup> )	K <sub>m</sub> (μM)	k <sub>cat</sub> /K <sub>m</sub> (s <sup>-1</sup> , μM <sup>-1</sup> )	k <sub>cat</sub> (s <sup>-1</sup> )
<i>C. imbricata</i> cHPL					
	wild-type	133.5 ± 5.0	3.8 ± 0.5	35.1	3
Heme region	F150L	49.6 ± 1.5	1.8 ± 0.4	27.6	14
	P65A	40.3 ± 2.5	15.3 ± 2.5	2.6	22
	I357V	63.9 ± 3.2	5.0 ± 1.0	12.8	8
Substrate channel	R56G	304.5 ± 22.8	19.0 ± 4.0	16.0	3
	YS176-177NL	218.1 ± 13.8	3.9 ± 0.9	56.0	31
	ME59-60LK	7.5 ± 0.6	7.3 ± 1.9	1.0	16
	SSSAGE155-160PVKEG fragment	52.1 ± 3.4	2.0 ± 0.8	26.1	35
<i>C. imbricata</i> cAOS					
	wild-type	1835.0 ± 196.3	46.6 ± 9.0	39.4	303
Heme region	L150F	203.3 ± 8.1	6.7 ± 1.0	30.3	127
<i>P. homomalla</i> cAOS*					
	wild-type	1409.2 ± 84.8	45.3 ± 7.5	31.1	insignificant#

The k<sub>cat</sub> and K<sub>m</sub> values determined with 8R-HpETE are presented with the corresponding standard error (n = 3). The k<sub>cat</sub> values with H<sub>2</sub>O<sub>2</sub> were determined as described in Materials and methods.

\*—values obtained from the article by Boutaud *et al.* [26].

#—value obtained from the article by Tosha *et al.* [32].

<https://doi.org/10.1371/journal.pone.0185291.t001>

correlation with those of wt cAOS and *P. homomalla* cAOS (Table 1). All the mutations influenced the reaction rate and/or the affinity of cHPL with the 8R-HpETE substrate referring that all the substituted residues are necessary for the efficient catalysis.

To study the catalase activity of *C. imbricata* wt cHPL, wt cAOS and selected mutants, incubations with the H<sub>2</sub>O<sub>2</sub> substrate were conducted. Wt cHPL and cHPL R56G had a very low reaction rate with H<sub>2</sub>O<sub>2</sub>, resulting in the initial production of 10 μM O<sub>2</sub> per minute with the corresponding k<sub>cat</sub> value of 2.5 s<sup>-1</sup> which is in correlation with the measurements of *P. homomalla* cAOS [33]. With cHPL ME59-60LK, P65A, F150L, YS176-177NL, I357V, PVKEGD155-160SSSAGE, the oxygen levels increased up to 100 μM O<sub>2</sub>/min (k<sub>cat</sub> = 8–35 s<sup>-1</sup>). In contrast, a considerably higher catalase activity was detected in the reactions using wt cAOS and cAOS L150F. The oxygen evolution by wt cAOS and cAOS L150F was determined as 1090 μM (k<sub>cat</sub> = 303 s<sup>-1</sup>) and 450 μM O<sub>2</sub>/min (k<sub>cat</sub> = 127 s<sup>-1</sup>), respectively. These values are about two orders of magnitude higher compared to wt cHPL's. A similar catalase activity of *C. imbricata* cAOS-S-LOX to the individual cAOS domain was detected in parallel. In comparison with *P. homomalla* cAOS T66V [33], the oxygen evolution by *C. imbricata* cAOS was about 30-fold higher. *C. imbricata* and *P. homomalla* cAOSs share 82.8% of their amino acid sequences and there are no remarkable differences in the active site residues (Fig 1, S1A and S1B Fig), therefore, the higher ability of *C. imbricata* cAOS to break down H<sub>2</sub>O<sub>2</sub> requires further investigation.

### Product synthesis by cHPL mutants

Wt cHPL catalyzes the formation of C8-oxo acid and C12 aldehyde (Fig 1)[12]. On the radiochromatogram, C8-oxo acid, which retains the [1-<sup>14</sup>C] label, was the early-eluting peak at 2.5 minutes (Fig 6A). The detected product patterns of cHPL R56G, P65A, ME59-60LK, and SSSAGE155-160PVKEGD were identical to wt cHPL's. In contrast to wt cHPL, cHPL F150L catalyzed the formation of C8-oxo acid and also α-ketol eluting at 2.5 and 17 min with

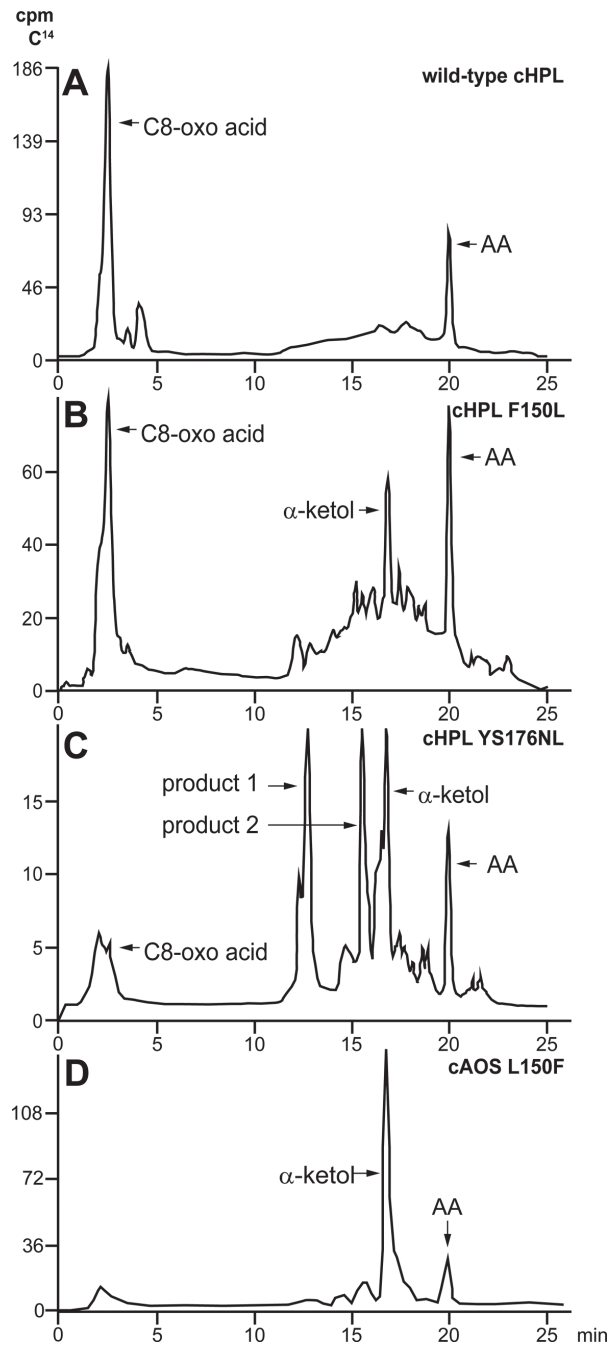


**Fig 6. The products derived from the radiolabeled 8R-HpETE substrate by wt cHPL, selected cHPL mutants, and cAOS L150F.** **A**– C8-oxo acid formed by wt cHPL representing also the products formed by cHPL R56G, P65A, ME59-60LK, and SSSAGE155-160PVKEG; **B**– C8-oxo acid and  $\alpha$ -ketol formed by cHPL F150L; **C**– C8-oxo acid,  $\alpha$ -ketol and product 1 and product 2 formed by cHPL YS176-177NL; **D**– $\alpha$ -ketol formed by cAOS L150F. The product pattern is identical to wt cAOS's (data not shown).

<https://doi.org/10.1371/journal.pone.0185291.g006>

conversion rates of 60% and 16% of total cpm value, respectively (Fig 6B). The cHPL YS176-177NL gave rise to the C8-oxo acid,  $\alpha$ -ketol and also to two additional products, product 1 and 2. The conversion rates of corresponding products were determined as 18%, 9%, 46%, 15% (Fig 6C), respectively. The conversion rate to C8-oxo acid was determined as 18% whereas the corresponding value for  $\alpha$ -ketol, product 1 and product 2 was about 23% (Fig 6C). Products 1 and 2 having the UV chromophore at 205 nm (data not shown) eluted at 12.5 and 16 min, respectively. The respective [M] values of products 1 and 2 were determined to be 353 and 335 which correspond those of trihydroxy and epoxy alcohol derivatives, respectively. The product formation by cAOS was not altered by the opposite substitution, cAOS L150F, producing only the wt products,  $\alpha$ -ketol and cyclopentenone [11], with elution times at 17 and 17.5 min, respectively (Fig 6D). The altered product profile and the docking analysis (see Results above) indicate that F150 and YS176-177 are involved in the correct substrate positioning.

## Discussion

Coral cAOS and cHPL catalyze the same initial steps until the formation of the 8R-HpETE-derived epoxy allylic radical (Fig 1). The further transformations of intermediates by cAOS and cHPL are controlled differently. In cAOS, H67 is involved in the initiation of the homolytic cleavage of hydroperoxide (Fig 1) and also in the abstraction of hydrogen from the C9 of the epoxy allylic carbocation resulting in the formation of AO [18](Fig 7). We suggest that in the cHPL-catalyzed mechanism, H67 might not be able to abstract hydrogen at C9 (Fig 7). Instead, the epoxy ring opening occurs via the breakage of C8-C9 bond resulting in the formation of an oxonium ion [34,35]. Next, the resonance structure of the oxonium ion, allylic ether

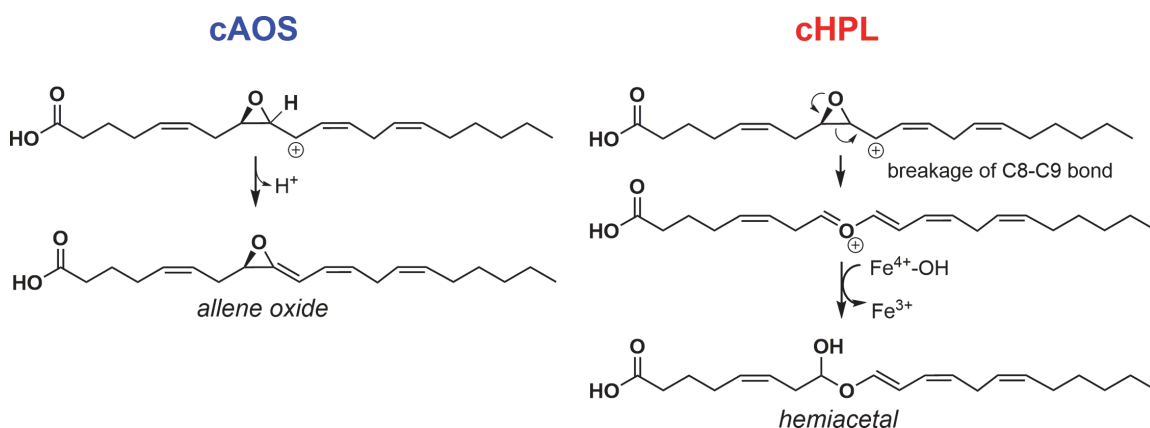


**Fig 7. The proposed difference in reaction mechanisms between coral cAOS and cHPL.** The hydrogen abstraction at C9 of the epoxy allylic carbocation is initiated by His67 of cAOS (blue). In cHPL-catalyzed reaction (red), no hydrogen abstraction occurs and instead, an unstable hemiacetal forms via the breakage of C8-C9 bond of the epoxide and the subsequent rebound of hydroxide.

<https://doi.org/10.1371/journal.pone.0185291.g007>

carbocation, binds the hydroxide from the ferryl-hydroxo complex forming the highly unstable hemiacetal. In both reactions, the carbocation of cAOS- or cHPL-derived epoxy allylic intermediate [14,36] is stabilized at C10. In the cHPL-catalyzed reaction, the inability of H67 to abstract the hydrogen at C9 can be explained with the greater distance and/or unfavored positioning between the intermediate and H67. Moreover, there is no consensus describing AOS and HPL reactions in regard of ionic or radical intermediates. Both intermediates are possible, however, the most accepted way of presenting the AOS reaction is using a carbocation intermediate [14]. Therefore, for clarity in explaining the formation of multiple products from a common intermediate by cHPL F150L or YS176-177NL, only ionic intermediates were presented in Fig 7.

As suggested by Oldham *et al.* 2005, either the positively charged K107 or K60 could interact with the carboxy group of the 8R-HpETE substrate. K107 is present in the active site entrance of both enzymes, cAOS and cHPL. However, the 60th residue in cHPL is the negatively charged Glu (E60) which should have an opposite effect on the coordination of the negatively charged carboxy group of 8R-HpETE. In our study, the E60 of cHPL was replaced with the positively charged Lys (K60) of cAOS in regard to the double mutation, ME59-60LK, and instead of the expected improvement in activity and/or affinity, the reaction efficiency dropped remarkably. It indicates that although E60 in cHPL is necessary for the good activity of cHPL, the 60th residue might not be located near the carboxy head of 8R-HpETE. Instead, it could influence the reaction efficiency via conformational changes in the active site. As K107 of cAOS was located closer to the carboxy head of 8R-HpETE according to docking analysis, we postulate that K107 in cHPL and cAOS might be the main residue coordinating the carboxy group. However, the influence on the coordination of 8R-HpETE by K60 or K107 in cAOS and cHPL needs further investigation to confirm the obtained results. The positively charged R56 may also have an effect on the coordination of the carboxy head of 8R-HpETE. However, the replacement of R56 with G56 resulted in the unexpected increase in  $k_{cat}$  (Table 1) showing that R56 is not essential for the coordination of the carboxy group of 8R-HpETE and is also irrelevant in the matter of the cHPL-catalyzed reaction but seems to be necessary for stronger binding of the substrate.

Our data supports the hypothesis that the main differences between cHPL and cAOS in the interaction with a ligand were determined in the residues of F150/L150 and YS176-177/NL176-177 (cHPL/cAOS, respectively). Among other mutants, only the F150L and YS176-177NL substitutions resulted in the change of product pattern and influenced the catalysis process. A precedent can be found in the structural-functional study on the plant AOS where a single replacement of F to L resulted in the exchanged specificity from AOS to HPL [37]. As mentioned in the Introduction, cAOS and cHPL do not share any common structural elements with corresponding plant enzymes and therefore in coral isozymes, F150 and L150 may serve a different role in the reaction with the 8R-HpETE substrate. Based on ligand binding analysis, L150 of *P. homomalla* cAOS interacts with the C5-C6 double bond of 8R-HpETE (Fig 3A) and thus the corresponding residue in cHPL, bulkier F150, might direct the epoxy allylic carbocation into a position where the hydrogen abstraction at C9 is not possible (Fig 7). The opposite mutation in cAOS, L150F, did not cause any change in the product profile, indicative that the corresponding residue in cAOS, L150, is not directly involved in the catalysis. A similar phenomenon can be observed in the structural-functional analysis of the plant enzymes where the mutations between the Cyp74 family members, AOS, HPL or DES, were not interchangeable [38,39]. Moreover, the inability of cAOS L150F to synthesize aldehydes might be explained by the proposed theory about the evolution of plant AOS from HPL [38]. Based on our results, the distinct effect of a mutation on product formation implies that L150 of cAOS and F150 of cHPL interact with the substrate differently due to slight variances in the active site and/or the positioning of the substrate.

According to our docking analysis, the L177 of *P. homomalla* cAOS interacted with the aliphatic tail of 8R-HpETE. We suggest that as a result of the YS176-177NL mutation, the repositioning of the epoxy allylic radical intermediate took place which resulted in the increased activity of cHPL and in the production of multiple products. The formation of unexpected products (Fig 6C) can be explained by the uncontrolled catalysis. Presumably, the initial step in the reaction remained unaltered but the further intramolecular rearrangements of the epoxy allylic radical were taking different directions as it has been described with the formation of AO, hemiacetal, divinyl ether or epoxy alcohol by the closely related enzymes of the Cyp74 family [14]. The increase in the activity of cHPL YS176-177NL cannot be explained by the change of the volume of substrate channel as it is nearly identical with wt cHPL's (S2 Table). Probably, the nonpolar properties of NL instead of polar YS provided stronger interactions with the hydrophobic tail of 8R-HpETE and promoted a faster reaction rate by directing the substrate in a more favorable position. As with both mutants, F150L and YS176-177NL, there was no total shift in the activity from cHPL to cAOS, we suggest that alternative conformations of the intermediate in the active site were possible. Therefore, the capability of corresponding cHPL mutants to abstract hydrogens by H67 was dependent on the conformation of the intermediate.

In the current study, we elucidated how the site-specific mutations in the substrate channel influenced the reaction efficiency, specificity and oligomerization of *C. imbricata* cHPL. Based on the altered product formation, F150 and YS176-177 were established as the reaction-specific residues of cHPL. As the determinants of the reaction mechanism and the substrate coordination of coral cHPL and cAOS are not fully understood, additional structural-functional studies are a matter of future research.

## Supporting information

**S1 Table. Forward and reverse primers of *C. imbricata* cHPL mutants, wt cAOS domain, cAOS L150F and 8R-LOX domain.**

(PDF)

**S2 Table. The surface volume and area analysis of *C. imbricata* wt cHPL, wt cAOS, *P. homomalla* cAOS and selected mutants.**

(PDF)

**S1 Fig. The sequence comparison of *P. homomalla* cAOS, *C. imbricata* cHPL domain. A—**the amino acid identity and divergence between *P. homomalla* cAOS domain, *C. Imbricata* cHPL domain and mutants; **B—**the sequence alignment of *P. homomalla* cAOS and *C. imbricata* cAOS.

(PDF)

**S2 Fig. The oligomerization state of *P. homomalla* cAOS-LOX.** Size exclusion chromatography was performed the same way as described in Materials and Methods.

(PDF)

**S1 File. The homology model of *C. imbricata* cHPL.** The model was prepared based on the X-ray structures of *P. homomalla* cAOS (PDB IDs: 1u5u and 3dy5) using the CPHmodels-3.2 server.

(PDB)

**S1 Text. The topography of *C. imbricata* cHPL.**

(PDF)

## Acknowledgments

We thank Prof. Alan R. Brash for providing beneficial information about the reactions of fatty acid-metabolizing hemoproteins and Priit Eek for helpful comments on the manuscript.

## Author Contributions

**Conceptualization:** Tarvi Teder, Helike Lõhelaid, Nigulas Samel.

**Formal analysis:** Tarvi Teder, Helike Lõhelaid.

**Funding acquisition:** Helike Lõhelaid, Nigulas Samel.

**Investigation:** Tarvi Teder, Helike Lõhelaid.

**Validation:** Tarvi Teder, Helike Lõhelaid, Nigulas Samel.

**Visualization:** Tarvi Teder.

**Writing – original draft:** Tarvi Teder, Helike Lõhelaid, Nigulas Samel.

**Writing – review & editing:** Tarvi Teder, Helike Lõhelaid, Nigulas Samel.

## References

1. Mosblech A, Feussner I, Heilmann I. Oxylipins: Structurally diverse metabolites from fatty acid oxidation. *Plant Physiol Biochem*. 2009. pp. 511–517. <https://doi.org/10.1016/j.plaphy.2008.12.011> PMID: 19167233
2. Andreou A, Feussner I. Lipoxygenases—structure and reaction mechanism. *Phytochemistry*. 2009. pp. 1504–1510. <https://doi.org/10.1016/j.phytochem.2009.05.008> PMID: 19767040
3. Schneider C, Pratt DA, Porter NA, Brash AR. Control of oxygenation in lipoxygenase and cyclooxygenase catalysis. *Cell Chemical Biology*. 2007. pp. 473–488. <https://doi.org/10.1016/j.chembiol.2007.04.007> PMID: 17524979
4. Griffiths G. Biosynthesis and analysis of plant oxylipins. *Free Radic Res*. 2015; 49: 565–82. <https://doi.org/10.3109/10715762.2014.1000318> PMID: 25536417
5. Hecker M, Ullrich V. On the mechanism of prostacyclin and thromboxane A2 biosynthesis. *J Biol Chem*. 1989; 264: 141–150. PMID: 2491846
6. Hughes RK, De Domenico S, Santino A. Plant cytochrome CYP74 family: Biochemical features, endocellular localisation, activation mechanism in plant defence and improvements for industrial applications. *ChemBioChem*. 2009. pp. 1122–1133. <https://doi.org/10.1002/cbic.200800633> PMID: 19322850
7. Wasternack C, Hause B. Jasmonates: Biosynthesis, perception, signal transduction and action in plant stress response, growth and development. An update to the 2007 review in *Annals of Botany*. *Annals of Botany*. 2013. pp. 1021–1058. <https://doi.org/10.1093/aob/mct067> PMID: 23558912
8. Matsui K. Green leaf volatiles: hydroperoxide lyase pathway of oxylipin metabolism. *Curr Opin Plant Biol*. 2006. pp. 274–280. <https://doi.org/10.1016/j.pbi.2006.03.002> PMID: 16595187
9. Koljak R, Boutaud O, Shieh BH, Samel N, Brash AR, Hamberg M, et al. Identification of a naturally occurring peroxidase-lipoxygenase fusion protein. *Science*. 1997; 277: 1994–6. <https://doi.org/10.1126/science.277.5334.1994> PMID: 9302294
10. Lõhelaid H, Järving R, Valmsen K, Varvas K, Kreen M, Järving I, et al. Identification of a functional allene oxide synthase-lipoxygenase fusion protein in the soft coral *Gersemia fruticosa* suggests the generality of this pathway in octocorals. *Biochim Biophys Acta—Gen Subj*. 2008; 1780: 315–321. <https://doi.org/10.1016/j.bbagen.2007.10.010> PMID: 17996204
11. Lõhelaid H, Teder T, Töldsepp K, Ekins M, Samel N. Up-regulated expression of AOS-LOXa and increased eicosanoid synthesis in response to coral wounding. *PLoS One*. 2014; 9. <https://doi.org/10.1371/journal.pone.0089215> PMID: 24551239
12. Teder T, Lõhelaid H, Boeglin WE, Calcutt WM, Brash AR, Samel N. A catalase-related hemoprotein in coral is specialized for synthesis of short-chain aldehydes: Discovery of P450-type hydroperoxide lyase activity in a catalase. *J Biol Chem*. 2015; 290. <https://doi.org/10.1074/jbc.M115.660282> PMID: 26100625
13. Lõhelaid H, Teder T, Samel N. Lipoxygenase-allene oxide synthase pathway in octocoral thermal stress response. *Coral Reefs*. 2015; 34. <https://doi.org/10.1007/s00338-014-1238-y>



14. Brash AR. Mechanistic aspects of CYP74 allene oxide synthases and related cytochrome P450 enzymes. *Phytochemistry*. 2009; 70: 1522–1531. <https://doi.org/10.1016/j.phytochem.2009.08.005> PMID: 19747698
15. Tijet N, Brash AR. Allene oxide synthases and allene oxides. *Prostaglandins Other Lipid Mediat*. 2002; 68–69: 423–431. [https://doi.org/10.1016/S0090-6980\(02\)00046-1](https://doi.org/10.1016/S0090-6980(02)00046-1) PMID: 12432934
16. Hamberg M. Fatty acid allene oxides. *J Am Oil Chem Soc*. 1989; 66: 1445–1449.
17. Olliv EH, Aragó M, Chen Y, Jernerén F. A new class of fatty acid allene oxide formed by the DOX-P450 fusion proteins of human and plant pathogenic fungi, *C. immitis* and *Z. tritici*. *J Lipid Res*. 2016; 57: 1518–1528. <https://doi.org/10.1194/jlr.M068981> PMID: 27282156
18. Oldham ML, Brash AR, Newcomer ME. The structure of coral allene oxide synthase reveals a catalase adapted for metabolism of a fatty acid hydroperoxide. *Proc Natl Acad Sci U S A*. 2005; 102: 297–302. <https://doi.org/10.1073/pnas.0406352102> PMID: 15625113
19. Nielsen M, Lundegaard C, Lund O, Petersen TN. CPHmodels-3.0—remote homology modeling using structure-guided sequence profiles. *Nucleic Acids Res*. 2010; 38. <https://doi.org/10.1093/nar/gkq535> PMID: 20542909
20. Binkowski TA, Naghibzadeh S, Liang J. CASTp: Computed Atlas of Surface Topography of proteins. *Nucleic Acids Res*. 2003; 31: 3352–3355. <https://doi.org/10.1093/nar/gkq512> PMID: 12824325
21. Grosdidier A, Zoete V, Michielin O. SwissDock, a protein-small molecule docking web service based on EADock DSS. *Nucleic Acids Res*. 2011; 39. <https://doi.org/10.1093/nar/gkr366> PMID: 21624888
22. Pettersen EF, Goddard TD, Huang CC, Couch GS, Greenblatt DM, Meng EC, et al. UCSF Chimera—A visualization system for exploratory research and analysis. *J Comput Chem*. 2004; 25: 1605–1612. <https://doi.org/10.1002/jcc.20084> PMID: 15264254
23. Liu H, Naismith JH. An efficient one-step site-directed deletion, insertion, single and multiple-site plasmid mutagenesis protocol. *BMC Biotechnol*. 2008; 8: 91. <https://doi.org/10.1186/1472-6750-8-91> PMID: 19055817
24. De Luna P, Bushnell EAC, Gauld JW. A molecular dynamics examination on mutation-induced catalase activity in coral allene oxide synthase. *J Phys Chem B*. 2013; 117: 14635–14641. <https://doi.org/10.1021/jp408486n> PMID: 24164352
25. Gao B, Boeglin WE, Brash AR. Role of the conserved distal heme asparagine of coral allene oxide synthase (Asn137) and human catalase (Asn148): Mutations affect the rate but not the essential chemistry of the enzymatic transformations. *Arch Biochem Biophys*. 2008; 477: 285–290. <https://doi.org/10.1016/j.abb.2008.07.011> PMID: 18652800
26. Boutaud O, Brash AR. Purification and catalytic activities of the two domains of the allene oxide synthase-lipoxygenase fusion protein of the coral *Plexaura homomalla*. *J Biol Chem*. 1999; 274: 33764–33770. <https://doi.org/10.1074/jbc.274.47.33764> PMID: 10559269
27. Nagai M, Nagai Y, Imai K, Neya S. Circular dichroism of hemoglobin and myoglobin. *Chirality*. 2014. pp. 438–442. <https://doi.org/10.1002/chir.22273> PMID: 24425582
28. Hillar A, Peters B, Pauls R, Loboda A, Zhang H, Mauk AG, et al. Modulation of the activities of catalase-peroxidase HPI of *Escherichia coli* by site-directed mutagenesis. *Biochemistry*. 2000; 39: 5868–5875. <https://doi.org/10.1021/bi0000059> PMID: 10801338
29. Floris R, Moguilevsky N, Puppels G, Jacquet A, Renirie R, Bollen A, et al. Heme-protein interaction in myeloperoxidase: Modification of spectroscopic properties and catalytic activity by single residue mutation. *J Am Chem Soc*. 1995; 117: 3907–3912. <https://doi.org/10.1021/ja00119a003>
30. Neri F, Indiani C, Baldi B, Vind J, Welinder KG, Smulevich G. Role of the distal henylalanine 54 on the structure, stability, and ligand binding of Coprinus cinereus peroxidase. *Biochemistry*. 1999; 38: 7819–7827. <https://doi.org/10.1021/bi982811+> PMID: 10387022
31. Roncone R, Monzani E, Labò S, Sanangelantoni AM, Casella L. Catalytic activity, stability, unfolding, and degradation pathways of engineered and reconstituted myoglobins. *J Biol Inorg Chem*. 2005; 10: 11–24. <https://doi.org/10.1007/s00775-004-0606-4> PMID: 15565498
32. Gilbert NC, Niebuhr M, Tsuruta H, Bordelon T, Ridderbusch O, Dassey A, et al. A covalent linker allows for membrane targeting of an oxylipin biosynthetic complex. *Biochemistry*. 2008; 47: 10665–10676. <https://doi.org/10.1021/bi800751p> PMID: 18785758
33. Tosha T, Uchida T, Brash AR, Kitagawa T. On the relationship of coral allene oxide synthase to catalase: A single active site mutation that induces catalase activity in coral allene oxide synthase. *J Biol Chem*. 2006; 281: 12610–12617. <https://doi.org/10.1074/jbc.M600061200> PMID: 16513636
34. Crombie L, Morgan DO. Synthesis of [14,14-2H<sub>2</sub>]-linolenic acid and its use to confirm the pathway to 12-oxophytodienoic acid (12-oxoPDA) in plants: a conspectus of the epoxy-carbonium ion derived family of metabolites from linoleic and linolenic acid hydroperoxides. *J Chem Soc Perkin Trans 1*. 1991; 581–587. <https://doi.org/10.1039/P19910000581>

35. Lakshmipathi P, Grée D, Grée R. A facile C–C bond cleavage in the epoxides and its use for the synthesis of oxygenated heterocycles by a ring expansion strategy. *Org Lett*. 2002; 4: 451–454. <https://doi.org/10.1021/ol017164k> PMID: 11820902
36. Gerwick WH. Epoxy allylic carbocations as conceptual intermediates in the biogenesis of diverse marine oxylipins. *Lipids*. 1996. pp. 1215–1231. <https://doi.org/10.1007/BF02587906> PMID: 8972454
37. Lee D-S, Nioche P, Hamberg M, Raman CS. Structural insights into the evolutionary paths of oxylipin biosynthetic enzymes. *Nature*. 2008; 455: 363–8. <https://doi.org/10.1038/nature07307> PMID: 18716621
38. Ermilova VS, Gorina SS, Osipova E V, Toporkova YY, Mukhtarova LS, Gogolev Y V, et al. Alteration of the catalytic properties of divinyl ether synthase as a result of substitutions of unique amino acids. *Dokl Biochem Biophys*. 2013; 452: 251–254. <https://doi.org/10.1134/S1607672913050128> PMID: 24150585
39. Toporkova YY, Mukhtarova LS, Gogolev Y V, Grechkin AN. Origins of the diversity of cytochrome P450 CYP74 family based on the results of site-directed mutagenesis. *Moscow Univ Biol Sci Bull*. 2010; 65: 155–157. <https://doi.org/10.3103/S0096392510040085>

## PUBLICATION III

T. Teder, N. Samel, H. Lõhelaid

**Distinct characteristics of the substrate binding between highly homologous catalase-related allene oxide synthase and hydroperoxide lyase**

*Archives of Biochemistry and Biophysics* 676 (2019) 108216





Contents lists available at ScienceDirect

## Archives of Biochemistry and Biophysics

journal homepage: [www.elsevier.com/locate/yabbi](http://www.elsevier.com/locate/yabbi)

## Distinct characteristics of the substrate binding between highly homologous catalase-related allene oxide synthase and hydroperoxide lyase

Tarvi Teder, Nigulas Samel, Helike Lõhelaid\*

Department of Chemistry and Biotechnology, Tallinn University of Technology, Tallinn, Estonia



## ARTICLE INFO

## Keywords:

Allene oxide synthase  
Catalase  
Hydroperoxide lyase  
Molecular modeling  
Oxylipins  
Site-directed mutagenesis

## ABSTRACT

A catalase-related allene oxide synthase (cAOS) or a hydroperoxide lyase (cHPL) fused together with an 8R-lipoxygenase is involved in the stress signaling of corals via an arachidonic acid pathway. cAOS gives rise to  $\alpha$ -ketol and cyclopentenone, while cHPL catalyzes the cleavage of 8R-hydroperoxyeicosatetraenoic acid (8R-HpETE) to C8-oxo acid and C12 aldehyde. *In silico* analysis of the substrate entry sites of highly identical coral cAOS and cHPL indicated that two positively charged residues of cAOS, K60 and K107, and the corresponding residues of cHPL, E60 and K107, may be involved in the anchoring of the carboxy group of polyunsaturated fatty acid (PUFA) hydroperoxides. A mutational analysis of cAOS and cHPL revealed that K60 or E60 and K107 were not necessary in the tethering of 8R-HpETE, however, the E60 of cHPL was essential in the productive binding of PUFA hydroperoxides. The substrate preferences of cAOS and cHPL were determined with hydroperoxy derivatives of C18, C20, C22 PUFAs, anandamide (AEA), 1-arachidonoyl glycerol (1-AG) and selected methylated substrates. Although cAOS and cHPL were able to metabolize different free PUFA substrates and arachidonoyl derivatives, only cHPL catalyzed the reaction with methylated PUFA hydroperoxides. The differences in the substrate binding and preferences between cAOS and cHPL can be explained by the distinct properties of their substrate entry sites. The current study demonstrated that homologous PUFA metabolizing enzymes may contribute to the versatile usage of the substrate pool.

## 1. Introduction

A catalase-related allene oxide synthase (cAOS) or a hydroperoxide lyase (cHPL) and an 8R-lipoxygenase (8R-LOX) in corals are expressed together as a single protein, cAOS-LOX [1] or cHPL-LOX, initially designated as cAOS-LOXb [2], respectively. Despite the functionally conserved C-terminal 8R-LOX domains, the highly homologous N-terminal domains of both fusion proteins synthesize different products. Specifically, the C-terminal 8R-LOX domain performs the oxygenation of arachidonic acid (AA) to 8R-hydroperoxyeicosatetraenoic acid (8R-HpETE) which is subsequently converted to an unstable allene-8,9-epoxide by the N-terminal catalase-related cAOS [3]. In contrast to cAOS, cHPL catalyzes the cleavage of 8R-HpETE to the short-chain aldehydes, 8-oxo-(6E)-octenoic acid and (3Z,6Z)-dodecadienal [4]. Although coral cAOS and cHPL catalyze the same reaction as the corresponding enzymes in plants [5], the latter belong to the cytochrome P450

superfamily and therefore are structurally unrelated to catalase-related enzymes [6]. Nevertheless, similarly to LOX-dependent pathways in plants [5], coral cAOS-LOX and cHPL-LOX, being at the center of the eicosanoid synthesis [7,8], are involved in the mechanical [2] and thermal stress response [9] of corals. Regardless of the conserved catalytic center between coral cAOS, cHPL and catalase [1,2,10], the cHPL-specific activity is achieved by F150 and S177 residues in the substrate channel of cHPL instead of L150 and L177 in cAOS [11]. However, structural aspects in the substrate binding and the substrate preference between cAOS and cHPL have not been studied. The elucidation of the X-ray structure of *Plexaura homomalla* cAOS proposed two positively charged lysines, K60 and K107 (Fig. 1), in the substrate entry site as the potential anchoring residues of the negatively charged carboxy group of 8R-HpETE [10]. This type of interaction between the positively charged side chain of an amino acid and the negatively charged carboxy group of a polyunsaturated fatty acid (PUFA) substrate

**Abbreviations:** 1- or 2-AG, 1- or 2-arachidonoyl glycerol; 8R-HpETE, 8R-hydroperoxy-5Z,9E,11Z,14Z-eicosatetraenoic acid; 8R-HpETE, 8R-hydroperoxy-5Z,9E,11Z,14Z,17Z-eicosapentaenoic acid; 10R-HpDHE, 10R-hydroperoxy-4Z,7Z,11E,13Z,16Z,19Z-docosahexaenoic acid; AA, arachidonic acid; AEA, arachidonoyl ethanolamide; ALA, alpha-linolenic acid; cAOS, catalase-related allene oxide synthase; Cap8R-LOX, *Capnella imbricata* 8R-LOX; cHPL, catalase-related hydroperoxide lyase; DHA, docosahexaenoic acid; EPA, eicosapentaenoic acid; GLA, gamma-linolenic acid; PUFA, polyunsaturated fatty acid

\* Corresponding author.

E-mail address: [helike.lohelaid@taltech.ee](mailto:helike.lohelaid@taltech.ee) (H. Lõhelaid).<https://doi.org/10.1016/j.ab.2019.108126>

Received 29 July 2019; Received in revised form 30 September 2019; Accepted 2 October 2019

Available online 04 October 2019

0003-9861/© 2019 Elsevier Inc. All rights reserved.

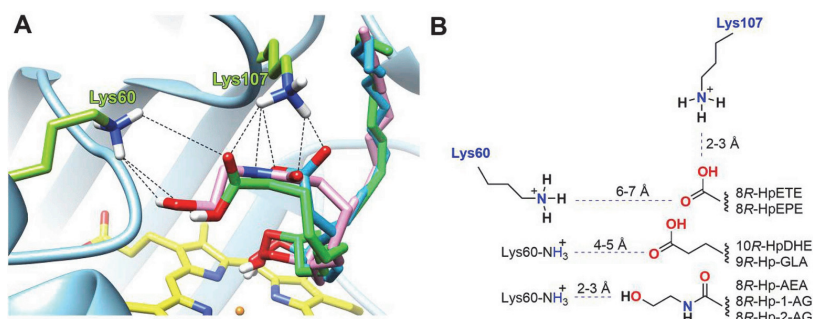


**Fig. 1.** The interactions between the head group of selected ligands and the K60 and K107 of cAOS determined by the docking simulations. (A) The docking results with 8R-HpETE (blue), 10R-HpDHE (green) and 8R-Hp-AEA (pink). The interactions between the residues and the head groups are presented as dotted lines. The heme is presented as yellow. (B) The schematic representation of docking results with used ligands. The proximity between the head group of ligands and K107 was 2–3 Å, while the distance from K60 varied due to the length differences between ligands. Based on the proximity to K60, the ligands were divided into the three following

groups: C20, C18 and C22, and endocannabinoid derivatives of PUFA hydroperoxides. Only the interactions between the head group of 8R-Hp-AEA and K60 are shown. (For interpretation of the references to colour in this figure legend, the reader is referred to the Web version of this article.)

is essential for many PUFA metabolizing enzymes. For example, R182 in the substrate entry site of *P. homomalla* 8R-LOX and R120 of two pro-inflammatory isozymes, cyclooxygenase-1 (COX-1) and cyclooxygenase-2 (COX-2), are necessary for the anchoring of PUFA substrates [12,13]. At the same time, the presence of E60 instead of K60 in the *Capnella imbricata* cHPL sequence (Fig. 1) indicates that the tethering of 8R-HpETE by cHPL might be different. The notion was supported by our previous mutagenesis experiment, where the replacement of E60 in regard of the ME59-60LK double mutation of cHPL reduced the activity significantly [11]. Although the most remarkable structural difference, the SSSAGE motif of cHPL instead of the PVEEGD of cAOS, adjacent to the substrate entry sites, is not involved in the reaction specificity [11], the effect of these motifs on the binding and selectivity of polyunsaturated fatty acid (PUFA) hydroperoxides was not examined. Despite the structural information of cAOS, the role of K60 and K107 in regard to the substrate binding and specificity is unknown. Therefore, the aim of this study was to compare the substrate binding of cAOS and cHPL by analyzing their substrate entry sites *in silico*, performing mutational analyses and conducting kinetic measurements with different hydroperoxy PUFAs as substrates.

## 2. Materials and methods

### 2.1. Materials

Arachidonic acid (20:4n-6, AA), eicosapentaenoic acid (20:5n-3, EPA), docosahexaenoic acid (22:6n-3, DHA),  $\alpha$ -linolenic acid (18:3n-3, ALA),  $\gamma$ -linolenic acid (18:3n-6, GLA), arachidonoyl ethanolamide (AEA) and 1-arachidonoyl glycerol (1-AG) were purchased from Cayman Chemical Company and [ $1-^{14}\text{C}$ ]-labeled AA were acquired from Amersham Pharmacia Biotech. Only HPLC grade solvents (Sigma-Aldrich) were used. All of the buffer components were purchased from Merck.

### 2.2. Structural analysis of cAOS and cHPL

The amino acid sequences of *P. homomalla* cAOS (GenBank accession nr: AF003692.1) and *C. imbricata* cHPL (GenBank accession nr: KF000374.1) were aligned using MegAlign software (DNASar 7.1) to determine the differences in residues of the substrate entry sites. The location of amino acid variances between cAOS and cHPL were determined based on the crystal structure of *P. homomalla* cAOS (PDB code: 1u5u) [10]. The 3D homology model of cHPL with Global Model Quality Estimation (GMQE) and Qualitative Model Energy Analysis (QMEAN) values of nearly 1 [14] were prepared based on the crystal structure of cAOS using SwissModel [15]. The electrostatic and hydrophilic properties of the substrate entry sites of cAOS and cHPL were determined and visualized by using UCSF Chimera (1.13.1) software

[16].

### 2.3. Docking simulations and homology modeling

The docking of 8R-hydroperoxy derivatives of AA (8R-HpETE), EPA (8R-HpEPE), DHA (8R-HpDHE), AEA (8R-Hp-AEA), 1-AG (8R-Hp-1-AG), 2-AG (8R-Hp-2-AG), and 6R- or 9R-hydroperoxy ALA (6R- or 9R-Hp-ALA) and GLA (6R- or 9R-Hp-GLA) as ligands into the X-ray structure of cAOS or the model of cHPL were conducted using AutoDock Vina (ADV) [17] and SwissDock (SW) [18] tools in parallel for the reproducibility purposes. Although the expected outcome of both docking tools should be highly similar, the docking process and the scoring function of ADV and SW are different [17,18]. The ligands were prepared by using ChemDraw Professional 16 and the PRODRG server [19]. As the crystallization and the incubations with cAOS were performed around physiological pH [10,20], positively charged residues, e.g. R and K, were protonated in the docking simulations. The docking with a ligand having either a charged ( $\text{RCOO}^-$ ) or neutral ( $\text{RCOOH}$ ) carboxy group gave similar results and therefore only the neutral ligands were presented in this work. Formed enzyme-ligand complexes were evaluated by the docking geometry and docking affinity [21]. Based on the geometric attributes of the substrate binding site [10,22], cAOS should bind PUFA hydroperoxides in a catalytically productive conformation with their hydroperoxy group (-OOH) placed near H67, T66 and the heme, and with their head group (RCOOH) located near K107 and/or K60 at the opening of the substrate channel. The distance for a strong hydrogen bond or an electrostatic interaction should be less than 5 Å, and ideally around 3 Å [23]. The correctly formed enzyme-ligand complexes were scored based on the binding energy and the best outcomes were presented in the results. Protein structures and protein-ligand complexes were visualized using UCSF Chimera (1.13.1) software [24]. The 2D interpretation of the interactions in enzyme-ligand complexes were generated by using LigPlot+ v 2.1 [25]. The MODELLER tool [26] in Chimera software was used to remodel the cHPL SSSAGE fragment in the substrate channel opening. The best model having the refined loop with the highest GA341 as a statistical potential value [27], the lowest zDope as a Discrete Optimized Protein Energy value [28] and the smallest estimated overlap with the loop of the initial cHPL model were used in the docking simulations by SW.

### 2.4. Site-directed mutagenesis

The replacements of existing residues, E60 and K107, of cHPL with similar-sized residues containing the side chain with either neutral or opposite charge were carried out using the site-directed mutagenesis method. The E60M, E60K, K107M, and K107E mutations of cHPL were inserted into the cHPL-His4+ pET11a construct [4] by using the whole plasmid PCR [29]. The cAOS domain was PCR-amplified from the His6-

cAOS-LOX sequence [1] and cloned into the pET11a expression vector using the previously described protocol [11]. Analogously to cHPL, the K60M, K60E, K107M and K107E mutants of cAOS were prepared using the cAOS-His4 + pET11a template. To exclude the possible co-operativity between K60 and K107, the double mutant K60M + K107M was prepared in parallel. Complementary primers with silent mutations for the restriction analysis used in the whole plasmid PCR are presented in Table S1. The mutations were screened by restriction analysis and the constructs were sequenced (Agowa, Germany).

### 2.5. Expression and purification

The expression and the purification of wild-type (wt) enzymes and mutants were carried out as described previously [11] with slight modifications. The cHPL and cAOS mutants were expressed at 10 °C and 15 °C, respectively, in 0.5 L of lysogeny broth (LB) medium overnight. The cell pellets were resuspended in a lysis mixture containing 20 mM Tris (pH 8.0), 100 μM phenylmethylsulfonyl fluoride (Sigma-Aldrich), 0.2% Tergitol NP-40 (Sigma-Aldrich), 1 mg/mL of lysozyme (Sigma-Aldrich) and 10U/mL benzonase nuclease (Santa Cruz Biotechnology), and incubated on ice, stirring for 30 min prior to the sonication. Cells were sonicated for 10 × 5 s on ice using a Bandelin Sonopuls HD 2200 ultrasonic homogenizer at about 30% power and centrifuged at 40 000 × g in 1 h at 4 °C. The supernatant was applied on the nickel-NTA column (1 mL of bed volume, Sigma-Aldrich) equilibrated with the loading buffer (20 mM Tris, 300 mM NaCl, pH 8.0). The protein was eluted with the elution buffer (20 mM Tris, 300 mM NaCl, 200 mM imidazole, pH 8.0) and the 1 mL fractions were collected and assayed for activity. The positive fractions were dialyzed in a 50 mM Tris (pH 8.0) and 150 mM NaCl buffer by using regenerated cellulose tubular dialysis membrane (MWCO: 12000 ± 14000 Da; Orange Scientific) with constant stirring at 4 °C overnight. The dialyzed proteins were stored at –80 °C for further use. The level of protein purity over 80% was determined by the analysis of SDS-PAGE using GeneTools software (Syngene).

### 2.6. Protein quantification and heme analysis

Protein samples were quantified at 406 nm ( $\epsilon \sim 100\,000\text{ M}^{-1}\text{ cm}^{-1}$ ), characteristic for heme proteins, by using a 1601 UV–visible spectrometer (Shimadzu). The  $\lambda$  maxima of mutants were compared to the corresponding values of wt cHPL or wt cAOS, 406 nm and 407 nm, respectively [11]. Wt cHPL, wt cAOS and mutants with the same heme concentration were compared by SDS-PAGE to estimate the relative quantities of heme-free protein by using GeneTools densitometry (Syngene). The ratio between heme-containing and heme-free protein was determined by size exclusion chromatography using a Superdex 200 Increase 10/300 GL (GE Healthcare) column with a 50 mM Tris (pH 8.0) and 150 mM NaCl buffer at a flow rate of 0.7 mL/min on an AKTA FPLC system (GE Healthcare) at 406 nm and 280 nm. The extension coefficients at 280 nm were calculated by using an EXPASy ProtParam web tool (<https://web.expasy.org/protparam>).

### 2.7. Enzyme assay

Incubations with 10 nM wt cHPL, wt cAOS and each mutant were performed using 10 μM 8R-HpETE synthesized from AA by 1 nM C. imbricata 8R-lipoxygenase (Cap8R-LOX) of cHPL-LOX fusion protein [11] in a 50 mM Tris (pH 8.0) buffer containing 100 mM NaCl and 1 mM CaCl<sub>2</sub> in a quartz cuvette, with constant stirring at 20 °C. The appearance and disappearance of a conjugated diene chromophore ( $\epsilon \sim 25\,000\text{ M}^{-1}\text{ cm}^{-1}$ ) at 235 nm was recorded using a 1601 UV–visible spectrometer (Shimadzu). The capabilities of wt cHPL and wt cAOS to metabolize neutral PUFA hydroperoxides were tested by using 12 μM hydroperoxy derivatives of endocannabinoids, AEA and 1-AG, as well as AA and DHA containing methylated head groups, Met-AA and

Met-DHA. Methylated substrates were prepared using diazomethane. Incubations with PUFA hydroperoxides derived from ALA, GLA, EPA, DHA, AEA or 1-AG by Cap8R-LOX were carried out as with the 8R-HpETE substrate.

The kinetic measurements were conducted using 5–80 μM PUFA hydroperoxides of AA, EPA, DHA, ALA, GLA, Met-AA or Met-DHA and the initial reaction velocity was determined from the linear part of the curve. The  $k_{\text{cat}}$  and  $K_{\text{m}}$  values and the corresponding standard errors (SE) were calculated employing the nonlinear regression analysis of the Michaelis-Menten equation using PRISM 6 (GraphPad) program. The catalytic efficiency was calculated based on the  $k_{\text{cat}}/K_{\text{m}}$  ratio. The standard errors of the  $k_{\text{cat}}/K_{\text{m}}$  values were estimated from the following equation: the SE of  $k_{\text{cat}}/K_{\text{m}} = (k_{\text{cat}}/K_{\text{m}})[(\text{the SE of } k_{\text{cat}}/k_{\text{cat}})^2 + (\text{the SE of } K_{\text{m}}/K_{\text{m}})^2]^{1/2}$ .

Incubations with 20 μM [<sup>1-14</sup>C]-AA-derived 8R-HpETE substrate were performed for the product analysis. The reactions were stopped using the mild reducing agent SnCl<sub>2</sub> (final concentration at 1 mg/mL) and acidified with HCl to pH 3.5. The products were extracted using ethyl acetate, taken to dryness and dissolved in an HPLC eluent prior to further analysis.

### 2.8. HPLC-MS analysis

The PUFA hydroperoxides synthesized from AA, DHA, EPA, ALA and GLA by 8R-LOX and the metabolites derived from corresponding PUFA hydroperoxides by wt cAOS or wt cHPL were analyzed with RP-HPLC connected to MSMS using the same protocol as described previously [2]. The PUFA metabolites catalyzed by the cHPL and cAOS mutants were identified in a similar manner. The products synthesized from [<sup>1-14</sup>C]-8R-HpETE were analyzed by RP-HPLC connected to a radiodetector [2]. As the products derived from 8R-Hp-AEA and 8R-Hp-1-AG do not contain ionic groups, the positive mode of MS was used [30].

### 2.9. Methylation of surface lysines of cAOS

The methylation of surface lysines of cAOS (Met-cAOS) was carried out with a borane dimethylamine complex and formaldehyde in a 20 mM potassium phosphate (pH 8) buffer based on the published protocol [31]. The Met-cAOS was analyzed by SDS-PAGE and MALDI-TOF (Bruker) to control the dimethylation of the enzyme. The Met-cAOS was treated with trypsin, and the methylation of K60 and K107 were determined by nano-LC-MSMS (Thermo Fisher Scientific) in the Proteomics Core Facility at the University of Tartu. The activity of the Met-cAOS with 8R-HpETE was estimated as previously described for wt cAOS and wt cHPL (see “2.7. Enzyme assay”).

## 3. Results

### 3.1. Analysis of enzyme-ligand complexes

The docking results of cAOS with most of the selected ligands using either ADV or SW were in agreement with the docking criteria. Specifically, the ligands were placed inside the substrate channel in a catalytically productive conformation, with the carboxy group located near the K107 of cAOS. For clarity, only the docking poses with SW were presented and illustrated in figures (Figs. 1 and 2C). The binding energies of protein-ligand complexes and the distances of the hydroperoxy group and the head group of a ligand between selected residues and heme are summarized in Table S2. Both docking tools, SW and ADV, were not able to fit 9R-Hp-ALA into the substrate channel of cAOS possibly due to the conformational rigidity of the ligand. A docking simulation with 8R-Hp-2-AG was performed successfully only by ADV. The different outcomes by ADV and SW can be explained by the distinct docking processes.

The distances between the hydroperoxy group of 8R-HpETE and

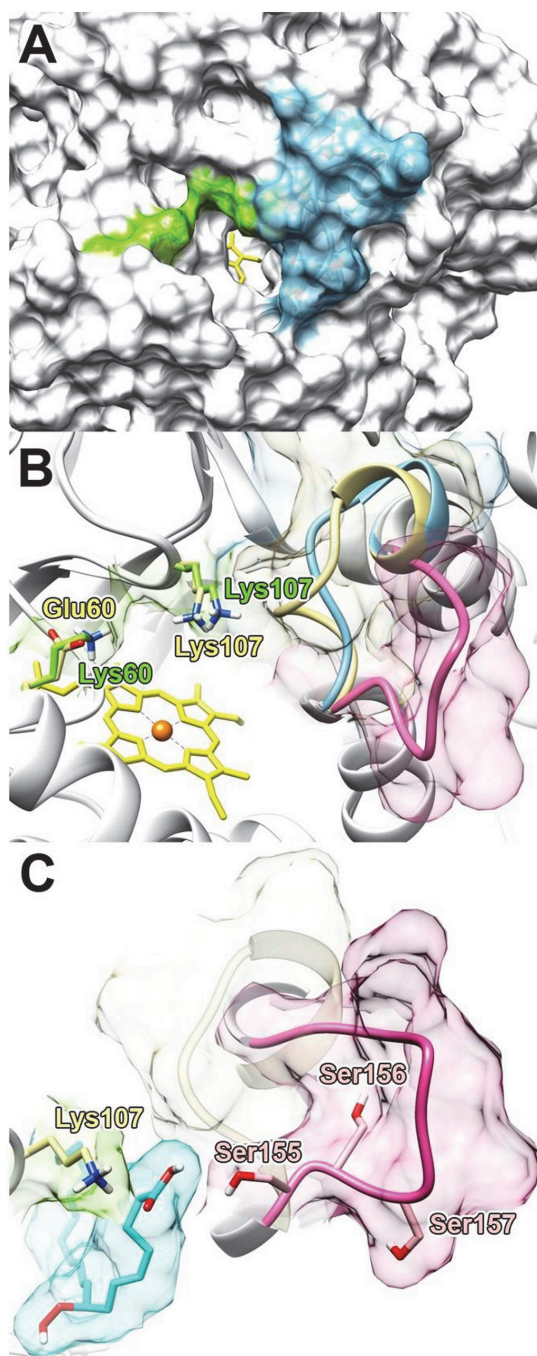


**Fig. 2.** The substrate entry sites of cAOS, the cHPL model and the cHPL-SSSAGE model. (A) The substrate entry site of cAOS with the green and blue surfaces presenting K60 and K107, and the PVEEGD region, respectively. The heme is presented as yellow. (B) The superimposed structures of cAOS (blue), the homology model of cHPL (beige) and the cHPL-SSSAGE model (pink). (C) The docking result of the cHPL-SSSAGE model with the head group of 8R-HpETE (cyan) placed between K107 (beige) and the SSSAGE loop (pink). (For interpretation of the references to colour in this figure legend, the reader is referred to the Web version of this article).

H67, T66 and the heme group of cAOS (Table S2) were comparable to the previously published docking simulations [11,22,32]. Although the alternative ligands were placed inside the substrate channel similarly to 8R-HpETE, the positioning near K60 and K107 varied due to the differences in the length and the double bonds of the aliphatic tails or the sizes of the head group of the ligands (Fig. 1A and B). Moreover, small differences in the distances were the results of the slight rotations between single C–C bonds, resulting in the placement of the -OOH group of a ligand closer to either H67, T66 or the heme (Table S2).

The wide opening of the substrate entry site allowed the binding of 8R-HpETE derivatives with different sizes of the head group without disrupting the binding of the aliphatic tails of substrates (Fig. 1A). From the docking simulation standpoint, the correctly formed enzyme-ligand complex was achieved mainly due to the suitable structural properties of the substrate cavity of cAOS, e.g. the size and shape, which were the basis for the binding of selected PUFA hydroperoxides. As the ion-ion interaction between the carboxy head group and K107 or K60 was not the primary criterion of docking programs, neutral PUFA hydroperoxides were placed in the substrate channel similarly to free PUFA ligands. Therefore, 8R-Hp-AEA, 8R-Hp-1-AG, 8R-Hp-2-AG, and methylated ligands were placed in the substrate channel in a productive conformation. All of the used ligands had the carbonyl oxygen in the head group which have the potential to interact with K107 via a hydrogen bond. Due to the larger head group of 8R-hydroperoxy derivatives of endocannabinoids, the hydrogen bonding between the hydroxy group and K60 of cAOS was possible (Fig. 1). The ability of cAOS and cHPL to use alternative substrates *in vitro* will be presented below.

### 3.2. Homology modeling and docking simulations of cHPL

Despite the good resolution of the X-ray structure of cAOS [10] and the high sequence identity between the template and the target, cAOS and cHPL [2], the docking simulations with the initial cHPL model were unsuccessful. It should be noted that > 30% of the amino acid identity and > 30% of the coverage between the model and the template are accurate enough to predict the structure of a protein [33]. Thus, only a significant difference in the structural motifs in comparison to cAOS, e.g. the SSSAGE loop in the substrate entry site of cHPL (Fig. 2), could have influenced the outcome of docking simulations. In our previous study, the replacement of the SSSAGE sequence of cHPL with the PVKEGD of *C. imbricata* cAOS only reduced the turnover rate but did not alter the reaction specificity, indicating that the loop did not have a major impact on the substrate coordination [11]. However, a model derived from a X-ray structure might ignore the flexibility of certain loops and dynamic domains, which together with the differences in residues might affect the docking results and consequently lead to misinterpretation. As stated previously [11], the substrate entry site of cHPL might be wider, which was not achieved with the homology modeling due to the high dependency of the structure of cAOS (Fig. 2A and B). The remodeling of the SSSAGE loop resulted in an extended substrate entry site (Fig. 2B), which was appropriate to perform successful docking simulations with the modified cHPL model (cHPL-SSSAGE model) (Fig. 2C). The shift in the SSSAGE loop away from the PVEEGD of cAOS as a template motif (Fig. 2B) was important evidence, pointing out the potential conformational difference between the substrate entry sites of cAOS and cHPL.



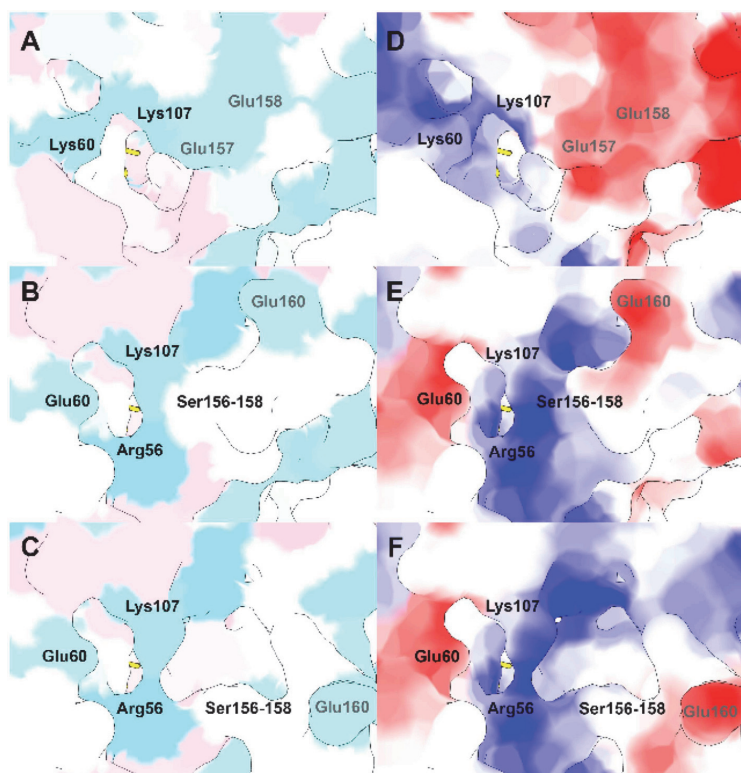


**Fig. 3.** The hydrophobic and electrostatic properties of the substrate entry sites of cAOS, the cHPL model and the cHPL-SSSAGE model. (A, B and C) The hydrophobic regions (pink) and hydrophilic regions (sky blue) of cAOS, the cHPL model and the cHPL-SSSAGE model. The heme is presented as yellow. (D, E and F) The electrostatic regions from positive to negative (from blue to red, respectively) of cAOS, the cHPL model and the cHPL-SSSAGE model. (For interpretation of the references to colour in this figure legend, the reader is referred to the Web version of this article).

### 3.3. Properties of the substrate entry sites of cAOS and cHPL

The hydrophobic and electrostatic properties of the substrate entry sites of cAOS, the initial cHPL model and the cHPL-SSSAGE model were compared (Fig. 3). Although K60 and K107 gave hydrophilic properties for the substrate entry site of AOS, the lower part contained only hydrophobic residues (Fig. 3A). In contrast, the substrate entry sites of cHPL and the cHPL-SSSAGE model were more hydrophilic (Fig. 3B and C), mainly due to R56 and the S156-158 motif, which are missing in the cAOS sequence. The K60 and K107 of cAOS made the substrate entry site positively charged (Fig. 3D), while E60 instead of K60 and R56 contributed to the more diverse electrostatic properties of the substrate binding site of cHPL (Fig. 3E and F).

### 3.4. Protein expression, quantification and heme analysis

The expression yields of wt cHPL and wt cAOS were determined to be 0.5 and 1.8 mg of purified protein per 1 g of biomass, respectively, correlating with our previous findings [11]. The cHPL and cAOS mutants were purified and yielded around 0.1–0.4 mg and 0.5–1.0 mg of protein per 1 g of biomass, respectively. The lower protein yields of cHPL can be explained by the cHPL's tendency to accumulate in the inclusion bodies at higher expression temperatures (personal data). Therefore, the expression temperature of cHPL was lowered to 10 °C, while cAOS was expressed at 15 °C.

The protein concentration determined based on the heme

absorbance around 406 nm represents the active part of the protein pool at 280 nm. The mixture of purified protein might contain the heme-containing and heme-free protein [11]. The ratios between the concentrations at 280 nm and at 406 nm of wt cHPL, E60M, E60K, K107M, and K107E were determined by size exclusion chromatography as follows: 2, 5, 2, 26, and 29, respectively. The K107 mutants contained significantly more heme-free protein than the wt cHPL and E60 mutants. The corresponding ratios for wt cAOS, K60M, K60E, K107M, and K107E mutants were calculated as 4, 11, 8, 7, and 12, respectively. These ratios indicate that all of the samples contained heme-free protein. These results are in correlation with the SDS-PAGE analysis (Table S3) (Fig. S1).

The UV–Vis spectra of all enzymes were compared to analyze the changes in the absorbance of the heme. The  $\lambda$  maxima of mutants corresponded to the wt enzymes, except for E60M and E60K mutants of cHPL which had corresponding values around 408 nm instead of 406 nm. There was an indication that the E60 replacements slightly influenced the heme chromophore by shifting the distances of conjugated bonds. As there were no significant shifts, over 10 nm, in the  $\lambda$  maxima, the oxidation state remained unaltered [34].

### 3.5. Products formed by the cAOS and cHPL mutants

The reaction specificities of cAOS and cHPL were not affected by the mutations as the radiochromatograms and RP-HPLC-MS profile of the products synthesized by cAOS and cHPL mutants correspond to wild-

type products [4]. The unaltered product profiles of cAOS and cHPL mutants implied that the mutated residues in the substrate channel opening did not influence the substrate positioning in the catalytic center.

### 3.6. Products formed from alternative substrates by coral 8R-LOX, cAOS and cHPL

The products formed from AA, EPA, DHA, ALA, GLA, AEA, and 1-AG by Cap8R-LOX were determined as 8R-HpETE, 8R-HpEPE, 10R-HpDHE, 8R-Hp-AEA, 9R-Hp-ALA, 9R-Hp-GLA and 8R-Hp-1-AG, respectively. All of the  $m/z$  values and retention times of formed product are presented in Table S4. Although the stereoconfiguration of the hydroperoxy group of each precursor substrate was not analyzed, *R*-specificity should have remained as cAOS and cHPL can metabolize only 8R-derivatives [4,20]. Although Cap8R-LOX was out of the scope of the study, it should be mentioned that the formation of 10R-HpDHE from DHA by Cap8R-LOX was in correlation with the regioselectivity of *P. homomalla* 8R-LOX [20]. Moreover, Cap8R-LOX synthesized only 9R-Hp-GLA instead of the expected 6R-Hp-GLA indicating that the shorter length of the molecule, C18 instead of C20 or C22, and the carboxy group interaction with the residues in the entry site of the substrate channel obstructed the complete entrance of the substrate to the bottom of the substrate channel. Based on the results with the C18 to C22 PUFA substrates, we can conclude that the distance of the catalytic center of Cap8R-LOX is about 12 carbons from the bottom and 9 carbons from the entry site of the substrate channel.

All 8R-hydroperoxy FAs derived from precursor PUFAs were metabolized to corresponding wt products by cAOS or cHPL in the same catalytic mechanism as determined for the natural 8R-HpETE substrate [1,4]. For instance, C10-oxo acid and C12 aldehyde formed from 10R-HpDHE by cHPL while cAOS gave rise to 10R-HpDHE-derived  $\alpha$ -ketol and cyclopentenone. Likewise, the 8R-hydroperoxy derivatives of AEA and 1-AG were metabolized to the corresponding products of cAOS or cHPL.

### 3.7. Kinetic parameters of wild-type enzymes and mutants

The kinetic parameters of wt cAOS, wt cHPL and mutants determined with different PUFA hydroperoxides are presented in Table 1 (the kinetic curves are given in Fig. S2 and Fig. S3). The  $k_{\text{cat}}$  and  $K_m$  of cAOS K60M, K60E, and K107M with 8R-HpETE were comparable to the values obtained with wt cAOS. The result with the K60M+K107M double mutant correlated with the single mutations, K60M and K107M, except for the fact that at higher substrate concentrations, a reaction inhibition occurred. In addition, the activity of Met-cAOS with 8R-HpETE was identical to the measurements with wt cAOS, showing the lack of necessity of the salt bridge formation between the head group of PUFA substrates and positively charged K60 and K107. However, the turnover rate of cAOS was reduced remarkably with the K107E substitution. Similar kinetic parameters were observed with 8R-HpEPE, except that the K60M and K60E mutants had higher  $K_m$  values. The  $k_{\text{cat}}$  values of cAOS K60M, K60E, and K107M with 10R-HpDHE were 1.5 times and the  $K_m$  values of corresponding mutants were 2.5 times lower than the values established with 8R-HpETE and 8R-HpEPE. In contrast to the result with 8R-HpETE and 8R-HpEPE, the  $k_{\text{cat}}$  value of the K107E mutant with 10R-HpDHE did not show any significant difference compared to the turnover rates of K60M and K60E mutants. Moreover, the  $k_{\text{cat}}$  value of K107M with 10R-HpDHE was similar to the turnover rates obtained with 8R-HpETE and 8R-HpEPE, which did not correlate with the measurements with other K107 and K60 mutants. This unexpected result cannot be explained with our current knowledge.

The  $k_{\text{cat}}$  and  $K_m$  values of cHPL were decreased remarkably as a result of the E60 mutations. Specifically, the kinetic parameters of cHPL E60M with all the selected substrates were about two times lower than the values obtained with wt cHPL. While the  $k_{\text{cat}}$  and  $K_m$  values of cHPL

E60K with 8R-HpETE and 10R-HpDHE were about 10 times lower, the  $k_{\text{cat}}$  value with 8R-HpEPE was only 2.5 times lower than the values of wt cHPL. In contrast to the K107 mutations of wt cAOS, the K107 replacements of cHPL increased the  $k_{\text{cat}}$  values remarkably. The kinetic parameters of cHPL K107M compared to the values obtained with wt cHPL and other mutants were the highest. The  $k_{\text{cat}}$  of cHPL K107E with 8R-HpETE was doubled in comparison to the values of wt cHPL while the  $K_m$  values were nearly identical. The  $k_{\text{cat}}$  of cHPL K107E with 8R-HpEPE and 10R-HpDHE were comparable to the  $k_{\text{cat}}$  of wt cHPL, however, the K107E mutation made the  $K_m$  value of cHPL about 2–3 times lower.

The  $k_{\text{cat}}$  values of wt cAOS and its mutants with 9R-Hp-ALA and 9R-Hp-GLA were significantly lower compared with the results obtained with C20 PUFA hydroperoxides. The turnover rates of cAOS with 9R-Hp-ALA increased as a result of the replacement of K60 or K107 with M while the corresponding value decreased with the change of K60 or K107 to E. The results suggested that the mutations influenced the binding of 9R-Hp-ALA more drastically compared to the measurements with other substrates. This observation can be explained by the more linear shape of the substrate molecule from the carboxy head to the hydroperoxy group which was also an obstacle in the docking simulations. The  $k_{\text{cat}}$  values of wt cAOS and mutants with 9R-Hp-GLA as the C18 PUFA derivative and 10R-HpDHE as the C22 PUFA derivative were comparable. In addition, the  $k_{\text{cat}}$  value of cAOS K107M with 9R-Hp-GLA, similarly to the results with 10R-HpDHE, was higher than the corresponding value obtained with other mutants. The  $k_{\text{cat}}$  values of wt cHPL and its mutants with 9R-Hp-ALA and 9R-Hp-GLA were similar to the turnover rates determined with 8R-HpEPE. The  $k_{\text{cat}}/K_m$  values of wt cAOS, wt cHPL and their mutants with C18 PUFA hydroperoxides were remarkably lower than determined with 8R-HpETE, 8R-HpEPE and 10R-HpDHE.

### 3.8. Substrate preferences of cAOS and cHPL

The substrate preferences of cAOS and cHPL (Scheme 1) were determined based on the  $k_{\text{cat}}/K_m$  values [35] obtained with the corresponding PUFA hydroperoxides (Table 1). In comparison between different PUFA hydroperoxides, cAOS metabolized 8R-HpETE and 8R-HpEPE with similar and 10R-HpETE with slightly lower catalytic efficiency, while the  $k_{\text{cat}}/K_m$  values with 9R-Hp-ALA and 9R-Hp-GLA were about two times lower. The substrate selectivity of cHPL was distinct from cAOS (Table 1). The best substrate for cHPL was determined to be 8R-HpETE while 8R-HpEPE and 10R-HpEPE were metabolized with lower efficiencies. The  $k_{\text{cat}}/K_m$  of cHPL with 9R-Hp-ALA and 9R-Hp-GLA was 3 and 1.5 times lower, respectively, compared to the value obtained with the best substrate, 8R-HpETE.

### 3.9. Activities of cAOS and cHPL with selected alternative substrates

The  $k_{\text{cat}}$  value of cHPL with 8R-HpETE was about 10 times lower compared to the turnover rate of cAOS (Table 1). In the case of AA derivatives with bulkier headgroups, endocannabinoids, the opposite trend was observed. Specifically, cHPL metabolized 8R-Hp-AEA and 8R-Hp-1-AG with a four-times higher reaction rate compared to the activity of cAOS (Table S5).

To test if the ionic state of the head group of a PUFA substrate influenced the reaction rates of cAOS and cHPL, Met-8R-HpETE and Met-10R-HpDHE were used as substrates. Wt cAOS and its mutants had no reaction with methylated substrates, while the  $k_{\text{cat}}$  and  $K_m$  values of cHPL with Met-8R-HpETE were determined as  $370 \pm 60 \text{ s}^{-1}$  and  $50 \pm 15 \mu\text{M}$ , respectively. The corresponding values of cHPL with Met-10R-HpDHE were measured as  $360 \pm 70 \text{ s}^{-1}$  and  $50 \pm 20 \mu\text{M}$ , respectively (Figs. S4A and S4B). Even though the turnover rates were twice as high compared to the value obtained with the free 8R-HpETE substrate (Table 1), the  $k_{\text{cat}}/K_m$  value with both methylated substrates,  $7 \text{ s}^{-1} \mu\text{M}^{-1}$ , was about two times lower. The  $K_m$  values around  $50 \mu\text{M}$

**Table 1**

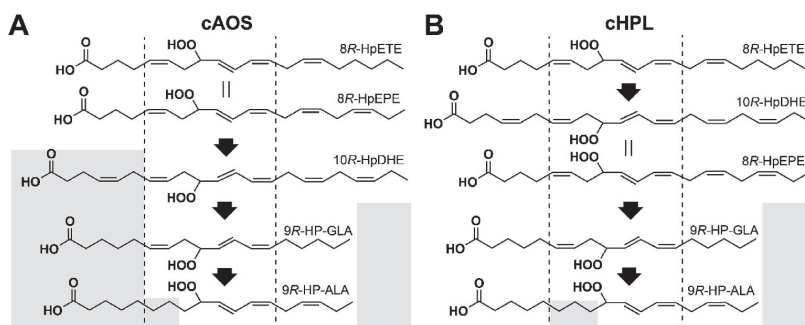
Kinetics of wt cAOS, wt cHPL and mutants determined with PUFA hydroperoxides. The kinetic parameters are presented with the corresponding standard error ( $n = 3$ ). The catalytic efficiency is presented as  $k_{\text{cat}}/K_m$  ( $\text{s}^{-1} \mu\text{M}^{-1}$ ).

ENZYME		8R-HpETE			8R-HpEPE			10R-HpDHE		
		$k_{\text{cat}}$ ( $\text{s}^{-1}$ )	$K_m$ ( $\mu\text{M}$ )	$k_{\text{cat}}/K_m$	$k_{\text{cat}}$ ( $\text{s}^{-1}$ )	$K_m$ ( $\mu\text{M}$ )	$k_{\text{cat}}/K_m$	$k_{\text{cat}}$ ( $\text{s}^{-1}$ )	$K_m$ ( $\mu\text{M}$ )	$k_{\text{cat}}/K_m$
cAOS	wild-type	2360 ± 230	50 ± 10	50 ± 10	2370 ± 230	40 ± 10	55 ± 10	1400 ± 170	35 ± 10	40 ± 10
	K60M	2580 ± 340	50 ± 10	50 ± 15	2950 ± 730	60 ± 20	50 ± 20	1100 ± 140	20 ± 5	50 ± 15
	K60E	2670 ± 230	50 ± 10	50 ± 10	2450 ± 390	70 ± 20	40 ± 10	1040 ± 180	30 ± 10	40 ± 15
	K107M	2400 ± 160	50 ± 5	50 ± 5	2460 ± 180	50 ± 5	55 ± 10	2800 ± 370	50 ± 10	60 ± 15
	K107E	1080 ± 110	30 ± 5	35 ± 10	1260 ± 100	25 ± 5	50 ± 10	1030 ± 140	30 ± 10	40 ± 15
cHPL	wild-type	170 ± 10	12.0 ± 1.5	15 ± 2	420 ± 30	50 ± 5	10 ± 1	700 ± 70	60 ± 10	10 ± 2
	E60M	90 ± 10	4.5 ± 1.5	20 ± 5	200 ± 10	20 ± 2	10 ± 1	300 ± 30	30 ± 5	10 ± 2
	E60K	20 ± 1	1.5 ± 0.2	15 ± 2	160 ± 20	40 ± 10	5 ± 1	55 ± 2	5 ± 1	10 ± 2
	K107M	580 ± 60	38.0 ± 6.5	15 ± 5	720 ± 60	70 ± 10	10 ± 2	1290 ± 220	90 ± 20	15 ± 5
	K107E	390 ± 30	12.5 ± 2.0	30 ± 5	460 ± 30	20 ± 5	25 ± 5	620 ± 50	15 ± 5	40 ± 15
cAOS		9R-Hp-ALA		9R-Hp-GLA						
		$k_{\text{cat}}$ ( $\text{s}^{-1}$ )	$K_m$ ( $\mu\text{M}$ )	$k_{\text{cat}}/K_m$	$k_{\text{cat}}$ ( $\text{s}^{-1}$ )	$K_m$ ( $\mu\text{M}$ )	$k_{\text{cat}}/K_m$			
	wild-type	1370 ± 130	80 ± 10	15 ± 2	1710 ± 200	75 ± 15	25 ± 6			
	K60M	2050 ± 510	90 ± 35	25 ± 10	1630 ± 340	75 ± 30	20 ± 10			
	K60E	1080 ± 120	50 ± 10	20 ± 5	1550 ± 160	90 ± 20	15 ± 5			
cHPL		9R-Hp-ALA		9R-Hp-GLA						
		$k_{\text{cat}}$ ( $\text{s}^{-1}$ )	$K_m$ ( $\mu\text{M}$ )	$k_{\text{cat}}/K_m$	$k_{\text{cat}}$ ( $\text{s}^{-1}$ )	$K_m$ ( $\mu\text{M}$ )	$k_{\text{cat}}/K_m$			
	wild-type	340 ± 25	60 ± 10	5 ± 1	550 ± 50	80 ± 15	6.5 ± 1.0			
	E60M	110 ± 10	25 ± 5	5 ± 1	220 ± 15	60 ± 10	4.0 ± 0.5			
	E60K	80 ± 15	50 ± 15	2 ± 1	70 ± 5	30 ± 5	2.0 ± 0.5			
K107M	700 ± 180	140 ± 50	5 ± 2	620 ± 90	80 ± 20	8.0 ± 2.5				
K107E	490 ± 90	80 ± 20	5 ± 2	460 ± 40	60 ± 10	8.5 ± 2.0				

with the methylated substrates were similar to the affinity obtained with the free 8R-HpEPE and 10R-HpDHE, but significantly higher compared to the  $K_m$  with 8R-HpETE (Table 1). Unexpectedly, the reaction rates of cHPL with Met-10R-HpDHE and Met-8R-HpETE were lower and higher, respectively, compared to the corresponding derivatives with the free carboxy head group. As the reaction rate of cHPL with Met-10R-HpDHE was lower than with the corresponding free PUFA derivative, we believe that more suitable interactions, e.g. ion-ion interactions or hydrogen bonding, were lost with the methylated substrate. In contrast, Met-8R-HpETE was a more favored substrate for cHPL than the respective free PUFA derivative, indicating that the carboxy group had a weaker effect on the binding of the C20 PUFA compared to the C22 derivative.

#### 4. Discussion

As the literature lacks comprehensive information about the binding mechanisms of PUFA hydroperoxides by cAOS, we used the X-ray structures of cAOS in structural modeling and docking experiments to determine the possible interactions between the residues in the substrate entry site of cAOS or cHPL and the carboxy group of PUFA hydroperoxides. Due to the high similarity and the dependency of the model from the template structure, conclusions about the structural-functional insights of cHPL based on the model are not definitive. On the other hand, as cAOS and cHPL are highly identical, a comparative analysis of the crystal structure of cAOS and the model of cHPL is appropriate for visualizing and presenting the locations of the variable



**Scheme 1. The substrate preferences of cAOS (A) and cHPL (B).** The substrate preference is presented from top to bottom, starting with the best substrate. The motifs of ligands lowering the catalytic efficiency are presented as dark gray. The similar kinetic parameters determined with different substrates are indicated by the equal sign.

residues/regions and the potential effects they might have on the substrate binding or catalysis. For instance, as shown in the present work, the substrate entry sites of cAOS and cHPL have distinct structural and electrostatic properties (Fig. 3).

In the current study, we observed that wt cAOS, wt cHPL and their mutants are able to metabolize 9R-hydroperoxy C18, 8R-hydroperoxy C20 and 10R-hydroperoxy C22 PUFAs, which is in correlation with the docking simulations of cAOS (Fig. 1). However, the mutational analysis of cAOS and cHPL in regard to the electrostatic interactions between K107 and the carboxy group of PUFA hydroperoxides was not consistent with the observations from computational methods. Based on the results obtained with the combination of *in silico* and *in vitro* approaches, the structural aspects of the differences in the substrate binding between cHPL and cAOS will be discussed.

The diminished catalytic rate of cHPL as a result of E60 replacements (Table 1) indicated that E60 seemed to be an important factor in the binding of PUFA hydroperoxides. Although the nature of the interaction between two negatively charged groups, the side chain of E60 and the carboxylate ion of a substrate, is repulsive, we cannot exclude the secondary contacts initiated by electrostatic interactions. The substrate entry site of cHPL contains a triad of charged residues, R56, E60 and K107, along with the SSSAGESA loop (Fig. 3B and C), which all together could produce a complex interaction with negatively charged PUFA hydroperoxides. In our previous work, we observed that the replacement of the R56 with the G56 of cAOS elevated the  $k_{cat}$  of cHPL, most likely by broadening the entry site of the substrate channel [11]. Similarly, the loss of positively charged K107, as presented in this work, increased the turnover rate of cHPL. Both residues, R56 and K107, most likely do not form a salt bridge with the carboxylate ion and therefore they are non-essential in regard to the substrate binding, but still may play a role in the shaping of the substrate entry site of cHPL. The  $k_{cat}$  and the  $k_{cat}/K_m$  of cHPL were increased, with the K107E mutation containing both negatively charged residues, E60 and E107 (Table 1). This indicated that, instead of the salt bridge formation with negatively charged carboxy head of the substrate, the coordination of PUFA substrates occurred in an alternative way. Such a repelling environment suggests that instead of the electrostatic anchoring, the E60 of cHPL could be involved in directing the carboxylate ion towards the productive binding. The SSSAGE replacement with the PVKEGD fragment of coral cAOS [11] reduced the turnover rate similarly to the E60 M mutation. However, the replacement of the E60 with positively charged K reduced the  $k_{cat}$  more drastically, almost resulting in the inactivation of cHPL. The E60K mutant having the lowest  $k_{cat}$  value is in agreement with the previously mentioned R56-E60-K107 triad concept. As all the key residues, E60K, K107 and R56, in the respective mutant were positively charged, the negatively charged carboxy head of substrates was probably retracted, resulting in less efficient binding and slower catalysis. To encapsulate the presented kinetic data, we can conclude that all of the mentioned negatively charged residues and the SSSAGE motif are necessary for the efficient catalysis of substrates, while the positively charged residues in the substrate entry site have a negative effect on the substrate binding by cHPL (Table 1).

Even though the kinetic properties between cAOS and cHPL (Table 1) with PUFA hydroperoxides were remarkably different, the substrate preferences derived based on the reaction efficiencies were comparable (Scheme 1). The substrate preference of an enzyme determined based on  $k_{cat}$  values is correct only if  $K_m$  values with different substrates are equivalent [35,36]. In spite of the fact that the substrate selectivity of cAOS correlates with the 8R-LOX domain [20], the results with LOX were established by comparing only the  $k_{cat}$  values. Based on this analogy, the highest and the lowest  $k_{cat}$  value of cHPL were determined with 10R-HpDHE and 8R-HpETE, respectively, which presented a notable effect of different substrates on the  $k_{cat}$  values of cHPL (Table 1). At the same time, it was difficult to comprehend the differences between the binding mechanisms with the C18, C20 and C22 PUFA hydroperoxides. Therefore, as the catalytic efficiency takes into

account both effects,  $k_{cat}$  and  $K_m$ , it was the best way to determine the substrate preferences of enzymes.

Even when cAOS was able to metabolize the endocannabinoid derivatives, probably due to the hydrogen bonding with K60 and/or K107, the conversion by cHPL was more efficient (Figs. 2B, S2C, S2D). The precedent of two human isozymes with the amino acid identity over 60% and with distinct substrate selectivity can be found in the comparison between COX-1 and COX-2 [37]. The wider channel opening of COX-2 due to a side pocket in the substrate channel gives COX-2 the ability to metabolize larger PUFA derivatives, e.g. AEA and 2-AG, which is also considered in a selective drug design [13]. Although ALA, GLA, DHA and EPA compared to AA are not good substrates for COX-2 and COX-1, COX-2 metabolizes these PUFAs more efficiently than COX-1 [37,38]. We can speculate that, similarly to COX-2, cHPL is able to bind free and neutral PUFA hydroperoxides due to the suitable size of the substrate entry site.

The fact that cHPL tolerated the missing carboxy ion of PUFA hydroperoxides while no reaction occurred with cAOS evoked many questions in regard to the substrate binding mechanisms of cAOS and cHPL. The inability to form any salt bridges by methylated substrates indicated that the substrate binding by cHPL took place via hydrophobic interactions. It also suggests that the cHPL might have the ability to interact with the membrane-bound substrates *in vivo*. For example, the binding specificity of phospholipases with PUFAs at the *sn*-1 and *sn*-2 positions is achieved via hydrophobic interactions [39]. Studies on albumin have demonstrated that PUFA substrates bind more strongly when electrostatic and hydrophobic interactions co-occur, although, the latter seems to be more essential due to the aliphatic tails of fatty acids [40]. It is difficult to envision whether the carbonyl group of Met-8R-HpETE or Met-10R-HpETE was in contact with hydrogen donors, e.g. K107, as the turnover rates of cHPL with corresponding substrates were quite similar. However, the differences between the kinetic parameters of cHPL with free and methylated substrates demonstrated a distinct effect on the binding, indicating that the interactions with free PUFAs were not purely hydrophobic. Clearly, the regio- and stereospecificity of the 8R-hydroperoxy group is essential in regard to the hydrophilic recognition by the catalytic center of cAOS and cHPL [4,20]. The inability of cAOS to metabolize methylated substrates can be explained by the structural characteristics of the substrate binding site of cAOS, which probably lacks the cleft with necessary interactions for binding hydrophobic substrates in a productive manner. Despite the fact that cAOS was not able to metabolize methylated substrates, the results obtained with cHPL and the K60 and K107 mutants of cAOS shed light on the importance of the hydrophobic interactions in substrate binding by cAOS and cHPL.

Substrates or substrate analogs are bound in a U-shaped substrate channel by plant AOSs in a fashion similar to that observed with coral cAOS. However, the substrate positioning and the interacting residues between homologous plant isozymes might differ. For instance, *Parthenium argentatum* AOS (PDB ID: 3DBM) binds the carboxy group of a substrate by K and S residues [41], while *Arabidopsis thaliana* AOS (PDB ID: 2RCH) forms hydrogen bonds via the T and nitrogen of a peptide bond instead [42]. Moreover, most of the characterized allene oxide cyclases (PDB IDs: 4CQ6, 4CQ7, 4HG6), enzymes responsible for the cyclization of allene oxide to jasmonic acid precursors, do not contain any positively charged residues in their substrate entry sites [43,44]. The latter examples also demonstrate that the PUFA binding does not occur necessarily via charged residues and the interacting residues might differ between homologs. Based on our *in vitro* results, the absence of direct evidence of the salt bridge formation between the positively charged K and negatively charged carboxy group of a substrate might indicate the presence of other interacting partners, e.g. water and hydrophilic residues, or the lack of the strength or the distance necessary for the proper ionic bond. The potency of an ionic interaction by R or K is influenced by its neighboring residues and also by whether the formed salt bridge is buried or solvent-exposed [45]. For

instance, an NMR study with liver FABP [46] revealed that in contrast to the crystal structure of FABP with two oleates, the mutations in the interacting residues, R122 and S124, of the carboxylate group of FAs did not influence the binding of one of the two oleates. Even though the structural data verified the electrostatic interactions, the contrary results by mutational analysis indicated the necessity of an alternative structural accommodation instead.

The total fatty acid composition of corals [47] shows that the most abundant PUFA is AA correlating with the PUFA derivatives of the soft corals *C. imbricata* and *P. homomalla* (unpublished data). The presence of EPA and DHA varies between coral species and is usually significantly underrepresented compared to AA [48]. Even when AA is the most abundant in *C. imbricata*, we speculate that cHPL might metabolize alternative PUFA hydroperoxides in parallel. As the cellular localization of cAOS-LOX or cHPL-LOX and the ability of 8R-LOX to oxidize membrane-bound PUFAs are not known, this is a matter of future research. In addition, the literature lacks data about the endocannabinoid systems in corals, however, the presence of endocannabinoid signaling in *Hydra* species [49] indicates the potential existence of endocannabinoid-like systems in *Cnidaria*, including corals.

## 5. Conclusion

In this study, we determined that the substrate preference and binding characteristics of two highly identical catalase-related PUFA metabolizing enzymes, cAOS and cHPL, are distinct due to the possible conformational variation in the substrate entry site. Our results indicate that the substrate accommodation between highly conserved enzymes can be different and a structural-functional analysis should be performed in order to understand the ligand preference. Although we determined that the K60 or E60 and K107 of cAOS and cHPL were not involved in the formation of a salt bridge, the reaction rates of cHPL mutants and cAOS K107E indicated their involvement in the conformational integrity of the substrate entry site. The conformational specificities of cHPL, especially in regard to the ability to bind neutral PUFA hydroperoxides, should be determined in future.

## Acknowledgements

This work was supported by the Estonian Ministry of Education and Research grant IUT 19-9 and the Estonian Science Foundation grant 9410. This work has been partially supported by “TTÜ arenguprogramm aastateks 2016–2022 Graduate School in Biomedicine and Biotechnology” receiving funding from the European Regional Development Fund under program ASTRA 2014-2020.4.01.16-0032 in Estonia. We would like to thank Prof. James W. Gauld and Dr. Abayomi S. Faponle for the consultations about the molecular dynamics of *P. homomalla* cAOS.

## Appendix A. Supplementary data

Supplementary data to this article can be found online at <https://doi.org/10.1016/j.abb.2019.108126>.

## References

- R. Koljak, O. Boutaud, B.H. Shieh, N. Samel, A.R. Brash, Identification of a naturally occurring peroxidase-lipoxygenase fusion protein, *Science* (80- ) 277 (1997) 1994–1996, <https://doi.org/10.1126/science.277.5334.1994>.
- H. Löhelaïd, T. Teder, K. Tõldsepp, M. Ekins, N. Samel, Up-regulated expression of AOS-LOXa and increased eicosanoid synthesis in response to coral wounding, *PLoS One* 9 (2014), <https://doi.org/10.1371/journal.pone.0089215>.
- A.R. Brash, Formation of an allene oxide from (8R)-8-hydroperoxyeicosatetraenoic acid in the coral *Plexaura homomalla*, *J. Am. Chem. Soc.* 111 (1989) 1891–1892, <https://doi.org/10.1021/ja00187a060>.
- T. Teder, H. Löhelaïd, W.E. Boeglin, W.M. Calcutt, A.R. Brash, N. Samel, A catalase-related hemoprotein in coral is specialized for synthesis of short-chain aldehydes: discovery of P450-type hydroperoxide lyase activity in a catalase, *J. Biol. Chem.* 290 (2015) 19823–19832, <https://doi.org/10.1074/jbc.M115.660282>.
- C. Wasternack, I. Feussner, The oxylipin pathways: biochemistry and function, *Annu. Rev. Plant Biol.* 69 (2017), <https://doi.org/10.1146/annurev-arplant-042817-040440>.
- A.R. Brash, Mechanistic aspects of CYP74 allene oxide synthases and related cytochrome P450 enzymes, *Phytochemistry* 70 (2009) 1522–1531, <https://doi.org/10.1016/j.phytochem.2009.08.005>.
- H. Löhelaïd, N. Samel, Eicosanoid diversity of stony corals, *Mar. Drugs* 16 (2018), <https://doi.org/10.3390/md16010010>.
- H. Löhelaïd, R. Järving, K. Valmsen, K. Varvas, M. Kreen, I. Järving, N. Samel, Identification of a functional allene oxide synthase-lipoxygenase fusion protein in the soft coral *Gersemia frutescens* suggests the generality of this pathway in octocorals, *Biochim. Biophys. Acta Gen. Subj.* 1780 (2008) 315–321, <https://doi.org/10.1016/j.bbagen.2007.10.010>.
- H. Löhelaïd, T. Teder, N. Samel, Lipoxygenase-allene oxide synthase pathway in octocoral thermal stress response, *Coral Reefs* 34 (2015) 143–154, <https://doi.org/10.1007/s00338-014-1238-y>.
- M.L. Oldham, A.R. Brash, M.E. Newcomer, The structure of coral allene oxide synthase reveals a catalase adapted for metabolism of a fatty acid hydroperoxide, *Proc. Natl. Acad. Sci.* 102 (2005) 297–302, <https://doi.org/10.1073/pnas.0406352102>.
- T. Teder, H. Löhelaïd, N. Samel, Structural and functional insights into the reaction specificity of catalase-related hydroperoxide lyase: a shift from lyase activity to allene oxide synthase by site-directed mutagenesis, *PLoS One* 12 (2017), <https://doi.org/10.1371/journal.pone.0185291>.
- D.B. Neau, G. Bender, W.E. Boeglin, S.G. Bartlett, A.R. Brash, M.E. Newcomer, Crystal structure of a lipoxygenase in complex with substrate: the arachidonic acid-binding site of 8R-lipoxygenase, *J. Biol. Chem.* 289 (2014) 31905–31913, <https://doi.org/10.1074/jbc.M114.599662>.
- K.M. Knights, A.A. Mangoni, J.O. Miners, Defining the COX inhibitor selectivity of NSAIDs: implications for understanding toxicity, *Expert Rev. Clin. Pharmacol.* 3 (2010) 769–776, <https://doi.org/10.1586/eczp.10.120>.
- P. Benkert, S.C.E. Tosatto, D. Schomburg, QMEAN: a comprehensive scoring function for model quality assessment, *Proteins Struct. Funct. Genet.* 71 (2008) 261–277, <https://doi.org/10.1002/prot.21715>.
- A. Waterhouse, M. Bertoni, S. Bienert, G. Studer, G. Tauriello, R. Gumienny, F.T. Heer, T.A.P. De Beer, C. Rempfer, L. Bordoli, R. Lepore, T. Schwede, SWISS-MODEL: homology modelling of protein structures and complexes, *Nucleic Acids Res.* 46 (2018) W296–W303, <https://doi.org/10.1093/nar/gky427>.
- E.F. Pettersen, T.D. Goddard, C.C. Huang, G.S. Couch, D.M. Greenblatt, E.C. Meng, T.E. Ferrin, UCSF Chimera - a visualization system for exploratory research and analysis, *J. Comput. Chem.* 25 (2004) 1605–1612, <https://doi.org/10.1002/jcc.20084>.
- O. Trott, A.J. Olson, Software news and update AutoDock Vina: improving the speed and accuracy of docking with a new scoring function, efficient optimization, and multithreading, *J. Comput. Chem.* 31 (2010) 455–461, <https://doi.org/10.1002/jcc.21334>.
- A. Grosdidier, V. Zoete, O. Michielin, SwissDock, a protein-small molecule docking web service based on EADock DSS, *Nucleic Acids Res.* 39 (2011), <https://doi.org/10.1093/nar/gkr366>.
- A.W. Schüttelkopf, D.M.F. Van Aalten, PRODRG: a tool for high-throughput crystallography of protein-ligand complexes, *Acta Crystallogr. Sect. D Biol. Crystallogr.* 60 (2004) 1355–1363, <https://doi.org/10.1107/S090744490401679>.
- O. Boutaud, A.R. Brash, Purification and catalytic activities of the two domains of the allene oxide synthase-lipoxygenase fusion protein of the coral *Plexaura homomalla*, *J. Biol. Chem.* 274 (1999) 33704–33710, <https://doi.org/10.1074/jbc.274.47.33764>.
- I.V. Oferkin, E.V. Katkova, A.V. Sulimov, D.C. Kutov, S.I. Sobolev, V.V. Voevodin, V.B. Sulimov, Evaluation of docking target functions by the comprehensive investigation of protein-ligand energy minima, *Adv. Bioinform.* 2015 (2015), <https://doi.org/10.1155/2015/126858>.
- E.A.C. Bushnell, R. Gherib, J.W. Gauld, Insights into the catalytic mechanism of coral allene oxide synthase: a dispersion corrected density functional theory study, *J. Phys. Chem. B* 117 (2013) 6701–6710, <https://doi.org/10.1021/jp403405b>.
- W. Kabsch, C. Sander, Dictionary of protein secondary structure: pattern recognition of hydrogen-bonded and geometrical features, *Biopolymers* 22 (1983) 2577–2637, <https://doi.org/10.1002/bip.360221211>.
- E.F. Pettersen, T.D. Goddard, C.C. Huang, G.S. Couch, D.M. Greenblatt, E.C. Meng, T.E. Ferrin, UCSF Chimera - a visualization system for exploratory research and analysis, *J. Comput. Chem.* 25 (2004) 1605–1612, <https://doi.org/10.1002/jcc.20084>.
- R.A. Laskowski, M.B. Swindells, LigPlot+: multiple ligand-protein interaction diagrams for drug discovery, *J. Chem. Inf. Model.* 51 (2011) 2778–2786, <https://doi.org/10.1021/ci200227u>.
- B. Webb, A. Sali, Comparative protein structure modeling using MODELLER, *Curr. Protoc. Bioinform.* 2016 (2016), <https://doi.org/10.1002/cpbi.3.5.6.1-5.6.37>.
- B. John, A. Sali, Comparative protein structure modeling by iterative alignment, model building and model assessment, *Nucleic Acids Res.* 31 (2003) 3982–3992, <https://doi.org/10.1093/nar/gkg460>.
- M. Shen, A. Sali, Statistical potential for assessment and prediction of protein structures, *Protein Sci.* 15 (2006) 2507–2524, <https://doi.org/10.1110/ps.062416606>.
- H. Liu, J.H. Naismith, An efficient one-step site-directed deletion, insertion, single and multiple-site plasmid mutagenesis protocol, *BMC Biotechnol.* 8 (2008) 91, <https://doi.org/10.1186/1472-6750-8-91>.
- M. Lehtonen, K. Reisner, S. Auriola, G. Wong, J.C. Callaway, Mass-spectrometric

- identification of anandamide and 2-arachidonoylglycerol in nematodes, *Chem. Biodivers.* 5 (2008) 2431–2441, <https://doi.org/10.1002/cbdv.200890208>.
- [31] N. Shaw, C. Cheng, Z.-J. Liu, Procedure for reductive methylation of protein to improve crystallizability, *Protoc. Exch.* (2007), <https://doi.org/10.1038/nprot.2007.287>.
- [32] P. De Luna, E.A.C. Bushnell, J.W. Gaudl, A molecular dynamics examination on mutation-induced catalase activity in coral allene oxide synthase, *J. Phys. Chem. B* 117 (2013) 14635–14641, <https://doi.org/10.1021/jp408486n>.
- [33] F. Melo, R. Sánchez, A. Sali, Statistical potentials for fold assessment, *Protein Sci.* 11 (2009) 430–448, <https://doi.org/10.1002/pro.110430>.
- [34] R. Floris, N. Moguilevsky, G. Puppels, A. Jacquet, R. Renirie, A. Bollen, R. Wever, Heme-protein interaction in myeloperoxidase: modification of spectroscopic properties and catalytic activity by single residue mutation, *J. Am. Chem. Soc.* 117 (1995) 3907–3912, <https://doi.org/10.1021/ja00119a003>.
- [35] R. Eisenthal, M.J. Danson, D.W. Hough, Catalytic efficiency and  $k_{cat}/K_M$ : a useful comparator? *Trends Biotechnol.* 25 (2007) 247–249, <https://doi.org/10.1016/j.tibtech.2007.03.010>.
- [36] N. Carrillo, E.A. Ceccarelli, O.A. Roveri, Usefulness of kinetic enzyme parameters in biotechnological practice, *Biotechnol. Genet. Eng. Rev.* 27 (2010) 367–382, <https://doi.org/10.1080/02648725.2010.10648157>.
- [37] O. Laneuville, D.K. Breuer, N. Xu, Z.H. Huang, D.A. Gage, J.T. Watson, M. Lagarde, D.L. DeWitt, W.L. Smith, Fatty acid substrate specificities of human prostaglandin-endoperoxide H synthase-1 and -2. Formation of 12-hydroxy-(9Z,13E/Z,15Z)-octadecatrienoic acids from  $\alpha$ -linolenic acid, *J. Biol. Chem.* 270 (1995) 19330–19336, <https://doi.org/10.1074/jbc.270.33.19330>.
- [38] A.J. Vecchio, D.M. Simmons, M.G. Malkowski, Structural basis of fatty acid substrate binding to cyclooxygenase-2, *J. Biol. Chem.* 285 (2010) 22152–22163, <https://doi.org/10.1074/jbc.M110.119867>.
- [39] V.D. Mouchlis, Y. Chen, J. Andrew McCammon, E.A. Dennis, Membrane allostery and unique hydrophobic sites promote enzyme substrate specificity, *J. Am. Chem. Soc.* 140 (2018) 3285–3291, <https://doi.org/10.1021/jacs.7b12045>.
- [40] M. Fasano, S. Curry, E. Terreno, M. Galliano, G. Fanali, P. Narciso, S. Notari, P. Ascenzi, The extraordinary ligand binding properties of human serum albumin, *IUBMB Life* 57 (2005) 787–796, <https://doi.org/10.1080/15216540500404093>.
- [41] L. Li, Z. Chang, Z. Pan, Z.-Q. Fu, X. Wang, Modes of heme binding and substrate access for cytochrome P450 CYP74A revealed by crystal structures of allene oxide synthase, *Proc. Natl. Acad. Sci.* 105 (2008) 13883–13888, <https://doi.org/10.1073/pnas.0804099105>.
- [42] D.-S. Lee, P. Nioche, M. Hamberg, C.S. Raman, Structural insights into the evolutionary paths of oxylipin biosynthetic enzymes, *Nature* 455 (2008) 363–368, <https://doi.org/10.1038/nature07307>.
- [43] E. Hofmann, P. Zerbe, F. Schaller, The crystal structure of Arabidopsis thaliana allene oxide cyclase: insights into the oxylipin cyclization reaction, *Plant Cell* 18 (2006) 3201–3217, <https://doi.org/10.1105/tpc.106.043984>.
- [44] P. Neumann, F. Brodhun, K. Sauer, C. Herrfurth, M. Hamberg, J. Brinkmann, J. Scholz, A. Dickmanns, I. Feussner, R. Ficner, Crystal structures of Physcomitrella patens AOC1 and AOC2: insights into the enzyme mechanism and differences in substrate specificity, *Plant Physiol.* 160 (2012) 1251–1266, <https://doi.org/10.1104/pp.112.205138>.
- [45] C.D. Waldburger, J.F. Schildbach, R.T. Sauer, Are buried salt bridges important for protein stability and conformational specificity? *Nat. Struct. Biol.* 2 (1995) 122–128, <https://doi.org/10.1038/nsb0295-122>.
- [46] Y. He, R. Estephan, X. Yang, A. Vela, H. Wang, C. Bernard, R.E. Stark, A nuclear magnetic resonance-based structural rationale for contrasting stoichiometry and ligand binding site(s) in fatty acid-binding proteins, *Biochemistry* 50 (2011) 1283–1295, <https://doi.org/10.1021/bi101307h>.
- [47] A.B. Imbs, N.A. Latyshev, T.N. Dautova, Y.Y. Latypov, Distribution of lipids and fatty acids in corals by their taxonomic position and presence of zooxanthellae, *Mar. Ecol. Prog. Ser.* 409 (2010) 65–75, <https://doi.org/10.3354/meps08622>.
- [48] A.B. Imbs, D.A. Demidkova, T.N. Dautova, Lipids and fatty acids of cold-water soft corals and hydrocorals: a comparison with tropical species and implications for coral nutrition, *Mar. Biol.* 163 (2016), <https://doi.org/10.1007/s00227-016-2974-z>.
- [49] L. De Petrocellis, D. Melck, T. Bisogno, A. Milone, V. Di Marzo, Finding of the endocannabinoid signalling system in Hydra, a very primitive organism: possible role in the feeding response, *Neuroscience* 92 (1999) 377–387, [https://doi.org/10.1016/S0306-4522\(98\)00749-0](https://doi.org/10.1016/S0306-4522(98)00749-0).

# Curriculum vitae

## Personal data

Name: Tarvi Teder

Date of birth: 14.04.1989

Place of birth: Valga

Citizenship: Estonian

## Contact data

E-mail: tarvi.teder@gmail.com

## Education

- 2015–... Tallinn University of Technology, Faculty of Science, Department of Chemistry and Biotechnology, Chemistry and Gene Technology, PhD
- 2012–2015 Tallinn University of Technology, Faculty of Science, Department of Gene Technology, Gene Technology, MSc (*cum laude*)
- 2008–2012 Tallinn University of Technology, Faculty of Science, Department of Chemistry, Applied Chemistry and Biotechnology, BSc (*cum laude*)
- 2005–2008 Valga Gymnasium (silver medal)

## Language competence

Estonian (native), English (competent), German (basic)

## Professional employment

- 2017–... Tallinn University of Technology, School of Science, Department of Chemistry and Biotechnology, Early Stage Researcher
- 2013–2014 Vanderbilt University (Nashville, Tennessee, USA) - Research Intern

## Honors and awards

- 2016 the research award by Estonian Biochemical Society - 1st prize
- 2015 the research award by Estonian Biochemical Society - 1st prize
- 2014 the research award by Estonian Biochemical Society - 2nd prize
- 2014 Estonian national research competition for university students - 2nd place, Master's students, biosciences and environment
- 2013 the science award by Estonian Academy of Sciences - Bachelor's thesis
- 2012 TUT Development Fund scholarship, AS Kevelt

## Other affiliations

- 2012–... Member of Estonian Biochemical Society

## Supervised dissertations

Relika Toome (BSc), 2017, "*Mutational analysis of Capnella imbricata hydroperoxide lyase*". Tallinn University of Technology, Faculty of Science, Department of Chemistry.

Reelika Sultson (BSc), 2017, "*Identification of Acropora sp. lipoxygenases*". Tallinn University of Technology, Faculty of Science, Department of Chemistry.

Jaroslav Marhivka (BSc), 2016, "*The influence of His-epitope on the expression, purification and activity of coral allene oxide synthase*". Tallinn University of Technology, Faculty of Science, Department of Chemistry.

Tähti Kull (BSc), 2013, "*Cloning of lipoxygenase sequences from soft coral Capnella imbricata*". Tallinn University of Technology, Faculty of Science, Department of Chemistry.

## Publications

Teder, T.; Samel, N; Lõhelaid, H. (2019). Distinct characteristics of the substrate binding between highly homologous catalase-related allene oxide synthase and hydroperoxide lyase - *Archives of Biochemistry and Biophysics*, 676 (108126).

Teder, T.; Boeglin, W. E.; Schneider, C.; Brash, A. R. (2017). A fungal catalase reacts selectively with the 13S fatty acid hydroperoxide products of the adjacent lipoxygenase gene and exhibits 13S-hydroperoxide-dependent peroxidase activity - *Biochimica et Biophysica Acta - Molecular and Cell Biology of Lipids*, 1862 (7), 706–715.

Teder, T.; Boeglin, W. E.; Brash, A. R. (2017). Oxidation of C18 hydroxy-polyunsaturated fatty acids to epoxide or ketone by catalase-related hemoproteins activated with iododibenzene - *Lipids*, 52 (7), 587–597.

Teder, T.; Lõhelaid, H.; Samel, N. (2017). Structural and functional insights into the reaction specificity of catalase-related hydroperoxide lyase: A shift from lyase activity to allene oxide synthase by site-directed mutagenesis - *PLoS One*, 12 (9), e0185291.

Teder, T.; Lõhelaid, H.; Boeglin, W. E.; Calcutt, W. M.; Brash, A. R.; Samel, N. (2015). A catalase-related hemoprotein in coral is specialized for synthesis of short-chain aldehydes: Discovery of P450-type hydroperoxide lyase activity in a catalase - *Journal of Biological Chemistry*, 290 (32), 19823–19832.

Lõhelaid, H.; Teder, T.; Samel, N. (2015). Lipoxygenase-allene oxide synthase pathway in octocoral thermal stress response - *Coral Reefs*, 34 (1), 143–154.

Teder, T.; Boeglin, W. E.; Brash, A. R. (2014). Lipoxygenase catalyzed transformation of epoxy fatty acids to hydroxy-endoperoxides: A potential P450 and lipoxygenase interaction - *Journal of Lipid Research*, 55 (12), 2587–2596.

Lõhelaid, H.; Teder, T.; Tõldsepp, K.; Ekins, M.; Samel, N. (2014). Up-Regulated Expression of AOS-LOXa and Increased Eicosanoid Synthesis in Response to Coral Wounding - *PLoS One* 9 (2), e89215.

## Science meetings and courses

2019, October – science meeting – Bioactive lipid mediators in cancer, inflammation and other diseases (St. Petersburg, Florida, USA)

2019, June – science meeting and oral presentation – FEBS3+ meeting (Riga, Latvia)



2019, May – advanced course – Trends in enzymology and biocatalysis (Rome, Italy)

2019, April – COST Short Term Scientific Mission (Naples, Italy)

2018, November – COST Action meeting – MARISTEM. (Banyuls-sur-mer, France)

2018, June – science meeting and poster presentation – XV Conference of the Lithuanian Biochemical Society (Dubingiai, Lithuania)

2018, March – science meeting and poster presentation – Bioactive lipids: from chemistry to biology and medicine (Athens, Greece)

2018, February – COST Action meeting and poster presentation – MARISTEM. Stem cells of marine invertebrates: from basic research to innovative applications (Piran, Slovenia)

2016, September – science meeting and poster presentation – 57th International Conferences on the Bioscience of Lipids (Chamonix, Mont-Blanc; France)

2015, November – advanced course – Lipid Biochemistry (Technical University of Denmark, Aarhus University; Denmark)

2014, September – science meeting – A Tribute to Bengt Samuelsson: Lipid Mediators in Health and Disease (Stockholm, Sweden)

2014, August – science meeting and poster presentation – Vanderbilt University Institute of Chemical Biology Symposium (Nashville, Tennessee, USA)

2014, May – science meeting and poster presentation – Lipid Maps Meeting (San Diego, California, USA)

2011, 2012, 2015–2018 – oral presentations – Estonian Biochemical Society Spring Seminar

## Elulookirjeldus

### Isikuandmed

Nimi: Tarvi Teder

Sünniaeg: 14.04.1989

Sünnikoht: Valga

Kodakondsus: Eesti

### Kontaktandmed

E-post: tarvi.teder@gmail.com

### Hariduskäik

2015–... TTÜ Matemaatika-loodusteaduskond, Keemiainstituut, Keemia ja geenitehnoloogia, PhD

2012–2015 TTÜ Matemaatika-loodusteaduskond, Geenitehnoloogia instituut; Geenitehnoloogia, MSc (*cum laude*)

2008–2012 TTÜ Matemaatika-loodusteaduskond, Keemiainstituut; Rakenduskeemia ja biotehnoloogia, BSc (*cum laude*)

2005–2008 Valga Gümnaasium, reaalkallak (hõbemedal)

### Keelteoskus

Eesti (emakeel), inglise (kõrgtase), saksa (algase)

### Teenistuskäik

2017–... Tallinna Tehnikaülikool, Loodusteaduskond, Keemia ja biotehnoloogia instituut, Doktorant-nooremteadur

2013–2014 Vanderbilt University (Nashville, Tennessee, USA) – Teaduspraktikant

### Teadusorganisatsiooniline tegevus

2012–... Eesti Biokeemia Seltsi liige

### Teaduspreemiad ja tunnustused

2016 Eesti Biokeemia Seltsi üliõpilastööde konkurss - I auhind

2015 Eesti Biokeemia Seltsi üliõpilastööde konkurss - I auhind

2014 Eesti Biokeemia Seltsi üliõpilastööde konkurss - II auhind

2014 Riiklik üliõpilastööde konkurss - II auhind, magistrandid, bio- ja keskkonnateaduste valdkond

2013 Eesti Teaduste Akadeemia teadusauhind - bakalaureusetöö

2012 TTÜ Arengufondi stipendium, AS Kevelt

## Lõputööde juhendamised

Relika Toome, BSc, 2017, "*Capnella imbricata* hüdroperoksiidi lüaasi mutantide valmistamine ja analüüs". TTÜ Matemaatika-loodusteaduskond, Keemiasstituut.

Jaroslav Marhivka, BSc, 2016, "*Histidiin-epitoobi mõju koralli alleenoksiidi süntaasi ekspresseerimisele, puhastamisele ja aktiivsusele*". TTÜ Matemaatika-loodusteaduskond, Keemiasstituut.

Reelika Sultson, BSc, 2017, "*Lipoksügenaasid kivikorallist Acropora sp.*". TTÜ Matemaatika-loodusteaduskond, Keemiasstituut.

Tähti Kull, BSc, 2013, "*Osaliste lipoksügenaaside kloneerimine pehmest korallist Capnella imbricata*". TTÜ Matemaatika-loodusteaduskond, Keemiasstituut.

## Publikatsioonid

Teder, T.; Samel, N.; Löhelaid, H. (2019). Distinct characteristics of the substrate binding between highly homologous catalase-related allene oxide synthase and hydroperoxide lyase - *Archives of Biochemistry and Biophysics*, 676 (108126).

Teder, T.; Boeglin, W. E.; Schneider, C.; Brash, A. R. (2017). A fungal catalase reacts selectively with the 13S fatty acid hydroperoxide products of the adjacent lipoxygenase gene and exhibits 13S-hydroperoxide-dependent peroxidase activity - *Biochimica et Biophysica Acta - Molecular and Cell Biology of Lipids*, 1862 (7), 706–715.

Teder, T.; Boeglin, W. E.; Brash, A. R. (2017). Oxidation of C18 hydroxy-polyunsaturated fatty acids to epoxide or ketone by catalase-related hemoproteins activated with iodobenzene - *Lipids*, 52 (7), 587-597.

Teder, T.; Löhelaid, H.; Samel, N. (2017). Structural and functional insights into the reaction specificity of catalase-related hydroperoxide lyase: A shift from lyase activity to allene oxide synthase by site-directed mutagenesis - *PLoS One*, 12 (9), e0185291.

Teder, T.; Löhelaid, H.; Boeglin, W. E.; Calcutt, W. M.; Brash, A. R.; Samel, N. (2015). A catalase-related hemoprotein in coral is specialized for synthesis of short-chain aldehydes: discovery of P450-type hydroperoxide lyase activity in a catalase - *Journal of Biological Chemistry*, 290 (32), 19823–19832.

Löhelaid, H.; Teder, T.; Samel, N. (2015). Lipoxygenase-allene oxide synthase pathway in octocoral thermal stress response - *Coral Reefs*, 34 (1), 143–154.

Teder, T.; Boeglin, W. E.; Brash, A. R. (2014). Lipoxygenase catalyzed transformation of epoxy fatty acids to hydroxy-endoperoxides: A potential P450 and lipoxygenase interaction - *Journal of Lipid Research*, 55 (12), 2587–2596.

Löhelaid, H.; Teder, T.; Töldsepp, K.; Ekins, M.; Samel, N. (2014). Up-Regulated Expression of AOS-LOXa and Increased Eicosanoid Synthesis in Response to Coral Wounding - *PLoS One*, 9 (2), e89215.

## Konverentsidel ja kursustel osalemine

2019, oktoober – teaduskonverents – Bioactive lipid mediators in cancer, inflammation and other diseases (St. Petersburg, Florida, USA)

2019, juuni – teaduskonverents ja suuline ettekanne – FEBS3+ meeting (Riga, Latvia)

2019, mai – erikursus – Trends in enzymology and biocatalysis (Rome, Italy)

2019, aprill – COST-i lühiajaline teaduskoostöö (Naples, Italy)

2018, november – COST Action meeting – MARISTEM. (Banyuls-sur-mer, France)

2018, juuni – teaduskonverents ja posterettekannne – XV Conference of the Lithuanian Biochemical Society (Dubingiai, Lithuania)

2018, märts – teaduskonverents ja posterettekannne – Bioactive lipids: from chemistry to biology and medicine (Athens, Greece)

2018, veebruar – COST Action meeting and poster presentation – MARISTEM. Stem cells of marine invertebrates: from basic research to innovative applications (Piran, Slovenia)

2016, september – teaduskonverents ja posterettekannne – 57th International Conferences on the Bioscience of Lipids (Chamonix, Mont-Blanc; France)

2015, november – erikursus – Lipid Biochemistry (Technical University of Denmark, Aarhus University; Denmark)

2014, september – teaduskonverents – A Tribute to Bengt Samuelsson: Lipid Mediators in Health and Disease (Stockholm, Sweden)

2014, august – teaduskonverents ja posterettekannne – Vanderbilt University Institute of Chemical Biology Symposium (Nashville, Tennessee, USA)

2014, mai – teaduskonverents ja posterettekannne – Lipid Maps Meeting (San Diego, California, USA)

2011, 2012, 2015–2018 – suulised ettekanded – Eesti Biokeemia Seltsi kevadseminarid